

TECHNICAL REPORT 1910  
February 2004

# **TST Reconfigurable Aperture RF MEMS for Antenna Applications**

E. W. Jacobs  
H. B. Simonds  
M. W. Roberts  
T. O. Jones III  
D. W. Brock  
C. E. Dempsey

Approved for public release;  
distribution is unlimited.

SSC San Diego



TECHNICAL REPORT 1910  
February 2004

# **TST Reconfigurable Aperture RF MEMS for Antenna Applications**

E. W. Jacobs  
H. B. Simonds  
M. W. Roberts  
T. O. Jones III  
D. W. Brock  
C. E. Dempsey

Approved for public release;  
distribution is unlimited.



SSC San Diego  
San Diego, CA 92152-5001

## EXECUTIVE SUMMARY

The ability of a modern U.S. Navy ship to perform its assigned mission is often “antenna-limited.” New antenna designs can only be accommodated onboard a U.S. Navy ship if they meet topside constraints. These constraints include (but are not limited to) size, weight, volume, moment, antenna pattern, and electromagnetic interference (EMI) characteristics. The explosive expansion of low-power wireless services in recent years has left the U.S. Navy in need of improving its signal intelligence (SIGINT) capability from surface platforms. To uniformly cover large bands of frequency, existing SIGINT antennas do not have sufficiently effective antenna aperture to yield signal levels useful for exploiting these modern signals. To further complicate matters, co-site/co-channel interference and jamming (now observed in the littoral environment) mask these signals.

An approach to these issues is to embed multiple reconfigurable antenna elements within a radome structure. Concepts for switched, reconfigurable antenna elements have existed for years. However, ordinary electrical switches are often unsuitable because the required metallic control wires perturb surrounding EM fields and suffer from EMI. The envisioned antenna concept for the Tactical SIGINT Technology (TST) Reconfigurable Aperture (RA) program calls for an array requiring a large number of switches on the antenna. Therefore, switches requiring little control power are desired. This report documents the progress of the TST program in investigating the pulsed RF performance of radio frequency (RF) microelectromechanical system (MEMS) switches, and the application of these devices to SIGINT reconfigurable antennas.

As a first phase in this project, RF pulse characterization of metal–metal contact RF MEMS switches, obtained from HRL Corporation, was performed, and a reconfigurable segmented dipole antenna incorporating these devices was designed, constructed, and tested. From the experimental RF pulse measurements presented here, it is estimated that these devices are likely to survive the voltages and currents induced in a dipole antenna from side-lobe radiation of co-site sources. Improvement in power capability would be required to survive main-lobe radiation. The HRL devices tested in this phase of the project were developmental devices. Reliability problems were an issue during the device testing. This reliability issue exemplifies the importance of the packaging and reliability work that is ongoing in the RF MEMS development community.

A reconfigurable, segmented dipole antenna was designed for improved operation in the ultra-high-frequency (UHF) range. The series of segments were connected via the HRL RF MEMS switches to change the length of the dipole antenna. Though these measurements successfully demonstrate the basic concept of a reconfigurable, segmented dipole, the resonances of this design were too narrow for the intended SIGINT application. Further study of the antenna design concluded that an unreasonably large number of switches would be required for a useful antenna using segmented dipoles.

Having verified the feasibility of using RF MEMS switches to reconfigure an antenna, but having determined that a reconfigurable antenna based on a segmented dipole-like concept was impractical, a new approach to the design of the antenna was undertaken. A hybrid design was selected where part of the antenna would consist of fixed tapered slot antennas, and part of the antenna would consist of several multiple-loop antennas intended to receive RF signals up to 100 MHz. The interconnections among the loops of these antennas would be made reconfigurable through RF MEMS switches. Commercially available RF MEMS switches were obtained from Teravicta Technologies for this development. Once again, the program was divided into two parts, RF pulse

power testing of the RF MEMS switches, and antenna design, construction, and testing. The RF pulse power testing results for the Teravicta RF MEMS switches were similar to those of the HRL devices. The intended loop-antenna design is advantageous for the implementation of RF MEMS switching because the current and voltage requirements of a switch in the loop antenna are less than in a dipole antenna.

Antenna patterns of a four-loop reconfigurable antenna and a single-loop non-reconfigurable test antenna were obtained. The shape of the received antenna pattern (azimuth versus power) for the antenna configured with four single-turn loops in parallel was similar to the single-loop test antenna, as expected. The received pattern also changed significantly for the different loop configurations. These measured antenna patterns were analyzed and additional antenna testing was recommended to achieve an understanding of the single-loop test antenna and to conduct new measurements of the reconfigurable loop antenna.

In conclusion, further study of fixed single-loop and reconfigurable multi-loop antennas is necessary to determine the benefits of the reconfigurable loop design for the intended TST application. The first step of the study would quantify the performance benefits of including the reconfigurable loop antenna with the tapered slot antenna in the hybrid antenna design. The next step of the study would focus on the design of a fixed-loop antenna, addressing the size of the loop, shielding of the loop, physical design of the feed, and impedance matching of the loop to the receiver. Based on this study, a new single-loop antenna would be constructed and tested. After experimental measurements of the single-loop antenna yield the predicted antenna pattern, the effort would proceed to the design and construction of a reconfigurable loop antenna to improve performance over the frequency range of interest. Depending on changes needed to the current reconfigurable loop antenna design, either the current RF MEMS-based switching circuit would be used in the new antenna design, or a new switching circuit would be designed and fabricated. The design study for the reconfigurable loop antenna would also consider the control line isolation requirement for the switching circuit. Based on this requirement, switches other than RF MEMS (e.g., electrically controlled PIN switches) might be considered.

# CONTENTS

<b>EXECUTIVE SUMMARY .....</b>	<b>iii</b>
<b>1. INTRODUCTION .....</b>	<b>1</b>
<b>2. RF MEMS SWITCHES .....</b>	<b>5</b>
2.1 RF MEMS SWITCH .....	5
2.2 RF MEMS SWITCHES: MECHANICAL ACTUATION SECTION .....	5
2.3 RF MEMS SWITCHES: ELECTRICAL SECTION .....	6
2.4 RF MEMS SWITCHES: OTHER FACTORS.....	7
2.5 COMPARISON WITH PIN DIODE AND FET SWITCHES.....	7
<b>3. SEGMENTED DIPOLE ANTENNA AND TESTING OF HRL RF MEMS SWITCHES.....</b>	<b>9</b>
3.1 HRL RF MEMS SWITCH CHARACTERIZATION AND TESTING .....	9
3.2 ANTENNA DESIGN, CONSTRUCTION, AND TESTING .....	12
<b>4. RECONFIGURABLE LOOP ANTENNA AND TESTING OF TERAVIDTA RF MEMS SWITCHES .....</b>	<b>19</b>
4.1 TERAVIDTA RF MEMS SWITCH CHARACTERIZATION AND TESTING .....	19
4.2 MULTIPLE-LOOP ANTENNA .....	21
4.3 FOUR-LOOP, SWITCHED ANTENNA .....	21
<b>5. CONCLUSION.....</b>	<b>33</b>
<b>APPENDICES</b>	
<b>A: HRL RF MEMS SWITCHES RF PULSE POWER TEST DATA.....</b>	<b>A-1</b>
<b>B: TERAVIDTA RF MEMS SWITCHES ISOLATION AND INSERTION DATA .....</b>	<b>B-1</b>
<b>C: TERAVIDTA RF MEMS SWITCHES RF PULSE POWER TEST DATA.....</b>	<b>C-1</b>

## Figures

3-1. HRL SL2 RF MEMS switch. Two control pads are on the right, and two RF pads are on the left. Hinges are just above the bottom contacts in the RF and control paths.....	13
3-2. HRL RF7A RF MEMS switch. RF path is on the right. Single hinge is located between two control pads on the left .....	13
3-3. HRL RF7A RF MEMS switch isolation data.....	14
3-4. HRL RF7A RF MEMS switch insertion loss data.....	14
3-5. Test setup with RF MEMS switch under test. Bottom trace on oscilloscope is gate of RF pulse and top trace shows the envelope of the RF pulse at the output of RF MEMS switch after attenuation. ....	15
3-6. RF MEMS switch test setup.....	15
3-7. HRL MEMS switch mounted for testing. ....	16

3.8. Summary: RF MEMS switch RF pulse power capability. Results from three pulse widths: 6.5, 65, and 125 $\mu$ sec are shown. Pulse width was kept constant during testing of a given individual switch. Higher power pulses could be tolerated at 6.5- $\mu$ sec pulse width than at 125- $\mu$ sec pulse width. ....	17
3-9. Segmented dipole antenna. ....	18
3-10. Measured S21 data for segmented dipole antenna. Lowest resonance shifts to lower frequency as RF MEMS switches are configured to make antenna longer. ....	18
4-1. Design of TST hybrid antenna. Lower part of antenna uses a radially sequenced array of tapered slot (TSA) elements designed to be the high-frequency section of antenna. No MEMS switches were to be used in this section of antenna. Upper, low-frequency part of antenna was designed to consist of several multiple-loop antennas. Interconnections among loops of these antennas were to be made reconfigurable through use of RF MEMS switches. ....	23
4-2. RF pulse power capability for pulse width = 6.5 $\mu$ sec. Results of RF pulse testing of Teravicta RF MEMS Device #8 and Device #11. Device #8 was also tested at two other pulse widths. RF output from Device #8 was randomly intermittent above 45 watts. However, Device #8 did not fail and functioned normally at end of the test. ....	24
4-3. RF pulse power capability for pulse width = 65 $\mu$ sec. Results of RF pulse testing of Teravicta RF MEMS Device #8 and Device #11. Note much lower power-handling capability at pulse width = 65 $\mu$ sec than at pulse width = 6.5 $\mu$ sec (Figure 4-2). ....	25
4-4. RF pulse power capability for pulse width = 125 $\mu$ sec. Results of RF pulse testing of seven Teravicta RF MEMS switches. Note reduced power-handling capability at 125 $\mu$ sec in comparison to that shown in previous two figures. Teravicta RF MEMS Device #3 failed during device characterization testing and was not RF pulse tested. ....	26
4-5. Gain maxima and minima for small-loop antenna. Antenna pattern of small-loop antenna has maximum gain parallel to plane of loops and has minimum gain perpendicular to plane of loops. ....	27
4-6. Two possible four-loop antenna configurations. Switching allows antenna to be reconfigured to better match "small-loop" criterion as the wavelength of incoming RF signal changes. At the highest frequencies, the antenna is configured to be four single-turn loops in parallel (top illustration). At low frequencies, the antenna is switched so that it becomes a single four-turn loop (bottom illustration), thereby improving gain of the antenna. Other loop combinations are possible at intermediate frequencies. ....	28
4-7. Connection board (top and bottom) design. ....	29
4-8. Connection board (top view). Six Teravicta RF MEMS switches are visible in photograph. The eight-loop connection pads (four pads across top, and four across bottom) are also visible. Scale is in inches. ....	30
4-9. Four-loop, switched antenna and control box. ....	31
A-1. Power through HRL Device #3. ....	A-2
A-2. Power through HRL Device #4 (31JUL02). ....	A-2
A-3. Power through HRL Device #4 (6AUG02). ....	A-3
A-4. Power through HRL Device #5. ....	A-3
A-5. Power through HRL Device #6. ....	A-4
A-6. Power through HRL Device #7. ....	A-4
B-1. TVM Device #2 RF1 isolation. ....	B-2
B-2. TVM Device #2 RF1 insertion loss. ....	B-2
B-3. TVM Device #2 RF2 isolation. ....	B-3

B-4. TVM Device #2 RF2 insertion loss. ....	B-3
B-5. TVM Device #4 RF1 isolation .....	B-4
B-6. TVM Device #4 RF1 insertion loss. ....	B-4
B-7. TVM Device #4 RF2 isolation .....	B-5
B-8. TVM Device #4 RF2 insertion loss. ....	B-5
B-9. TVM Device #5 RF1 isolation .....	B-6
B-10. TVM Device #5 RF1 insertion loss. ....	B-6
B-11. TVM Device #5 RF2 isolation. ....	B-7
B-12. TVM Device #5 RF2 insertion loss. ....	B-7
B-13. TVM Device #6 RF2 isolation. ....	B-8
B-14. TVM Device #6 RF2 insertion loss. ....	B-8
B-15. TVM Device #7 RF1 isolation. ....	B-9
B-16. TVM Device #7 RF1 insertion loss. ....	B-9
B-17. TVM Device #7 RF2 isolation. ....	B-10
B-18. TVM Device #7 RF2 insertion loss. ....	B-10
B-19. TVM Device #8 RF2 isolation. ....	B-11
B-20. TVM Device #8 RF2 insertion loss. ....	B-11
C-1. Power through TVM Device #1 RF2 output.....	C-2
C-2. Power through TVM Device #2 RF1 output.....	C-2
C-3. Power through TVM Device #4 RF1 output.....	C-3
C-4. Power through TVM Device #4 RF2 output.....	C-3
C-5. Power through TVM Device #5 RF1 output.....	C-4
C-6. Power through TVM Device #6 RF1 output.....	C-4
C-7. Power through TVM Device #7 RF1 output.....	C-5
C-8. Power through TVM Device #8 RF1 output (9JUL03).....	C-5
C-9. Power through TVM Device #11 RF2 output (26AUG03).....	C-6
C-10. Power through TVM Device #11 RF2 output (27AUG03).....	C-6
C-11. Power through TVM Device #8 RF1 output (28AUG03).....	C-7
C-12. Power through TVM Device #11 RF2 output (22SEP03).....	C-7
C-13. Power through TVM Device #8 RF1 output (23SEP03).....	C-8

## Tables

2-1. Comparison of RF MEMS actuation types.....	8
2-2. Comparison of RF MEMS, PIN diode, and FET switches.....	8



# 1. INTRODUCTION

The topside of a modern U.S. Navy ship carries a complex assortment of electromagnetic transmitters, receivers, and sensors, in addition to weapons and various other hardware. So many antennas are located topside that a modern U.S. Navy ship is often referred to as an “antenna farm.”

Antennas are the principal transducers for critical ship’s systems such as radar, communications, navigation, electronic warfare (EW), and information warfare (IW). The ability of a modern U.S. Navy ship to perform its assigned mission is often “antenna-limited.”

New antenna designs can only be accommodated onboard a U.S. Navy ship if they meet topside constraints. These constraints include (but are not limited to) size, weight, volume, moment, antenna pattern, and electromagnetic interference (EMI) characteristics.

Versatile, multi-functional antennas are of great interest to the U.S. Navy. These antennas could allow a single antenna to replace two or more antennas. Reducing the number of topside antennas would allow better siting and operation of the remaining required antennas, thus improving topside electromagnetic compatibility (EMC) and the performance of critical ship systems.

The explosive expansion of low-power wireless services in recent years has left the U.S. Navy in need of improving its signal intelligence (SIGINT) capability from surface platforms. To uniformly cover large bands of frequency, existing SIGINT antennas do not have sufficiently effective antenna aperture to yield signal levels useful for exploiting these modern signals. To further complicate matters, co-site/co-channel interference and jamming (now observed in the littoral environment) mask these signals.

An approach to these issues is to embed multiple reconfigurable antenna elements within a radome structure. Concepts for switched, reconfigurable antenna elements have existed for years. However, ordinary electrical switches are often unsuitable because the required metallic control wires perturb surrounding EM fields and suffer from EMI. The envisioned antenna concept for the Tactical SIGINT Technology (TST) Reconfigurable Aperture (RA) program calls for an array requiring a large number of switches on the antenna. Therefore, switches requiring little control power are desired.

Several optically controlled radio frequency (RF) switch configurations have been demonstrated that address reconfigurable antenna requirements. These devices include photoconductors, photo-transistors, photovoltaically biased field-effect transistor (PV-FET) (Sun et al., 1996), photovoltaically biased PIN diode (PV-PIN) (Sun et al., 1999), and the photo-injection PIN diode switches (PIPINS) (Jacobs et al., 2002). The performance characteristics of these optically controlled semiconductor switches are generally similar to their electrically controlled counterparts, where some performance improvement is gained by the optically isolated control. The FET-based optoelectronic (OE) switches are limited to switching only a few watts of RF power, though they have the advantage of requiring little optical control power. Compound FET switches, where the RF voltage swing is distributed across several FETs in series, enable significantly increased RF power capability, though no optically controlled version of this type of device has been reported. PV-PINs can be expected to handle more RF power than PV-FETs at the cost of increased optical power. The PV-FET and PV-PIN use indirect optical control where photovoltaic cells located near the switching elements provide charge to the switching elements via isolating chokes or resistors. The PIPINS is a

back-to-back PIN diode configuration where direct optical injection creates electron hole pairs in the intrinsic region of the PIN diodes, producing the on-state. The PIPINS requires no DC biasing. The direct optical injection eliminates the need for chokes and/or resistors that OE designs such as PV-PIN and PV-FET switches require, and the optical-to-electrical conversion efficiency is greater than that of the PV-PIN, though it is still significantly more than the PV-FET devices.

As the envisioned antenna design calls for a large number of switches, PIN-diode-type devices such as PV-PINs and PIPINS are not a good choice because they require relatively large control power. The PV-FET was considered for this study, but was eventually ruled out because FETs are susceptible to failure due to large voltage transients, which would be difficult to avoid for this application in the topside environment due to EMI. RF microelectromechanical (MEMS) switches are similar to FETs in the respect that they are voltage-controlled devices that can be configured for photovoltaic control and require little control power. However, they are very different from FETs in that they do not possess the semiconductor junctions that make FETs sensitive to voltage transients. As a result, RF MEMS switches may survive better in the presence of co-site interference. RF MEMS switches exhibit many characteristics of an “ideal” switch, including small size and exceptional high-isolation/low-insertion loss performance.

Along with the other armed services, the U.S. Navy participated in the recent (1999–2003) Defense Advanced Research Projects Agency (DARPA)-sponsored Reconfigurable Aperture (RECAP) program. The object of this program was to create new and innovative reconfigurable aperture antennas. Twelve principal investigators—including universities and private corporations—participated in the program. To realize the new reconfigurable antenna designs, new materials and devices were also investigated during the RECAP program. One of these devices was the RF MEMS switch.

Several principal investigators in the RECAP program prominently featured MEMS switches in their projects. In Raytheon’s project, “Reconfigurable Aperture—Decade Bandwidth Array,” MEMS switches were to be used in the feed of a flared notch antenna. The Georgia Tech Research Institute project, “Micro-Switched Percolating Reconfigurable Aperture,” used magnetically closed, electrostatically latched MEMS switches. The University of Colorado, Boulder project, “Programmable Aperture MEMS Interconnected Antennas Array Using Printed Circuit Technology,” proposed to use polyimide MEMS switches in their array antenna.

The University of Illinois, Urbana-Champaign project, “Mechanically Conformal and Electronically Reconfigurable Aperture Using Low Voltage MEMS and Flexible Membrane for Space-Based Radar Applications,” used hinged MEMS switches. In the Ball Aerospace and Technologies project, “Reconfigurable Aperture Program,” MEMS switches were to be integrated into a reconfigurable frequency selective surface (FSS). The BAE Systems project, “Reconfigurable Aperture,” intended to use photo-activated MEMS switches. The HRL Laboratories project, “A Novel Low-Cost Reconfigurable Aperture Antenna System,” used HRL-designed MEMS cantilever switches. HRL and its subcontractor, University of California, Los Angeles also proposed several innovative MEMS switch designs during the program.

Following RECAP, the DARPA Special Projects Office (SPO) initiated the “RF MEMS Improvement Program” in 2003. The goals of this program are to extend the lifetimes, develop inexpensive packaging techniques, and enhance the performance of X-, Ka-, and Ku- band RF MEMS devices. One major subtask of the program is to fully understand and predict failure mechanisms of RF MEMS and to generate the statistics necessary to predict the reliability of RF MEMS.

An even more recent DARPA-sponsored program in which RF MEMS switches are featured is Harsh Environment Robust Micromechanical Technology (HERMIT). Projects and principal investigators include “Self-Healing RF MEMS Switch with Liquid Gallium Contacts,” Honeywell; “Robust, Reliable RF MEMS Capacitive Switches,” Memtronics; “High Reliability, One Watt, Contact-Type RF Micromechanical Switches,” Northeastern University; “Encapsulated MEMS,” Stanford University; “Environment-Resistant Micromachined Inertial Gyroscopes,” University of Michigan; and “Bulk Titanium MEMS for Harsh Environments,” University of California, Santa Barbara.

In general, the motivation for using RF MEMS switches is the superior insertion loss and isolation performance resulting from the MEMS switches’ very small “on” resistance and very small “off” capacitance. Thus, RF MEMS switches are normally applied to high-frequency applications. Though these properties are important for the TST RA program, the motivation for using RF MEMS switches under this program also includes low control power and the possibility that these devices will be more resilient to co-site interference than FET-based switches. As evidenced by the broad base of development work in the community (summarized above), investigation of RF MEMS switch technology for SIGINT reconfigurable applications under the TST program is timely. This report documents the progress of the TST program in investigating RF MEMS pulsed RF performance, and application of these devices to SIGINT reconfigurable antennas.



## 2. RF MEMS SWITCHES

RF MEMS refers to the design and fabrication of MEMS for RF integrated circuits. RF MEMS switches are devices that use mechanical movement to achieve an open circuit or short-circuit condition in an RF transmission line or antenna (Rebeiz, 2003; Varadan, Vinoy, and Jose, 2003; De Los Santos, 2002; and Rebeiz and Muldavin, 2001).

MEMS were developed in the 1970s for various sensor applications. Laboratory versions of MEMS switches for low-frequency applications were demonstrated in the early 1980s. In 1990–1991, under DARPA support, Dr. Larry Larson at Hughes Research Labs in Malibu, California, developed the first MEMS switch specifically designed for microwave applications. Though not particularly reliable, the switch demonstrated excellent performance up to 50 GHz. This performance was better than anything that could be achieved using gallium/arsenide (GaAs) devices.

By 1995, Rockwell Science Center and Texas Instruments™ Incorporated had developed RF MEMS switches. The Rockwell switch was a metal-to-metal contact type, suitable for DC to 60-GHz applications. The Texas Instruments™ switch was a capacitive contact switch, suitable for 10- to 120-GHz applications.

By 1998, the University of Michigan, the University of California, Berkeley, Northeastern University, MIT Lincoln Labs, Columbia University, Analog Devices, Northrup Grumman, and several other companies were actively working on RF MEMS devices. More than 30 companies were working in the area by 2001.

### 2.1 RF MEMS SWITCH

An RF MEMS switch has two distinct parts: the mechanical actuation section and the electrical section.

To obtain the force required for mechanical movement in the actuation section, most MEMS switch designs use electrostatic fields, although magnetostatic, piezoelectric, thermal, or even gas-based microactuator structures have been developed. Electrostatic RF MEMS switches are available that can be used in RF circuits up to 100 GHz. RF MEMS switches have shown reliable switching for as many as 60 billion switch cycles.

As for the electrical section, the MEMS switch can be placed either in a series configuration or in a shunt configuration. The MEMS switch can also use either a metal-to-metal contact or a capacitive contact.

### 2.2 RF MEMS SWITCHES: MECHANICAL ACTUATION SECTION

Electrostatic actuation is the most common technique used in RF MEMS switches. Switches that use electrostatic actuation are small. They consume little power for control and have a short switching time relative to the other types of actuation (Table 2-1). Because RF MEMS require voltage and very low current for switch control, an electrostatic MEMS switch can be controlled remotely via an optical fiber illuminating a photovoltaic cell mounted next to the RF MEMS switch. Alternatively, high-resistance bias lines (e.g., carbon-fiber wires) can be used. Magnetostatic or thermal MEMS switches require a substantial amount of current for the switching cycle, and

therefore must be biased using low-resistance lines that may couple to surrounding microwave transmission lines.

All MEMS switch types require virtually zero power consumption once the switch is actuated. Electrostatic MEMS switches require the largest actuation voltages: 20 to 80 volts versus 3 to 5 volts for magnetostatic and thermal, and 5 to 20 volts for piezoelectric MEMS switches. However, electrostatic RF MEMS switches may be made smaller and have faster switching speeds than the other actuation types.

The two types of electrostatic RF MEMS switches are cantilever switches and membrane switches. For cantilever switches, a cantilever connected at one end is bent to create a contact at the other end. In membrane switches, a membrane is attracted to the substrate below it, thereby changing the capacitance.

Due to their reliance on the deflection/torsion properties of their constituent mechanical materials, cantilever and membrane switches have two basic drawbacks. First, isolation is limited because the deflections cannot traverse large distances. Second, because the deflections depend on the characteristics of the mechanical material, the switches are subject to environmental conditions such as temperature that may eventually cause changes in performance and degradation of switch reliability.

### **2.3 RF MEMS SWITCHES: ELECTRICAL SECTION**

Two basic electrical configurations are used in RF MEMS switch designs: the series switch and the shunt switch. The ideal series switch places an open circuit in the transmission line in the up-state when no bias voltage is applied. In the down-state, the ideal series switch causes a short circuit in the transmission line when a bias voltage is applied. An ideal series switch would have infinite isolation in the up-state position and zero insertion loss in the down-state position.

The MEMS shunt switch is placed in shunt between the transmission line and ground. Depending on the bias voltage, the shunt switch either does not affect the transmission line, or it connects the transmission line to ground. The ideal shunt switch would have zero insertion loss in the up-state when no bias is applied and infinite isolation in the down-state when bias is applied. Shunt capacitive switches are best suited for high-frequency applications ( $> 5$  GHz).

RF MEMS switches may be either metal-to-metal contact or capacitive contact types. Capacitive switches have larger contact area than metal-to-metal contact switches and therefore can handle more RF power. However, capacitive switches typically operate only at frequencies above 8 GHz due to their relatively small down-state capacitance (2 to 5 pF). Metal-to-metal contact switches are usually used in applications with frequencies below 8 GHz. TST application requirements dictate the use of series metal-to-metal contact devices.

Capacitive contact switches do not exhibit the same degree of surface stiction problems as metal-to-metal contact switches. Metal-to-metal contact switches are also subject to degradation of the metal contact. Capacitive contact switches are better suited for hot switching. However, capacitive contact MEMS switches are prone to problems associated with dielectric charging. These various problems eventually lead to performance degradation in both types of switch.

Specific failure mechanisms are complex and are different for capacitive versus metal-to-metal contact switches. Failure mechanisms depend on the RF power used and can be due to thermal stress,

dielectric breakdown, self-actuation, or critical current density issues. Other failure mechanisms include dielectric charging, surface pitting, and element hardening. Most MEMS switch failures are due to either stiction or contact wear.

## **2.4 RF MEMS SWITCHES: OTHER FACTORS**

Because they are relatively small, RF MEMS switches have little mass, and therefore they are far less sensitive to acceleration than larger switches or relays. RF MEMS switches can be manufactured on low-cost silicon or glass substrates. MEMS switches have been fabricated in GaAs and polished alumina, but they are mainly fabricated in high-resistivity silicon.

Water vapor, oxygen, hydrocarbons, or other contaminants can severely affect the operation of RF MEMS devices. This is due to the fact that contact or pull-up forces are small ( $< 500$  microNewtons), and there is not enough force to either pierce any contaminants or dielectrics that deposit or form on the contact surface, or to overcome the adhesive forces of water molecules on the contact surface.

Packaging critically affects MEMS switch reliability. Packaging of RF MEMS switches is often expensive because it requires hermetic or near-hermetic conditions. A non-hermetic package is inexpensive (20 to 50 cents per unit). However, hermetic packaging requires high temperatures and very smooth surfaces and is usually expensive (\$2 to \$50 per unit). Low-cost, wafer-scale manufacturing techniques can be used to produce the MEMS switches, but packaging costs per switch often represent up to 95% of the MEMS device cost.

Current application areas for RF MEMS switches are in radar systems, satellite communications systems, and wireless and other telecommunications systems. MEMS switches have been used in phased arrays, reconfigurable apertures, resonators, micro-mirrors, inertial sensors, and in low-power and low-noise oscillators and amplifiers. Other applications of RF MEMS switches have been in high-isolation switch circuits, low-loss phase shifters, tunable antennas, and low-loss tunable circuits such as filters and matching networks.

Though MEMS switches have become commonly used for commercial applications (e.g., in automotive safety systems), because of the degradation and packaging issues, use of RF MEMS switches remains largely limited to development and prototype systems. Even with many companies developing RF MEMS switches, few devices are available commercially.

## **2.5 COMPARISON WITH PIN DIODE AND FET SWITCHES**

RF MEMS switches have certain advantages over PIN diode or FET switches (Table 2-2). RF MEMS switches exhibit very small control power dissipation with respect to PIN diode switches. Typical electrostatic RF MEMS switches require 20 to 80 volts actuation, but draw very little current. Consequently, power consumption in these switches is similar to FET switches.

MEMS switches, with their extremely low on-state resistance and off-state capacitance (MEMS series switches), and their very high capacitance ratio (MEMS capacitance contact switches), offer superior performance compared to the solid-state switches in low- to medium-power applications. For a series switch, the figure of merit determining the insertion loss/isolation performance is the cutoff frequency,  $f_c = 1 / (2\pi C_{off} R_{on})$ . RF MEMS switches have superior cutoff frequency, 30 to 40 times higher than can be obtained with GaAs technology (for GaAs or InP diodes,  $f_c \approx 2$  THz; for RF MEMS,  $f_c$  can be up to 80 THz). Thus, RF MEMS switches exhibit higher isolation and lower

insertion loss than either PIN diode or FET switches, which makes them particularly attractive for high-frequency applications.

RF MEMS switches have certain disadvantages with respect to FET or PIN diode switches. RF MEMS switches have slower switching speed. The switching speed of RF MEMS switches is typically tens to a few hundred  $\mu\text{sec}$ . The switching speed of PIN diode or FET switches is tens of nanoseconds. RF MEMS switches also have an order of magnitude lower power-handling capability than PIN diode switches.

As noted above, RF MEMS switches also have reliability issues and packaging problems. The current maximum number of switching cycles before failure of research devices is 60 billion cycles.

Table 2-1. Comparison of RF MEMS actuation types (Rebeiz, 2003).

	Size	Voltage (V)	Current (mA)	Switching Time ( $\mu\text{sec}$ )
Electrostatic	Small	20 to 80	0	~ 200
Magnetostatic	Medium	~ 5	~ 150	~ 1,000
Piezoelectric	Medium	10 to 20	0	~ 500
Thermal	Large	~ 5	~ 100	1,000 to 10,000

Table 2-2. Comparison of RF MEMS, PIN diode, and FET switches (Rebeiz, 2003).

	RF MEMS	PIN Diode	FET
Control voltage (V)	20 - 80	~ 5	~ 5
Control current (mA)	0	~ 20	0
Control power (mW)	~ 0.1	10 - 100	~ 0.1
Cutoff frequency (THz)	80	4	2
Isolation (1 - 40 GHz)	Very High	High/Medium	Medium/Low
Insertion loss (dB)	~ 0.2	~ 1.2	~ 2.5
Switching time	~ 200 $\mu\text{s}$	~ 100 ns	~ 100 ns

### 3. SEGMENTED DIPOLE ANTENNA AND TESTING OF HRL RF MEMS SWITCHES

The first phase of this project was divided into two parts. In the first part, the RF pulse characterization of metal–metal contact RF MEMS switches obtained from HRL Corporation was performed. In the second part, a reconfigurable, segmented dipole antenna incorporating these devices was designed, constructed, and tested.

#### 3.1 HRL RF MEMS SWITCH CHARACTERIZATION AND TESTING

Approximately 30 RF MEMS switches were obtained from the HRL Corporation. These metal-to-metal contact series RF MEMS switches included two different types. The first type, designated RF7A, had two-contacts in the RF path, and the second type, designated SL2, had a single-contact in the RF path. Figure 3-1 shows an HRL SL2 RF MEMS switch. In the figure, the two control pads are on the right, and the two RF pads are on the left. Just above the bottom contacts in the RF and control path are the hinges. Figure 3-2 shows an HRL RF7A RF MEMS switch. In this figure, the RF path is on the right. The single hinge is located between the two control pads on the left.

MEMS switch characteristics were measured using a Hewlett Packard® 8753 network analyzer. Isolation and insertion loss values for several RF7A two-contact switches are shown in Figures 3-3 and 3-4, respectively. These isolation measurements were actually limited by the device mounting and test fixture, not the true off-capacitance of the device. The mounting method used was similar to that to be used in the antenna design, and as isolation at 3 GHz is more than adequate for the intended application, the isolation limitation was not a concern. Measurements of more carefully mounted devices yielded greater than 40-dB isolation at 3 GHz.

An analysis of the electromagnetic fields generated by shipboard radar and communications transmitters was completed as part of the TST effort.\* It was determined that shipboard pulsed RF systems, in particular, the SPS-49 and SPY-1 radars, could cause the RF MEMS switches mounted on the antenna to fail as a result of current and/or voltage transients. As a dipole takes advantage of resonance conditions and is connected to a relatively low impedance, current and voltage transients as a function of position on the antenna must be considered. This analysis considered the voltages and the currents induced in a segmented dipole antenna from these sources.

Based on this analysis, RF testing of the MEMS switches reproduced the shipboard environment in which the final antenna would be used. The MEMS switches were tested to determine their functionality in the presence of high-power RF pulses.

Figure 3-5 shows the test setup used in the RF pulse testing. The photograph was taken while a MEMS switch was being tested. Note that on the oscilloscope, the bottom trace is the gate of the RF pulse, and the top trace shows the envelope of the RF pulse at the output of the RF MEMS switch after attenuation. Figure 3-6 shows a schematic drawing of the test setup. The equipment used in the testing included a Hewlett Packard® 8642B signal generator, a Hewlett Packard® 8130A pulse generator, an Ophir RF power amplifier (rear view in Figure 3-5), a Channel Microwave Corporation BV393 circulator with attached 40-watt terminator, a Hewlett Packard® 6211A power supply, a

---

\* David W. Brock. 2002 (May 24). "RF Analysis for Reconfigurable Antenna." SPAWAR Systems Center, San Diego (Code 2738), San Diego, CA.

30-dB attenuator and a 20-dB attenuator in series, and a LeCroy® oscilloscope.

Figure 3-7 shows an HRL RF MEMS switch in test configuration. The MEMS switch (left center in the figure) is mounted on an aluminum nitrite substrate and is wire-bonded to two 50-ohm transmission lines (left, above and below the switch). The two other wire-bonds (extending horizontally across the figure) are used to bring the DC voltage, via current-limiting resistors, to the control pads of the MEMS switch. Though this figure shows an RF7A two-contact switch, all the high-power RF pulse measurements described were performed on SL2-type single-contact switches because the single-contact type switches have higher power capability than the two-contact devices.

In the initial set of RF pulse tests, a given MEMS switch was subjected in steps to increasing pulse power. Each power step was applied to the MEMS switch for 2 minutes. The switch was then tested for proper function before moving to the next higher power step. This procedure was continued until the switch failed. Only “cold-switching” was used during the testing.

The pulse generator was set to output pulses with a period of 3.51 milliseconds. The leading and trailing edges of each pulse were set to 700 picoseconds, and the pulse height was 3 volts from a 0-volt DC baseline. The pulse width was set to one of the three values: 6.5, 65, or 125  $\mu$ sec. The pulse width was kept constant at one of these values throughout the testing of an individual switch. The signal generator was set to output 375 MHz in pulse mode.

The test procedure began by applying 50 volts DC across the control inputs of the HRL MEMS switch to cause the switch to close (“cold-switching”). RF pulses were then applied to the RF input of the switch for 2 minutes. The RF output from the switch was monitored continuously on an oscilloscope during the 2 minutes.

Next, the RF power was turned off. The control voltage to the switch was then set to 0 volts, which caused the switch to open. The RF pulse signal was again applied to the RF input of the now open switch. The RF signal was applied for 1 minute. The RF output from the switch was again monitored on an oscilloscope during the 1-minute, open-switch test. If the switch passed the 2-minute “on” and 1-minute “off” RF pulse tests, the RF power was increased, and the procedure was repeated.

Appendix A shows the results of the RF pulse testing of the HRL RF MEMS switches. The power (ordinate) values in the Appendix A figures show the values of the power that passed through the MEMS switch during an RF pulse. The higher value is the power that passed through the switch during the 2-minute, closed-switch test. The lower value is the power that passed through the switch during the subsequent 1-minute, open-switch test. Note that the greater than 40-dB isolation at 375 MHz is consistent with the isolation data in Figure 3-3.

All switch failures during the RF pulse testing were due to the switch “shorting.” In all cases, the indication of failure was that the switch passed full power at the start of a 1-minute, open-switch test.

Data from the RF pulse tests are summarized in Figure 3-8. The figure shows the power-handling capability of the MEMS switches as a function of the pulse width of the RF pulsed input signal. The pulse width was kept constant during the testing of a given individual switch. The figure shows that the power-handling capability of the RF MEMS switches that were tested was a function of the pulse width used in the test. Higher power pulses could be tolerated at 6.5- $\mu$ sec pulse width than at 125- $\mu$ sec pulse width. At the intermediate pulse width of 65  $\mu$ sec, the tested device failed at lower power than the devices tested using 125- $\mu$ sec pulse width. Therefore, more statistics are needed for a conclusive

result. The results suggest that decreasing pulse widths to the order of microseconds allows these devices to survive higher pulsed powers. The device failure mode is believed to be localized heating at the metal-metal contact. A detailed study of thermal dissipation from the contact area of these devices would provide a better understanding of the experimental results.

In addition to the 2-minute RF pulse testing, one MEMS switch (HRL Device #4) was subjected to a sequence of fixed-power pulses of increasing duration. The same test setup (Figure 3-6) and equipment settings were used in the time duration tests as had been used in the 2-minute tests. The pulse width from the HP8130A pulse generator was set to 125  $\mu$ sec for all the time duration tests. Three sets of time duration measurements were made. Only “cold-switching” was used during the testing. In the first set, a 37.8-dBm RF signal was applied to the MEMS switch continuously for 2 minutes. The RF power was then removed, and the switch was tested to verify that it still functioned correctly. The same RF signal was then reapplied to the switch for 4 minutes. The RF power was again removed, and the switch was again tested for proper functionality. This procedure was repeated in time steps, increasing by 2 minutes for each step. In the final step, the RF pulsed signal was continuously applied to the HRL MEMS switch for 20 minutes. The switch functioned properly when tested after each step.

In the second set of continuous time duration steps, a 40-dBm pulsed RF signal was applied to the MEMS switch. The RF signal was initially applied to the switch for 5 minutes. The RF power was then removed, and the switch was tested to verify that it functioned properly. This procedure of application of the 40-dBm pulsed RF signal, followed by functionality testing, was subsequently repeated for time steps of 10, 15, 20, 30, 45, and 60 minutes. The MEMS switch functioned correctly when tested after each time-step.

For the third set of continuous time duration steps, a 40.7-dBm pulsed RF signal was applied to the MEMS switch. The procedure of continuous application of the pulsed RF signal to the MEMS switch, followed by functionality testing, was performed for time steps of 5, 10, 20, 30, 45, and 60 minutes. The MEMS switch functioned correctly when tested after each time-step.

From the experimental RF pulse measurements, it is estimated that these devices are likely to survive the voltages and currents induced in a dipole antenna from side-lobe radiation of co-site sources. Improvement in power capability would be required to survive main-lobe radiation.

The HRL devices tested were developmental devices. The devices were not hermetically sealed or packaged; rather, they were in chip form. Reliability problems were an issue during the testing of these devices. This reliability issue exemplifies the importance of the packaging and reliability work that is ongoing in the RF MEMS development community.

### 3.2 ANTENNA DESIGN, CONSTRUCTION, AND TESTING

A reconfigurable, segmented dipole antenna was designed for improved operation in the UHF frequency range. The series of segments were connected via the RF MEMS switches to change the length of the dipole antenna. Figure 3-9 shows the antenna.

Four HRL RF MEMS switches were used to construct the antenna. These switches were selected and their isolation and insertion loss values were tested before insertion into the antenna. As an alternative to optical control, the control voltages to the switches were made via high-resistance (1 k $\Omega$ /cm) carbon-fiber wire. Previous antenna measurements had shown that this resistive wire did not perturb the received antenna pattern. Use of high-resistance wire is possible because of the high-impedance control of the RF MEMS switches.

Return loss measurements were performed on the reconfigurable, segmented dipole antenna. Figure 3-10 shows the results. As expected, as the switches are configured to make the antenna longer, the lowest resonance shifts to lower frequency. Though these measurements successfully demonstrate the basic concept of a reconfigurable, segmented dipole, the resonances of this design are too narrow for the intended SIGINT application. Further study of the antenna design showed that an unreasonably large number of switches would be required for a useful antenna using segmented dipoles.

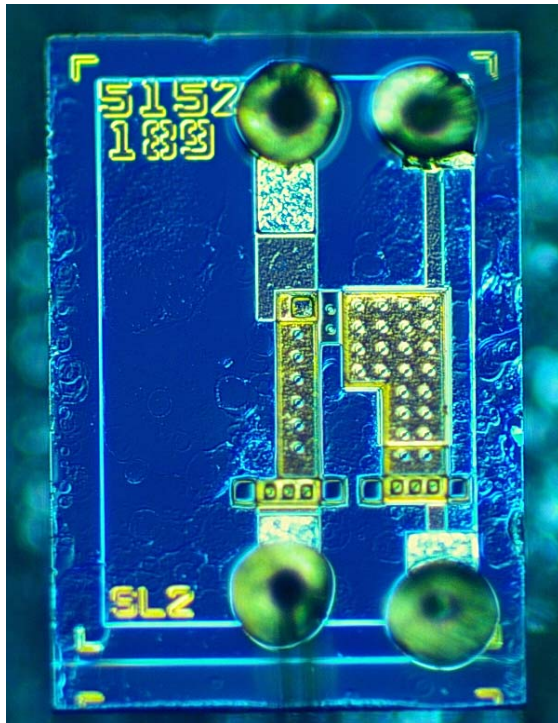


Figure 3-1. HRL SL2 RF MEMS switch. Two control pads are on the right, and the two RF pads are on the left. Hinges are just above the bottom contacts in the RF and control paths.

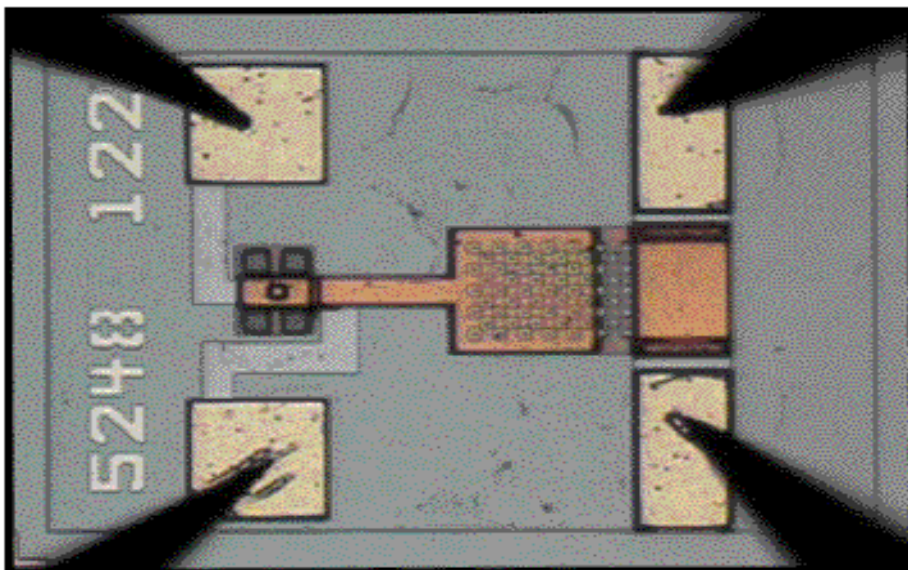


Figure 3-2. HRL RF7A RF MEMS switch. RF path is on the right. Single hinge is located between two control pads on the left.

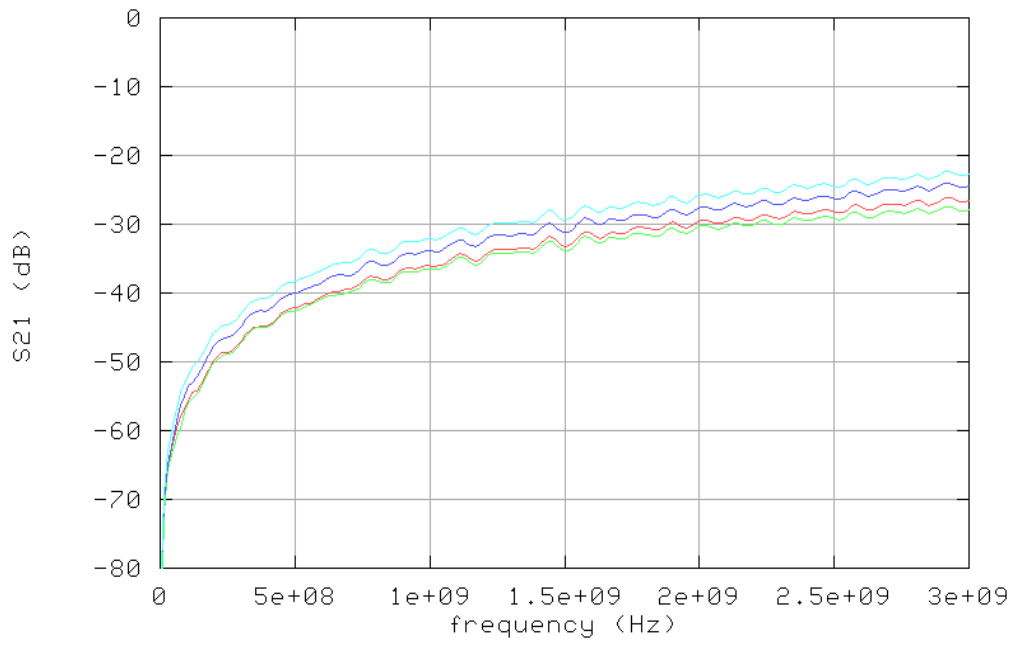


Figure 3-3. HRL RF7A RF MEMS switch isolation data.

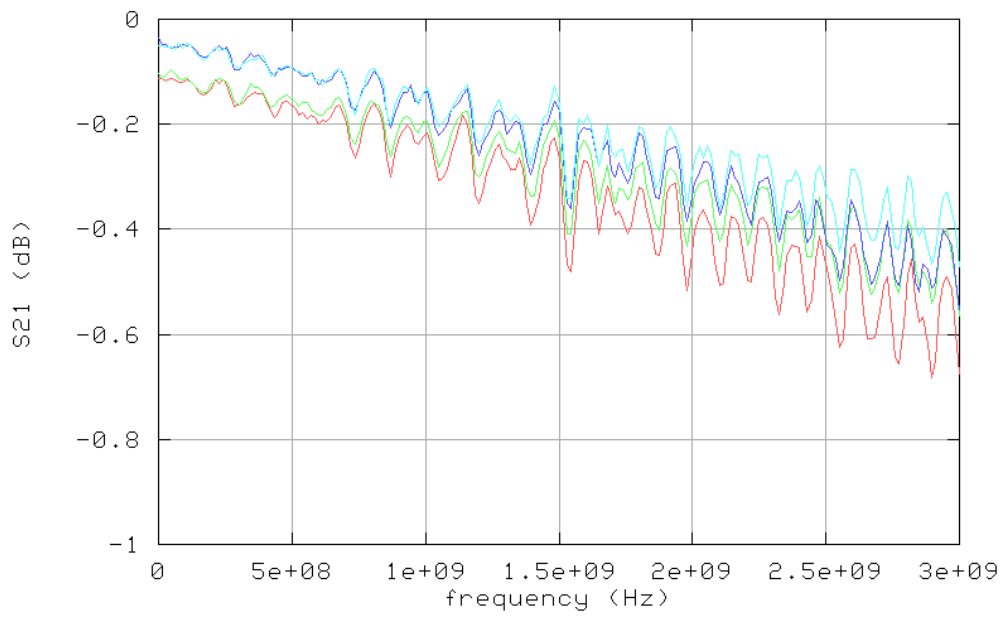


Figure 3-4. HRL RF7A RF MEMS switch insertion loss data.

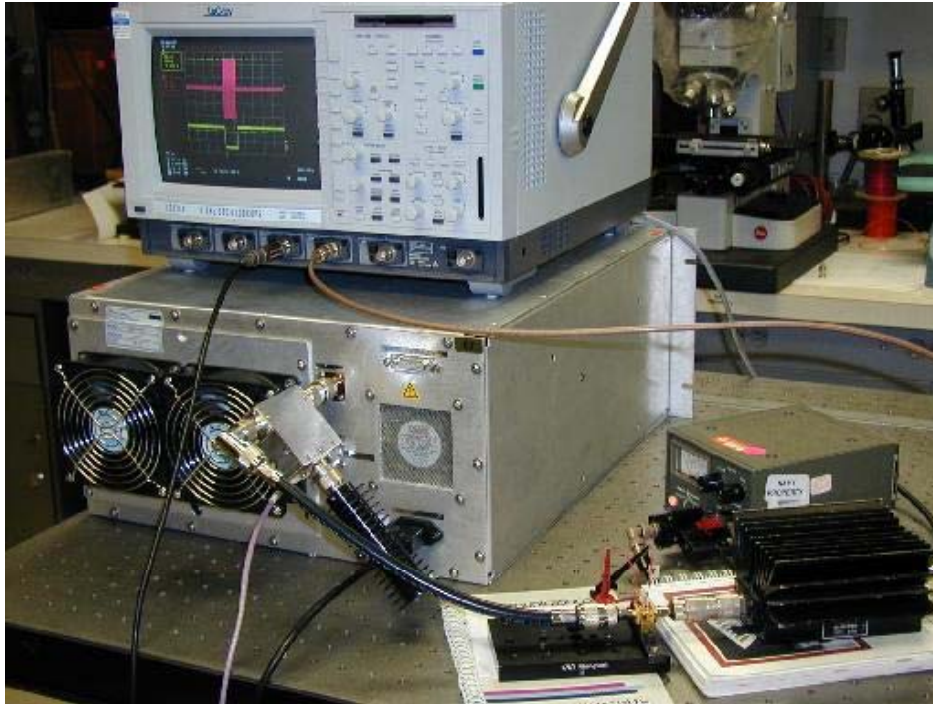


Figure 3-5. Test setup with RF MEMS switch under test. Bottom trace on oscilloscope is gate of RF pulse and top trace shows the envelope of the RF pulse at output of RF MEMS switch after attenuation.

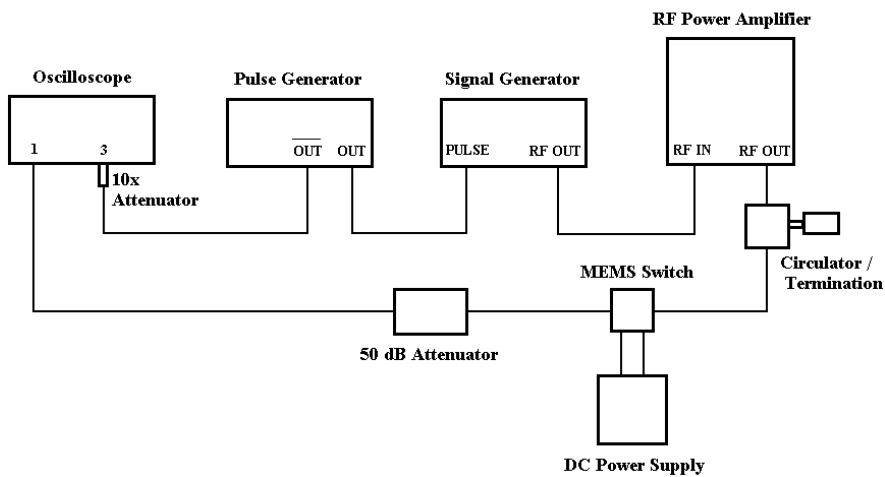


Figure 3-6. RF MEMS switch test setup.

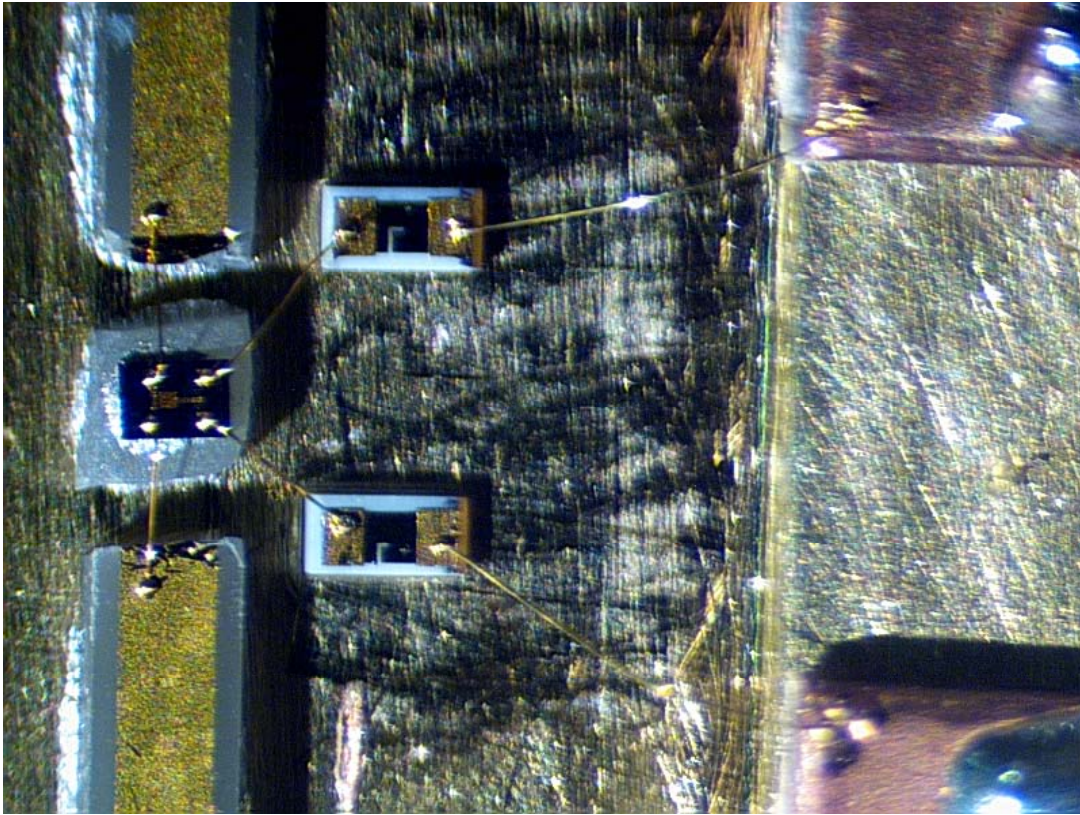


Figure 3-7. HRL MEMS switch mounted for testing.

The RF7A two-contact RF MEMS switch (left center in Figure 3-7) is mounted on an aluminum nitride substrate and is wire-bonded to two 50-ohm transmission lines (left, above and below the switch). The two other wire-bonds (extending horizontally across Figure 3-7) are used to connect DC voltage, via current limiting resistors, to the control pads of the MEMS switch.

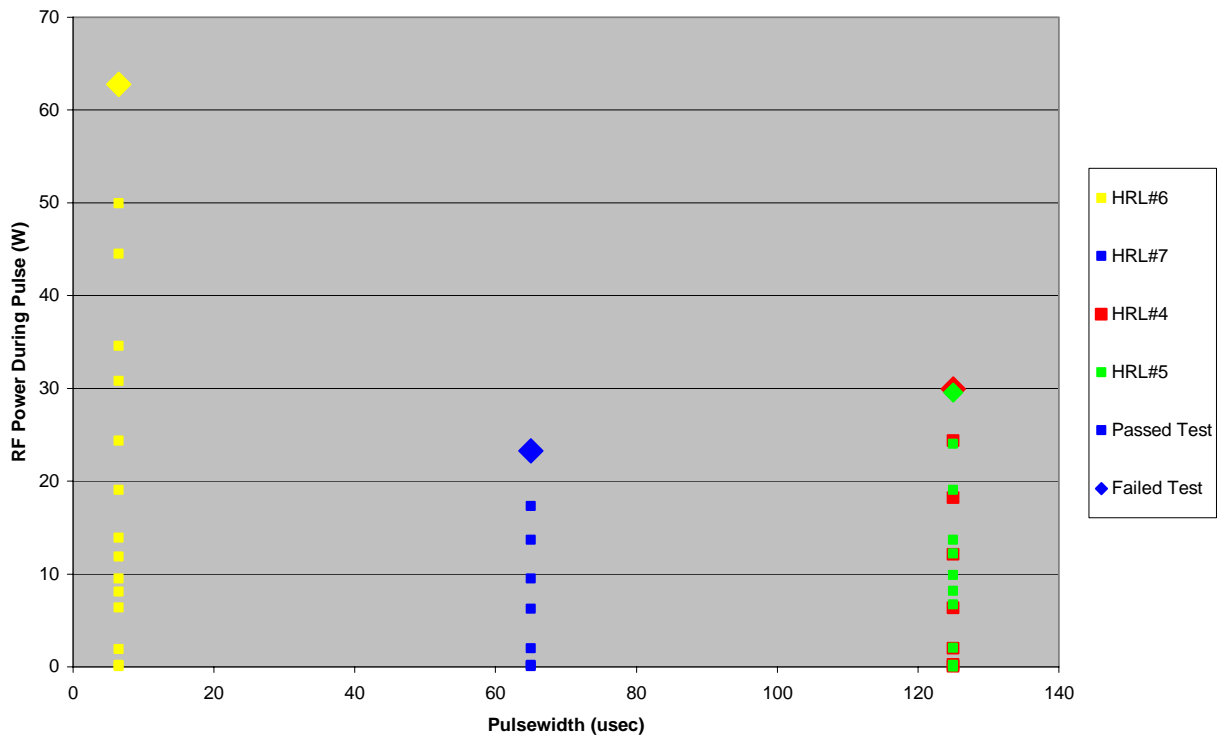


Figure 3-8. Summary: RF MEMS switch RF pulse power capability. Results from three pulse widths: 6.5, 65, and 125  $\mu$ sec are shown. Pulse width was kept constant during testing of a given individual switch. Higher power pulses could be tolerated at 6.5- $\mu$ sec pulse width than at 125- $\mu$ sec pulse width.

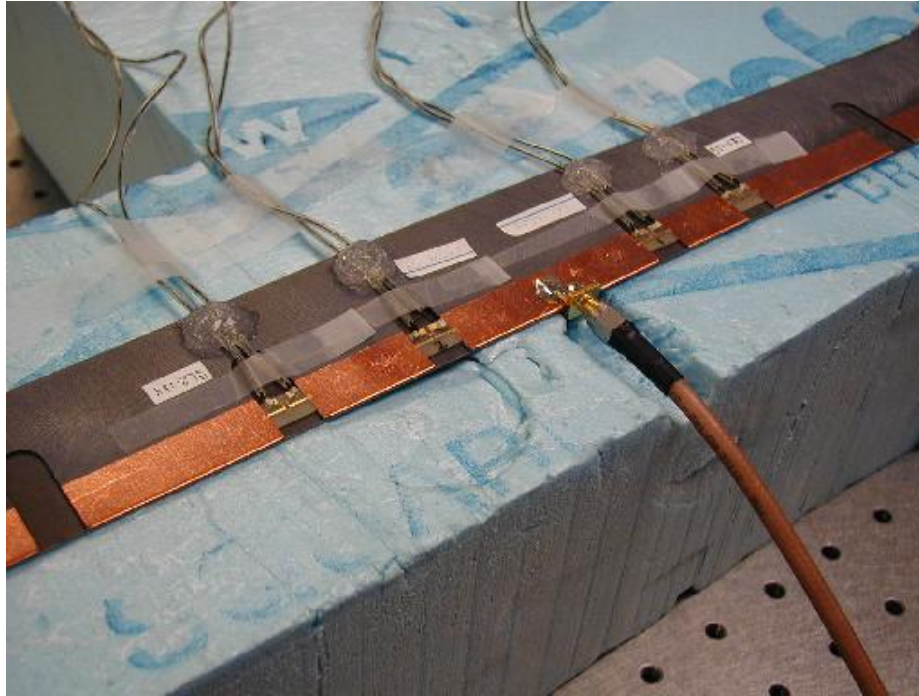


Figure 3-9. Segmented dipole antenna.

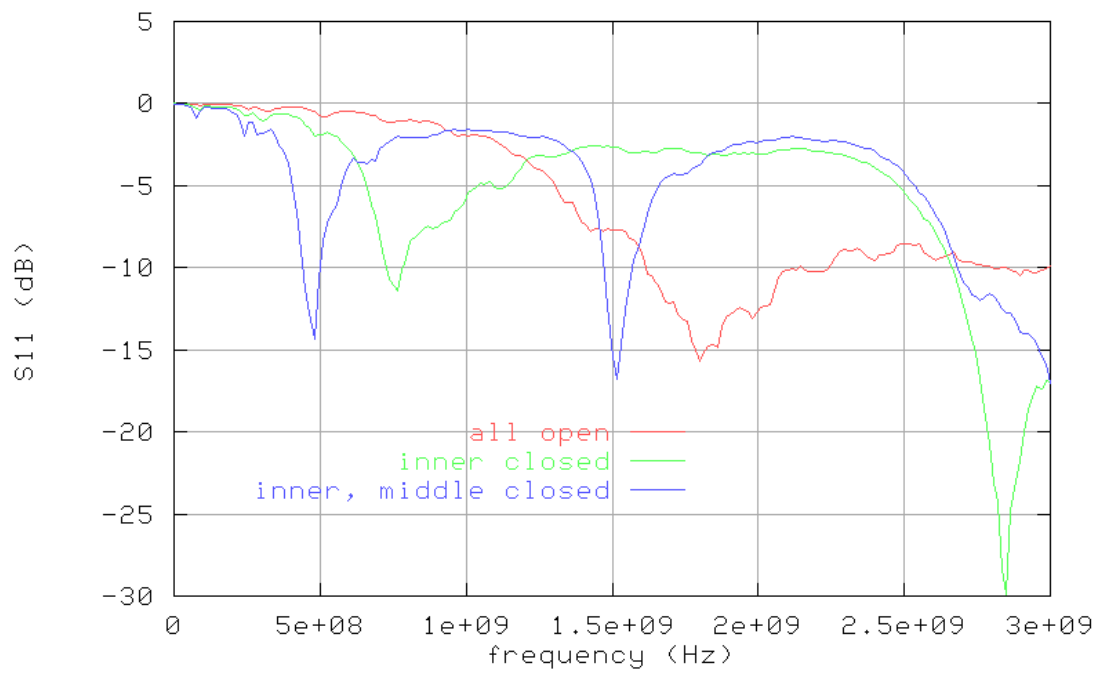


Figure 3-10. Measured S21 data for segmented dipole antenna. Lowest resonance shifts to lower frequency as RF MEMS switches are configured to make antenna longer.

## 4. RECONFIGURABLE LOOP ANTENNA AND TESTING OF TERAVIDTA RF MEMS SWITCHES

Having verified the feasibility of using RF MEMS switches to reconfigure an antenna, but having determined that a reconfigurable antenna based on a segmented dipole-like concept was impractical, a new approach to the antenna design was initiated. A hybrid design was selected (Figure 4-1). The lower part of the antenna uses a radially sequenced array of tapered slot elements designed to be the high-frequency section of the antenna. No MEMS switches were to be used in this section of the antenna.

The upper, low-frequency part of the antenna was designed to consist of several multiple-loop antennas. The interconnections among the loops of these antennas were to be made reconfigurable through RF MEMS switches. This multiple-loop section of the antenna was intended to receive RF signals up to 100 MHz.

Note that the use of RF MEMS switches in the low-frequency section of the antenna is unusual. Because of their high  $f_c$ , RF MEMS switches are typically used for high-frequency applications (e.g., up to 40 GHz). However, the metal-to-metal contact RF MEMS switches used for this project work at frequencies down to DC. Low control power and survivability in the topside EMI environment remain motivations for using RF MEMS switches for this application.

Once again, the program was divided into two parts. The first part consisted of RF MEMS switch testing and evaluation. The second part included antenna design, construction, and testing.

### 4.1 TERAVIDTA RF MEMS SWITCH CHARACTERIZATION AND TESTING

Near the start of this phase of the project, Teravicta Technologies substantially lowered the cost of their RF MEMS switches. Unlike the HRL developmental devices used in the first phase of the project, the Teravicta devices were commercial off-the-shelf (COTS), hermetically sealed, surface-mount devices. The Teravicta devices were the only COTS RF MEMS switches available. Twenty-four DKM812 model SPDT (1 x 2) Teravicta RF MEMS switches were purchased. These devices are specified to have DC to 6 GHz bandwidth, with an RF continuous wave (cw) maximum power of 3 watts.

Isolation and insertion loss data of each Teravicta MEMS switch was measured before the start of RF power testing. Appendix B shows the data for several of the switches as measured with a Hewlett Packard® 8753 network analyzer. These data indicate that the devices consistently meet specified performance. The insertion loss and particularly the isolation performance of these devices are relatively poor compared to state-of-the-art RF MEMS devices, but for the low-frequency application considered here, these devices easily meet the “on/off” requirement.

Pulsed testing and cw RF testing of the Teravicta MEMS switches were performed. The same test setup and the same test equipment were used to test the Teravicta MEMS switches as had been used in testing the HRL MEMS switches.

The following procedure was used for the cw RF testing. First, 60-volts DC was applied to the control input to close the MEMS switch contacts. Next, a cw RF signal (2 watts) was applied to the RF input of the switch for 15 seconds.

The RF power was then removed, and 0-volts DC was applied to the control input to cause the switch contacts to open. The cw RF signal was then reapplied to the RF input of the MEMS switch for 15 seconds. The output from the switch was observed on an oscilloscope during the time the RF signal was applied to the MEMS switch. All Teravicta RF MEMS switches tested in this manner passed the cw RF tests.

RF pulse testing of the Teravicta RF MEMS switches was also conducted. The testing procedure was similar to that used for the HRL devices described in the previous section. The testing consisted of applying sequences of RF pulses of increasing power to the switch under test.

Three different pulse widths, 6.5, 65, and 125  $\mu$ sec, with pulse repetition period of 3.51 milliseconds, were used during the RF pulse testing. The pulse width was kept constant during a given RF pulse test, but some of the Teravicta RF MEMS switches were tested more than once using different pulse width values.

The following procedure was used for the test. First, 60-volts DC was applied to the control inputs of the MEMS switch to cause the switch to close (“cold-switching”). RF pulses were then applied to the RF input of the switch for 2 minutes. The RF output from the switch was monitored continuously on an oscilloscope throughout the 2-minute test.

Next, the RF power was turned off, and the control voltage to the switch was set to 0 volts, which caused the switch to open. The RF pulse signal was then applied to the RF input for a 1 minute. The RF output from the switch was again monitored on an oscilloscope during the 1-minute, open-switch test. If the switch passed the RF pulse tests, the RF power was increased, and the procedure was repeated.

Appendix C shows the results of the pulse testing of the Teravicta RF MEMS switches. The higher power values in the Appendix C figures are those recorded during the 2-minute, closed-switch test. The lower power values are those observed during the subsequent 1-minute, open-switch test. In both cases, the power value shown is the power during the RF pulse.

Figures 4-2, 4-3, and 4-4 show a summary of the RF pulse testing. As was the case for the HRL RF MEMS switches tested previously, the power-handling capability of the Teravicta RF MEMS switches was a function of the pulse width used in the RF pulse test. The RF MEMS switches tolerated high-power pulses ( $\sim$  70 watts) when the pulse width was 6.5  $\mu$ sec (Figure 4-2). The power-handling capability of the MEMS switches was somewhat higher when the pulse width was 65  $\mu$ sec (Figure 4-3) than when the pulse width was 125  $\mu$ sec (Figure 4-4). However, both measurements were well below the power-handling capability exhibited when the pulse width was 6.5  $\mu$ sec.

As described in the next section, at their design frequency, loop antennas operate below resonance. They sense the magnetic field and provide a voltage proportional to the magnetic field to a high-impedance amplifier or meter. Therefore, for the receive signals of interest, resonant nodes (which could cause currents and voltage differences that could damage the RF MEMS switches) are not generated in the antenna. But these resonant conditions may occur for higher frequency co-site sources, so switch survivability in the presence of high-power RF pulses remains an issue.

## 4.2 MULTIPLE-LOOP ANTENNA

The design of the upper, low-frequency part of the hybrid antenna used “small-loop” antenna theory (Carr, 1999). By definition, a small-loop antenna has an overall wire length that is no greater than 10% of the RF wavelength (Kraus, 1988). In practice, even when this length criterion is somewhat exceeded, the loop antenna still behaves substantially as a “small” loop.

A small-loop antenna differs from a large-loop antenna in that the current distribution in the small loop antenna is uniform. In a large-loop antenna, current nodes and anti-nodes are at points around the loop. A small-loop antenna is less sensitive to local EMI than a large-loop antenna because the small-loop antenna responds primarily to the magnetic field of a transverse electromagnetic (TEM) wave. This response makes a small-loop antenna attractive for use in the high-EMI environment of the topside of a modern U.S. Navy ship.

As shown in Figure 4-5, the antenna pattern of a small-loop antenna has maximum gain parallel to the plane of the loops and has minimum gain perpendicular to the plane of the loops. This pattern is nearly opposite to the pattern of a large-loop antenna.

The equation for the output voltage of an untuned loop antenna is provided by Carr (1999):

$$V = [ 2 \pi A N E \cos(\theta) ] / \lambda.$$

The equation for the output voltage of a tuned loop antenna is also provided by Carr (1999):

$$V = [ 2 \pi A N Q E \cos(\theta) ] / \lambda.$$

In the above equations,  $V$  is the output voltage (volts),  $A$  is the area enclosed by the loop (square meters),  $N$  is the number of turns in the loop,  $Q$  is the loaded figure of merit of the tuned circuit,  $E$  is the strength of the incoming RF signal (volts/meter),  $\theta$  is the angle between the plane of the loop and the Poynting vector of the incoming RF signal, and  $\lambda$  is the wavelength of the incoming RF signal (meters).

## 4.3 FOUR-LOOP, SWITCHED ANTENNA

As part of the design process of the low-frequency loop section of the hybrid antenna, it was decided to construct and test a four-loop, switched antenna as a precursor to the reconfigurable multi-loop antenna array. The loops of the four-loop antenna were to be interconnected via a connection board that incorporated RF MEMS switches. The RF MEMS switches on the connection board reconfigured the four-loop antenna according to control voltages sent to the connection board from a control switch box.

To provide a high impedance at the loop antenna feed, a 16:1 transformer was placed between the reconfigurable loop antenna output and the 50-ohm impedance antenna feed coax, which then connected to the spectrum analyzer (50-ohm input impedance). In this configuration the center conductor of the feed coax was connected to one side of the transformer and the feed coax ground was connected to the other side of the transformer.

Figure 4-6 shows two possible reconfiguration patterns of the four-loop, switched antenna. The switching allows the antenna to be reconfigured to better match the “small-loop” criterion as the wavelength of the incoming RF signal changes. At the highest frequencies, the antenna is configured

to be four, single-turn loops in parallel. At low frequencies, the antenna is switched so that it becomes a single, four-turn loop, thereby improving the antenna gain. Other loop combinations are possible at intermediate frequencies.

Figure 4-7 shows the design for the connection board (front and back). Figure 4-8 shows the completed connection board. Figure 4-9 shows the four-loop, switched antenna with its control box. The dimensions of each loop are 15 inches x 15 inches.

The control voltages from the control box were sent to the connection board at the antenna via high-resistance (1 k $\Omega$ /cm) carbon-fiber wire so as not to perturb the received antenna pattern. Use of high-resistance wire is permitted because of the high-impedance control of the RF MEMS switches. As a consequence, there was essentially no voltage drop across the 2-meter-long, high-resistance control lines.

Antenna testing is ongoing. Antenna patterns of the four-loop, reconfigurable antenna and a single-loop, non-reconfigurable test antenna have been obtained. The shape of the received antenna pattern (azimuth versus power) for the antenna configured with four single-turn loops in parallel is similar to that of the single-loop test antenna, as expected. The received pattern also changed significantly for the different loop configurations. These measured antenna patterns have been analyzed, and additional antenna testing has been recommended to achieve an understanding of the single-loop test antenna and to perform new measurements of the reconfigurable loop antenna.

Further recommendations include the following:

1. Reduce the size of the loops to be more conservative in meeting the small-loop antenna requirement.
2. Modify the feed to the antenna by using a coax connected to each side of the output transformer.
3. Use a 1-GHz digital oscilloscope to provide high-input impedance differential measurement.
4. Remove the transformer between the antenna and the feed.
5. Procure a high-input impedance differential amplifier to place between the antenna and the measurement system.
6. Investigate proper shielding of the antenna loops.

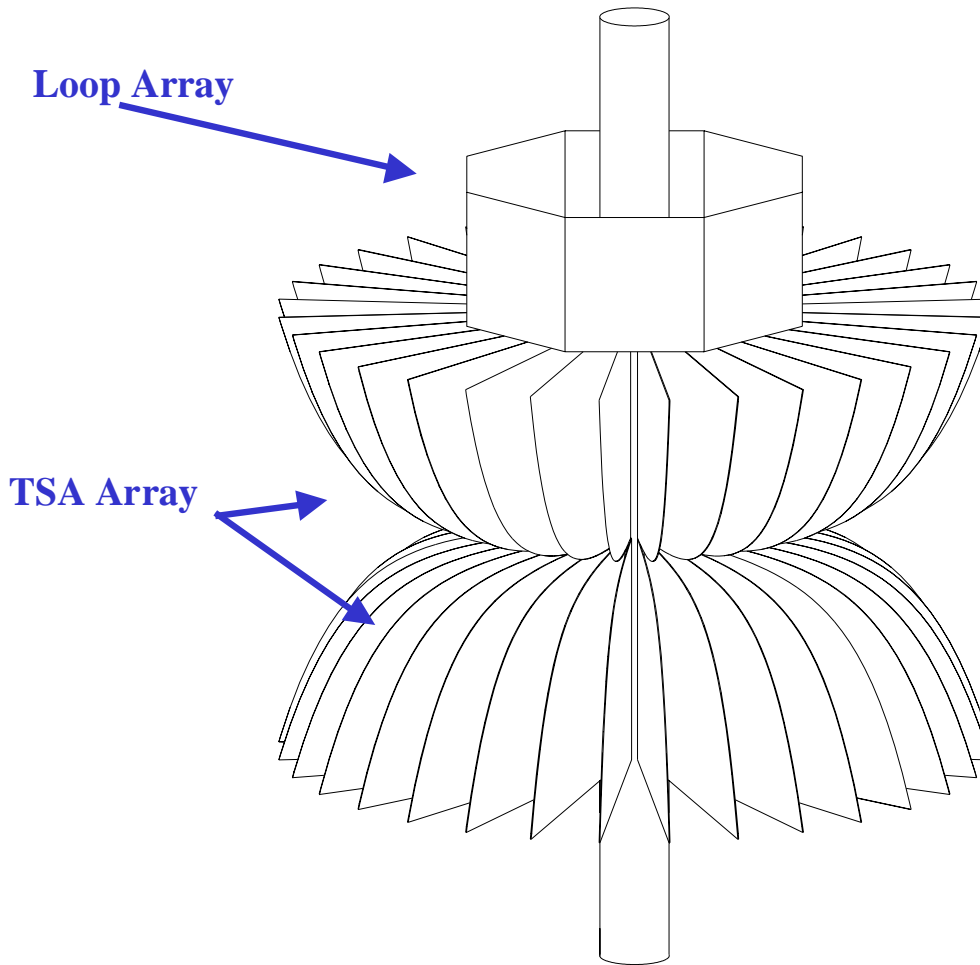


Figure 4-1. Design of TST hybrid antenna. Lower part of antenna uses a radially sequenced array of tapered slot elements designed to be the high-frequency section of antenna. No MEMS switches were to be used in this section of antenna. Upper, low-frequency part of antenna was designed to consist of several multiple-loop antennas. Interconnections among loops of these antennas were to be made reconfigurable through use of RF MEMS switches.

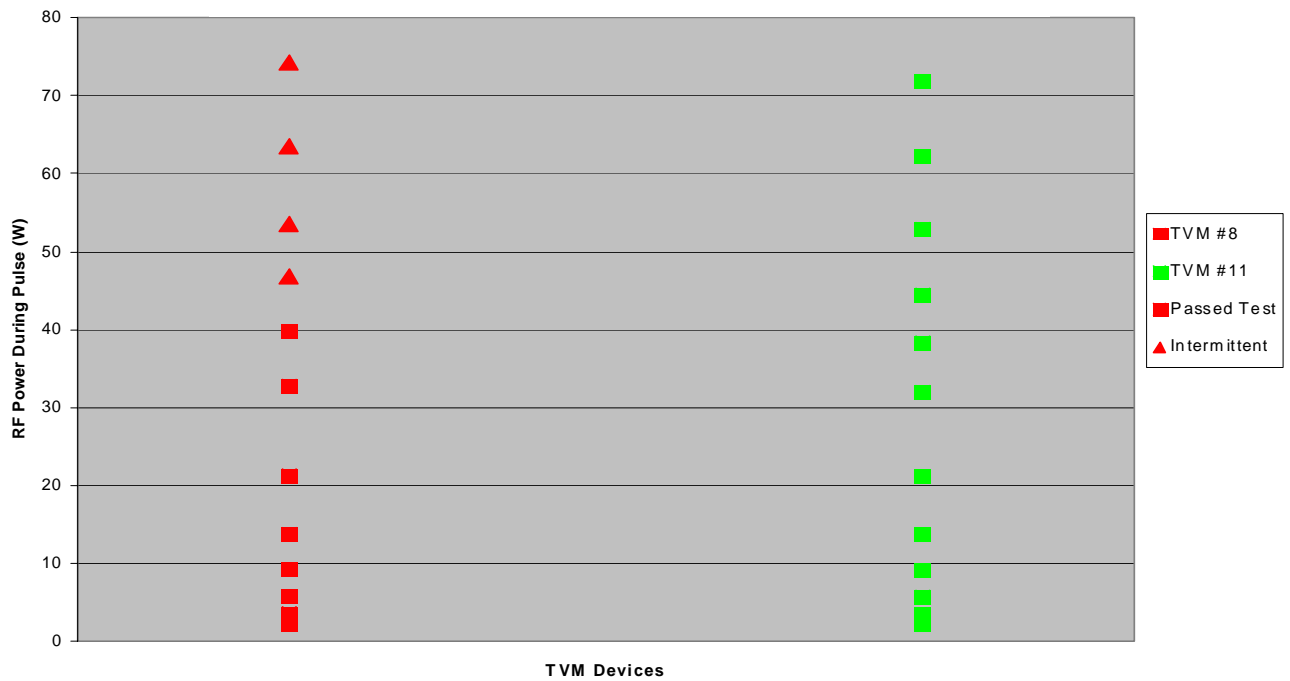


Figure 4-2. RF pulse power capability for pulse width = 6.5  $\mu$ sec. Results of RF pulse testing of Teravicta RF MEMS Device #8 and Device #11. Device #8 was also tested at two other pulse widths. RF output from Device #8 was randomly intermittent above 45 watts. However, Device #8 did not fail and functioned normally at end of the test.

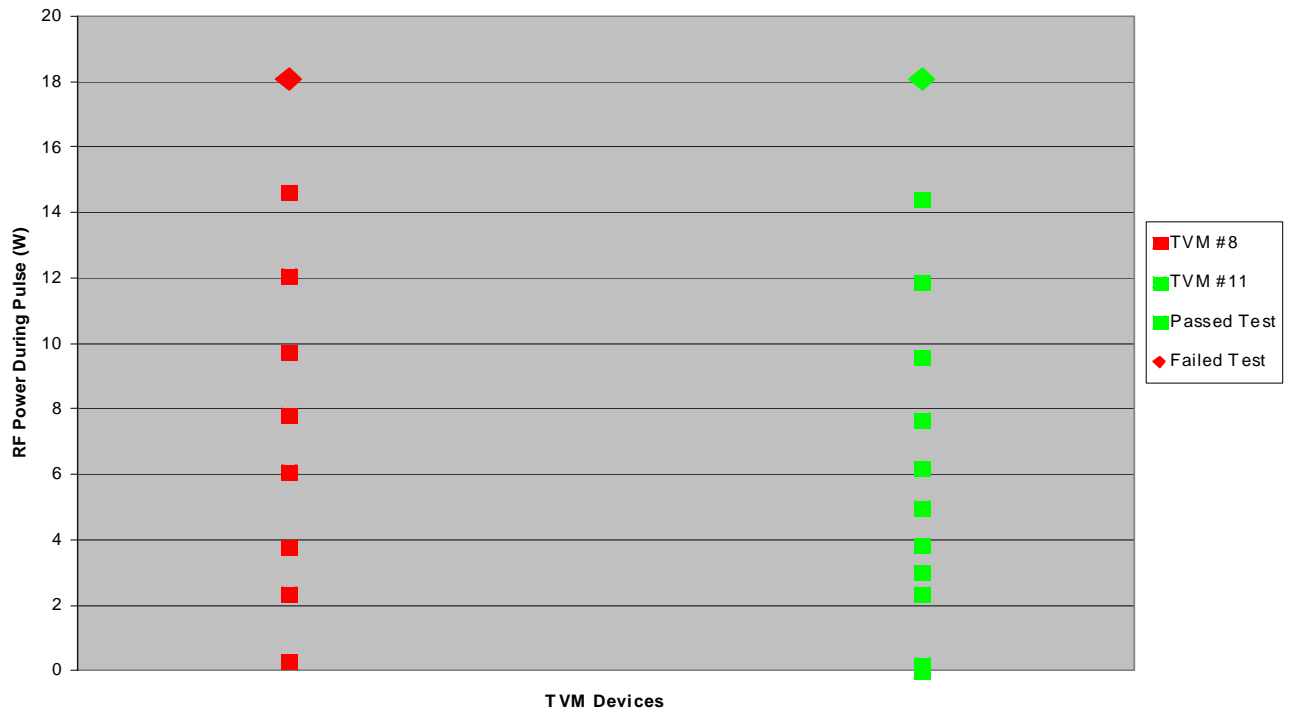


Figure 4-3. RF pulse power capability for pulse width = 65  $\mu$ sec. Results of RF pulse testing of Teravicta RF MEMS Device #8 and Device #11. Note much lower power-handling capability at pulse width = 65  $\mu$ sec than at pulse width = 6.5  $\mu$ sec (Figure 4-2).

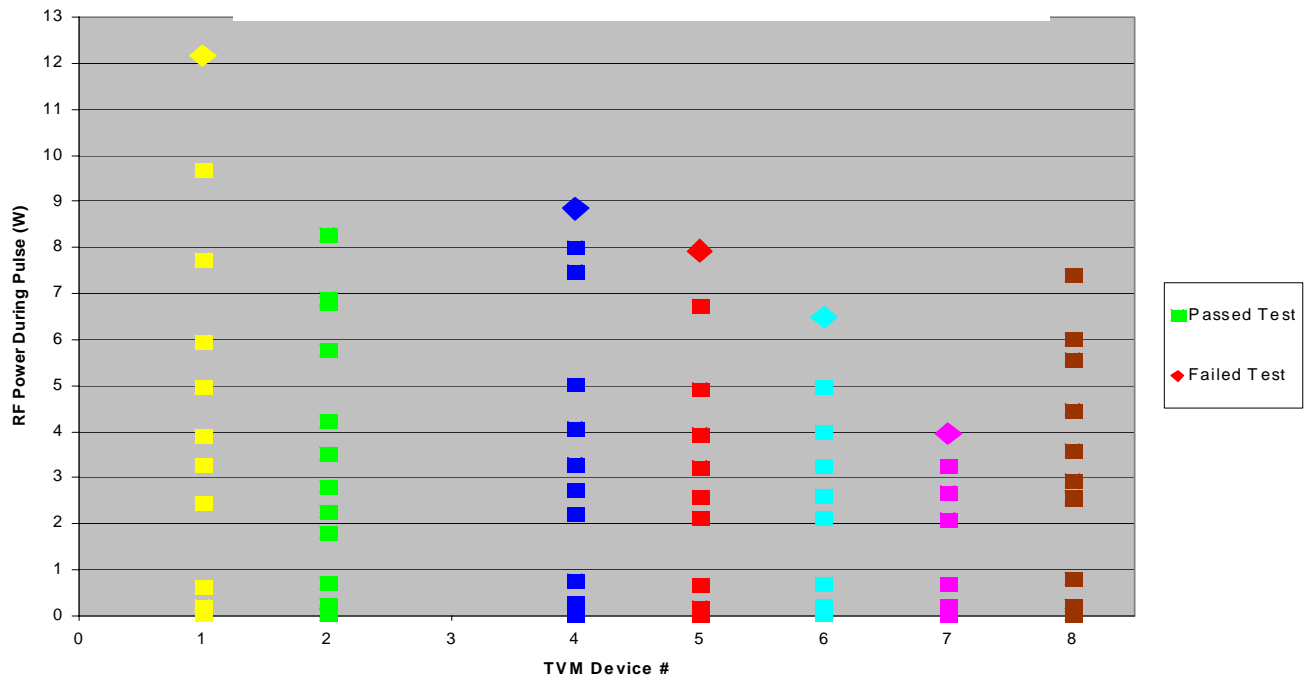


Figure 4-4. RF pulse power capability for pulse width = 125  $\mu$ sec. Results of RF pulse testing of seven Teravicta RF MEMS switches. Note reduced power-handling capability at 125  $\mu$ sec in comparison to that shown in previous two figures. Teravicta RF MEMS Device #3 failed during device characterization testing and was not RF pulse tested.

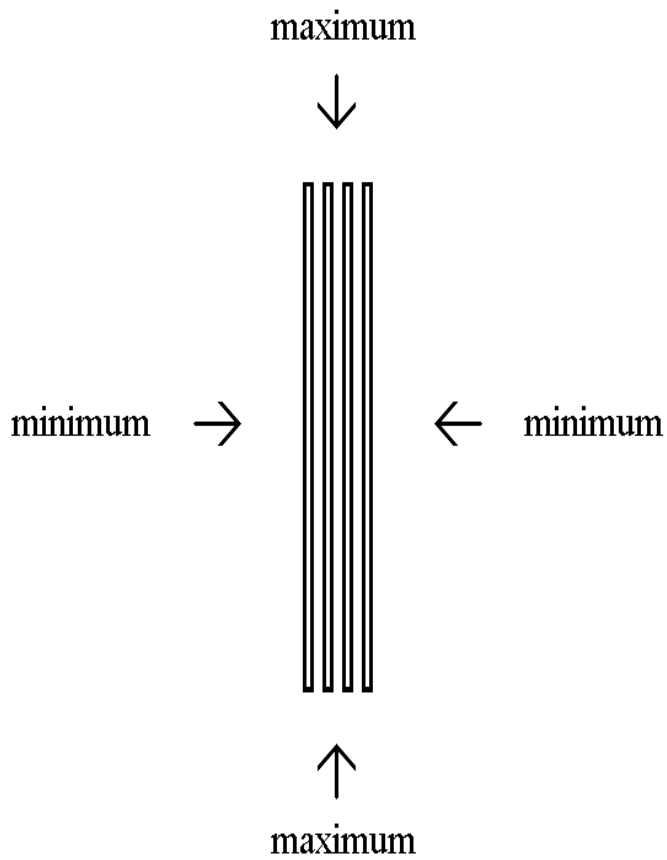


Figure 4-5. Gain maxima and minima for small-loop antenna. Antenna pattern of small-loop antenna has maximum gain parallel to plane of loops and has minimum gain perpendicular to plane of loops.

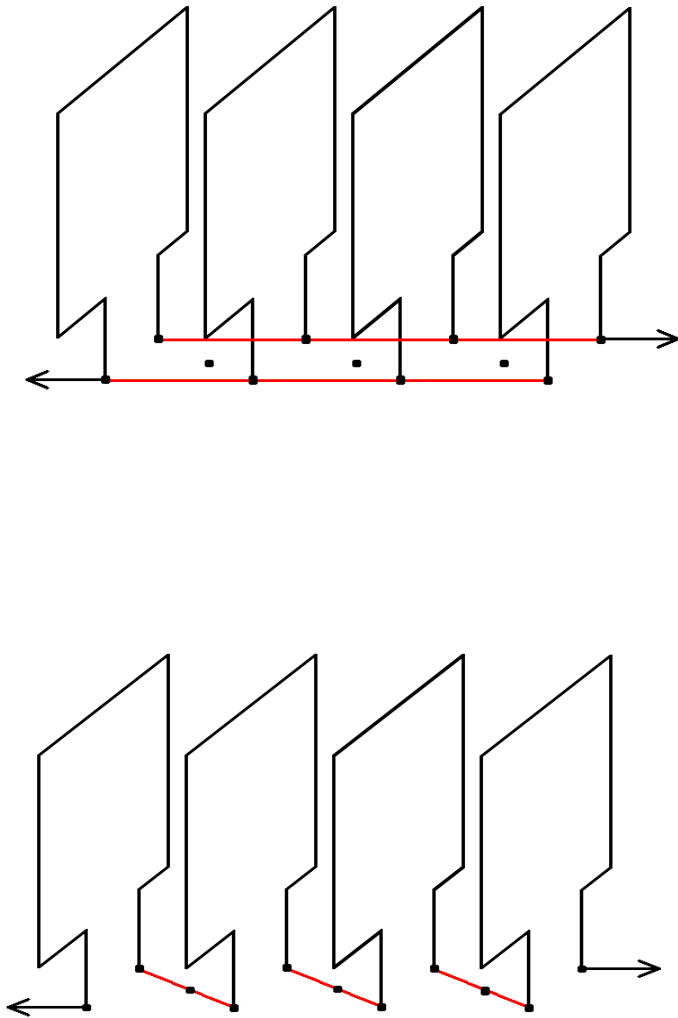


Figure 4-6. Two possible four-loop antenna configurations. Switching allows antenna to be reconfigured to better match “small-loop” criterion as wavelength of incoming RF signal changes. At highest frequencies, antenna is configured to be four single-turn loops in parallel (top illustration). At low frequencies, antenna is switched so that it becomes a single four-turn loop (bottom illustration), thereby improving gain of antenna. Other loop combinations are possible at intermediate frequencies.

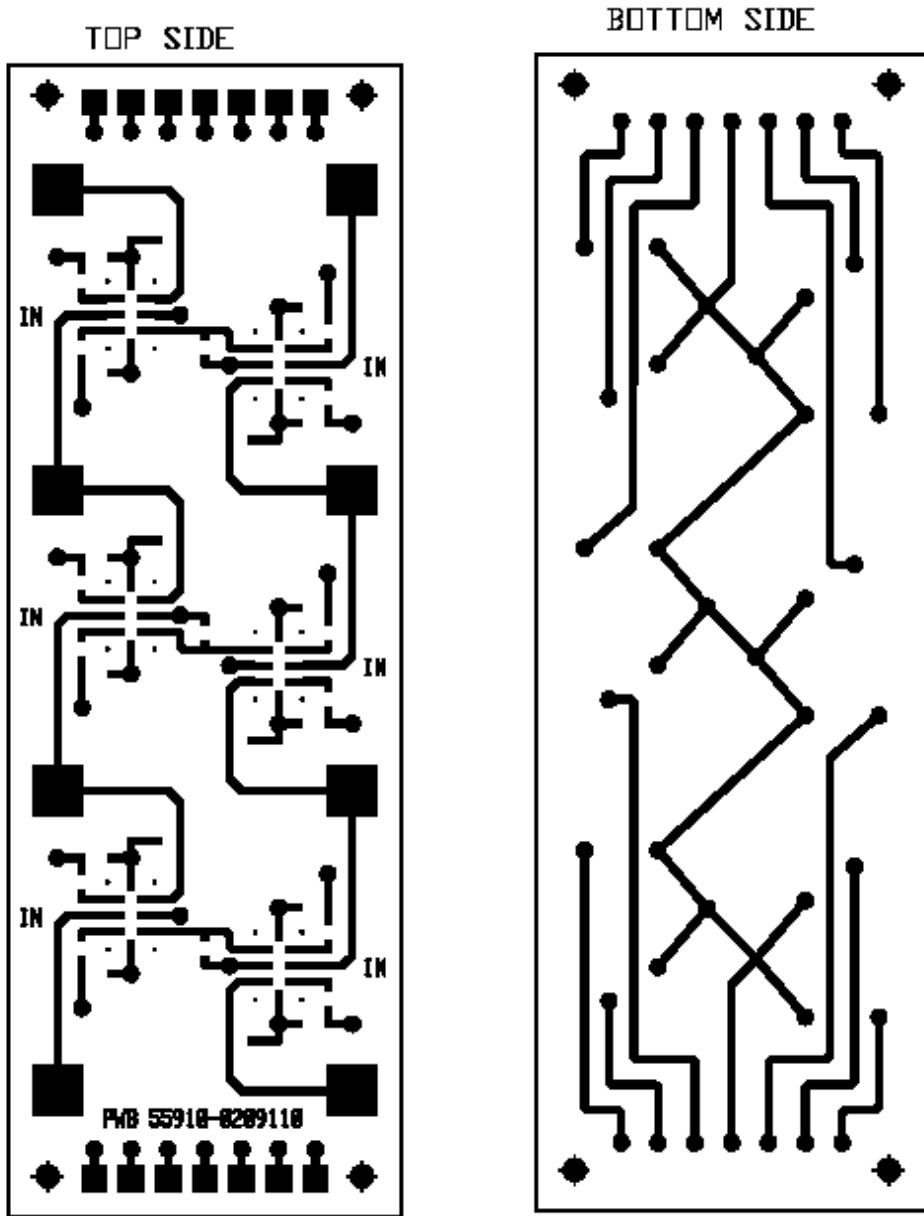


Figure 4-7. Connection board (top and bottom) design.

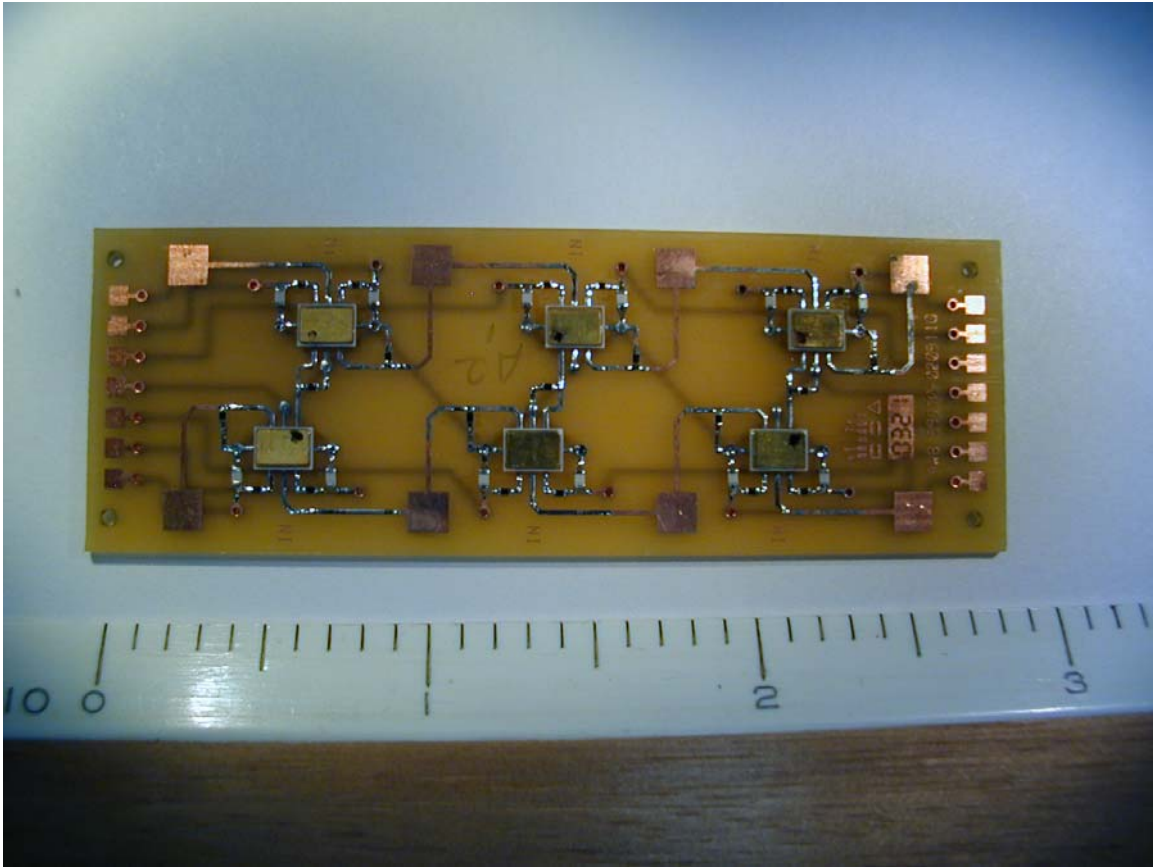


Figure 4-8. Connection board (top view). Six Teravicta RF MEMS switches are visible in photograph. The eight-loop connection pads (four pads across top, and four across the bottom) are also visible. Scale is in inches.

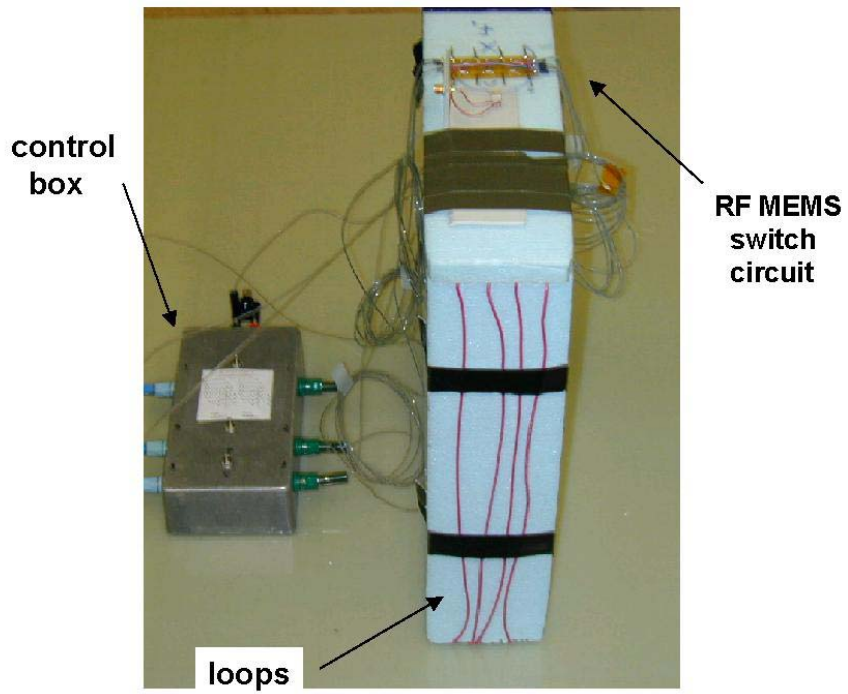


Figure 4-9. Four-loop, switched antenna and control box.



## 5. CONCLUSION

This report documents the progress of the TST RA program in investigating RF MEMS pulsed RF performance and the application of these devices to SIGINT reconfigurable antennas.

As a first phase in this project, RF pulse characterization of metal–metal contact RF MEMS switches (obtained from HRL Corporation) was performed, and a reconfigurable, segmented dipole antenna incorporating these devices was designed, constructed, and tested. From the experimental RF pulse measurements presented here, it is estimated that these devices are likely to survive the voltages and currents induced in a dipole antenna from side-lobe radiation of co-site sources. Improvement in power capability would be required to survive main-lobe radiation. The HRL devices tested were developmental devices. Reliability problems were an issue during the testing of these devices. This reliability issue exemplifies the importance of the packaging and reliability work that is ongoing in the RF MEMS development community.

A reconfigurable, segmented dipole antenna was designed for improved operation in the UHF frequency range. The series of segments were connected via the HRL RF MEMS switches to change the length of the dipole antenna. Measurements obtained in testing this antenna successfully demonstrate the basic concept of a reconfigurable segmented dipole, though the resonances of this design were too narrow for the intended SIGINT application. Further study of the antenna design showed that an unreasonably large number of switches would be required for a useful antenna using segmented dipoles.

Having verified the feasibility of using RF MEMS switches to reconfigure an antenna, but having determined that a reconfigurable antenna based on a segmented dipole-like concept was impractical, a new antenna design approach was initiated. A hybrid design was selected where part of the antenna would consist of fixed tapered-slot antennas, and part of the antenna would consist of several multiple-loop antennas intended to receive RF signals up to 100 MHz. The interconnections among the loops of these antennas were to be made reconfigurable through RF MEMS switches. Commercially available RF MEMS switches from Teravicta were obtained for this development. Once again, the program was divided into two parts, RF pulse power testing of the RF MEMS switches, and antenna design, construction, and testing. The RF pulse power testing results for the Teravicta RF MEMS switches were similar to those of the HRL devices. The loop-antenna design is also advantageous for the implementation of RF MEMS switching because the current and voltage requirements of a switch in the loop antenna are less than in a dipole antenna.

Antenna patterns of a four-loop reconfigurable antenna and a single-loop non-reconfigurable test antenna were obtained. The shape of the received antenna pattern (azimuth versus power) for the antenna configured with four single-turn loops in parallel was similar to that of the single-loop test antenna, as expected. The received pattern also changed significantly for the different loop configurations. These measured antenna patterns have been analyzed, and additional antenna testing has been recommended to achieve an understanding of the single-loop test antenna and to perform new measurements of the reconfigurable loop antenna.

Further study of fixed single-loop and reconfigurable multi-loop antennas is necessary to determine the benefits of the reconfigurable loop design for the intended TST application. The study would first quantify the performance benefits of including the reconfigurable loop antenna with the tapered-slot antenna in the hybrid antenna design. The next step of the study would focus on the design of a fixed-loop antenna. This step would address the size of the loop, the shielding of the loop,

the physical design of the feed, and the impedance matching of the loop to the receiver. Based on this study, a new single-loop antenna would be constructed and tested. After experimental measurements of the single-loop antenna yield the predicted antenna pattern, the effort would proceed to the design and construction of a reconfigurable loop antenna to improve performance over the frequency range of interest. Depending on changes needed to the current reconfigurable loop antenna design, either the current RF MEMS-based switching circuit would be used in the new antenna design, or a new switching circuit would be designed and fabricated. The design study for the reconfigurable loop antenna would also consider the control line isolation requirement for the switching circuit. Based on this requirement, switches other than RF MEMS (e.g., electrically controlled PIN switches) might be considered.

## REFERENCES

- Carr, J. J. 1999. *Joe Carr's Loop Antenna Handbook*. Universal Radio Research, Reynoldsburg, OH.
- De Los Santos, H. J. 2002. *RF MEMS Circuit Design*. Artech House, Boston, MA.
- Jacobs, E. W., D. W. Fogliatti, H. Nguyen, D. J. Albares, C. T. Chang, and C. K. Sun. 2002. "Photo-Injection P-I-N Diode Switch for High Power RF Switching," *IEEE Transactions on Microwave Theory and Techniques*, vol. 50, pp. 413–419.
- Kraus, J. D. 1988. *Antennas*. Second Edition. McGraw-Hill, Inc., New York, NY.
- Rebeiz, G. M. 2003. *RF MEMS Theory, Design, and Technology*. John Wiley & Sons, Inc., Hoboken, NJ.
- Rebeiz, G. M. and J. B. Muldavin, 2001. "RF MEMS Switches and Switch Circuits," *IEEE Microwave*, Dec., pp. 59–71.
- Sun, C. K., R. Nguyen, C. T. Chang, and D. J. Albares. 1996. "Photovoltaic-FET for Optoelectronic RF/ $\mu$ wave Switching," *IEEE Trans Microwave Theory and Techniques*, vol. 44, pp. 1747–1750.
- Sun, C. K., R. Nguyen, C. T. Chang, and D. J. Albares. 1999. "Photovoltaic-PIN Diodes for RF Control—Switching Application," *IEEE Transactions on Microwave Theory and Techniques*, vol. 47, pp. 2034–2036.
- Varadan, V. K., K. J. Vinoy, and K. A. Jose. 2003. *RF MEMS and Their Applications*. John Wiley & Sons, Ltd., Chichester, West Sussex, England.



## BIBLIOGRAPHY

- Anagnostou, D., M. Khodier, J. C. Lyke, C. G. Christodoulou. 2002. "Fractal Antenna with RF MEMS Switches for Multiple Frequency Applications." *Antennas and Propagation Society International Symposium, 2002, IEEE*, 16–21 June, vol. 2, pp. 22–25.
- Bernhard, J. T., R. Wang, R. Clark, and P. Mayes. 2001. "Stacked Reconfigurable Antenna Elements for Space-Based Radar Applications." *Antennas and Propagation Society, 2001 IEEE International Symposium*, 8–13 July, vol. 1, pp. 158–161.
- Bozler, C., R. Drangmeister, S. Duffy, M. Gouker, J. Knecht, L. Kushner, R. Parr, S. Rabe, and L. Travis. 2000. "MEMS Microswitch Arrays for Reconfigurable Distributed Microwave Components." *Antennas and Propagation Society International Symposium 2000, IEEE*, 16–21 July, vol. 2, pp. 587–591.
- Brown, E. R. 2001. "On the Gain of a Reconfigurable-Aperture Antenna." *Antennas and Propagation, IEEE Transactions on Antennas and Propagation*, vol. 49, issue. 10 (Oct), pp. 1357–1362.
- Cetiner, B. A., L. Jofre, C. H. Chang, J. Y. Qian, M. Bachman, G. P. Li, F. De Flaviis. 2002. "Integrated MEM Antenna System for Wireless Communications." *Microwave Symposium Digest, 2002 IEEE MTT-S International*, 2–7 June, vol. 2, pp. 1333–1336.
- Cetiner, B. A., J. Y. Qian, S. Liu, L. Jofre, G. P. Li, F. De Flaviis. 2003. "A Compact Wideband MEM Switched Diversity Antenna for Indoor Mobile Channels." *Microwave Symposium Digest, 2003 IEEE MTT-S International*, 8–13 June, vol. 3, pp. 1711–1714.
- Chiao, J. -C. 2000. "MEMS RF Devices for Antenna Applications." *Microwave Conference, 2000 Asia-Pacific*, 3–6 December, pp. 895–898.
- Chiao, J. -C., Y. Fu, I. M. Chio, M. DeLisio, and L.-Y. Lin. 1999. "MEMS Reconfigurable Vee Antenna." *Microwave Symposium Digest, IEEE MTT-S International*, 13–19 June, vol. 4, pp. 1515–1518.
- Kim, M., J. B. Hacker, R. E. Mihailoviich, and J. F. DeNatale. 2001. "MEMS True-Time Delay Circuit for Broadband Antennas." *Antennas and Propagation Society, 2001 IEEE International Symposim*, 8–13 July, vol. 3, pp. 662–665.
- Kiriazzi, J., H. Ghali, H. Ragaie, H. Haddara. 2003. "Reconfigurable Dual-Band Dipole Antenna on Silicon Using Series MEMS Switches." *Antennas and Propagation, 2003 IEEE Society International Conference*, 22–27 June, vol. 1, pp. 403–406.
- Norvell, B. R., R. J. Hancock, J. K. Smith, M. L. Pugh, S. W. Theis, and J. Kriatkofsky. "Micro Electro Mechanical Switch (MEMS) Technology Applied to Electronically Scanned Arrays for Space Based Radar." *Proceedings of 1999 IEEE Aerospace Conference*, 6–13 March, vol. 3, pp. 239–247.
- Rose, J., L. Roy, and N. Tait. 2003. "Development of a MEMS Microwave Switch and Application to Adaptive Integrated Antennas." *Electrical and Computer Engineering, IEEE CCECE 2003. Canadian Conference*, 4–7 May, vol. 3, pp. 1901–1904.

- Schaffner, J. H., R. Y. Loo, D. F. Sievenpiper, F. A. Dolezal, G. L. Tangonan, J. S. Colburn, J. J. Lynch, J. J. Lee, S. W. Livingston, R. J. Broas, and M. Wu. 2000. "Reconfigurable Aperture Antennas Using RF MEMS Switches for Multi-Octave Tunability and Beam Steering." *Antennas and Propagation Society International Symposium 2000*, IEEE, 16–21 July, vol. 1, pp. 321–324.
- Schaffner, J. H., D. F. Sievenpiper, R. Y. Loo, J. J. Lee, and S. W. Livingston. 2001. "A Wideband Beam Switching Antenna Using RF MEMS Switches." *Antennas and Propagation Society, 2001 IEEE International Symposium*, 8–13 July, vol. 3, pp. 658–661.
- Sievenpiper, D., H. J. Song, H. P. Hsu, G. Tangonan, R. Y. Loo, J. Schaffner. 2002. "MEMS-Based Switched Diversity Antenna at 2.3 GHz for Automotive Applications." *Wireless Personal Multimedia Communications. The 5<sup>th</sup> International Symposium*, 27–30 Oct, vol. 2, pp. 762–765.
- Simons, R. N., D. Chun, and L. P. B. Katehi. 2001. "Reconfigurable Array Antenna Using Microelectromechanical Systems (MEMS) Actuators." *Antennas and Propagation Society, 2001 IEEE International Symposium*, 8–13 July, vol. 3, pp. 674–677.
- Simons, R. N., D. Chun, L. P. B. Katehi. 2002. "Polarization Reconfigurable Patch Antenna Using Microelectromechanical Systems (MEMS) Actuators." *Antennas and Propagation Society International Symposium, 2002. IEEE*, 16–21 June, vol. 2, pp. 6–9.
- Tangonan, G., R. Loo, J. Schaffner, and J. J. Lee. 1999. "Microwave Photonic Applications of MEMS Technology." *Microwave Photonics, MWP '99. International Topical Meeting*, 17–19 November, vol. 1, pp. 109–112.
- Weedon, W. H., W. J. Payne, G. M. Rebeiz, J. S. Herd, and M. Champion. 1999. "MEMS-Switched Reconfigurable Multi-Band Antenna: Design and Modeling." *Proceedings of the 1999 Antenna Applications Symposium*, Monticello, Illinois, 15–17 September.
- Weedon, W. H., W. J. Payne, and G. M. Rebeiz. 2001. "MEMS-Switched Reconfigurable Antennas." *Antennas and Propagation Society, 2001 IEEE International Symposium*, 8–13 July, vol. 3, pp. 654–657.
- Veihl, J. C., R. E. Hodges, D. McGrath, and C. Monzon. 2000. "Reconfigurable Aperture Decade Bandwidth Array." *Antennas and Propagation Society International Symposium, IEEE*, 16–21 July, vol. 1, pp. 314–317.

# **APPENDIX A**

## **HRL RF MEMS Switches**

### **RF Pulse Power Test Data**

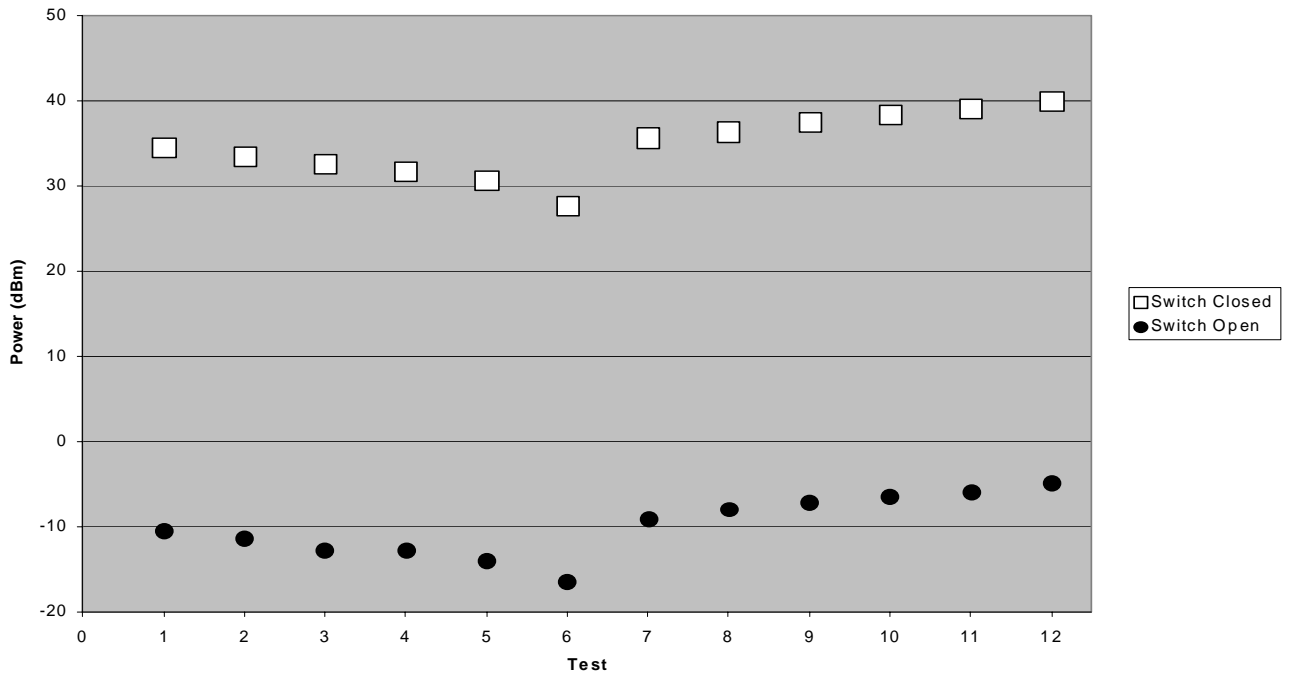


Figure A-1. Power Through HRL Device #3

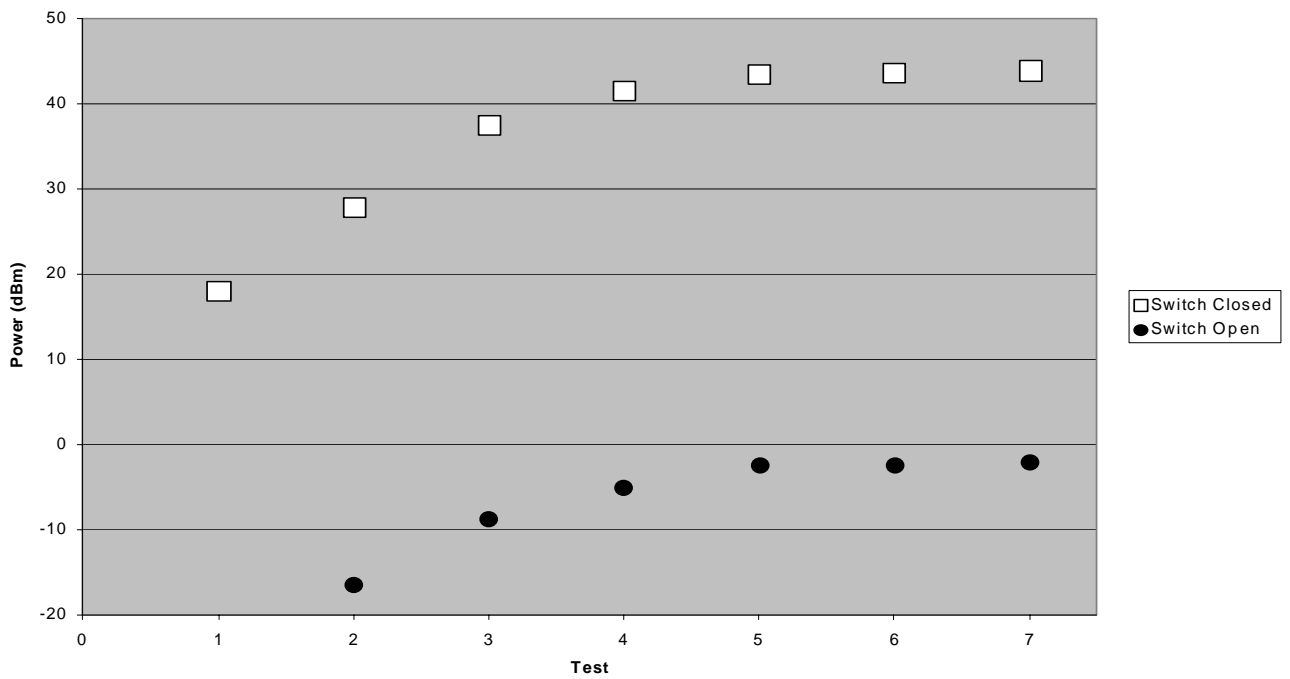


Figure A-2. Power Through HRL Device #4 (31JUL02)

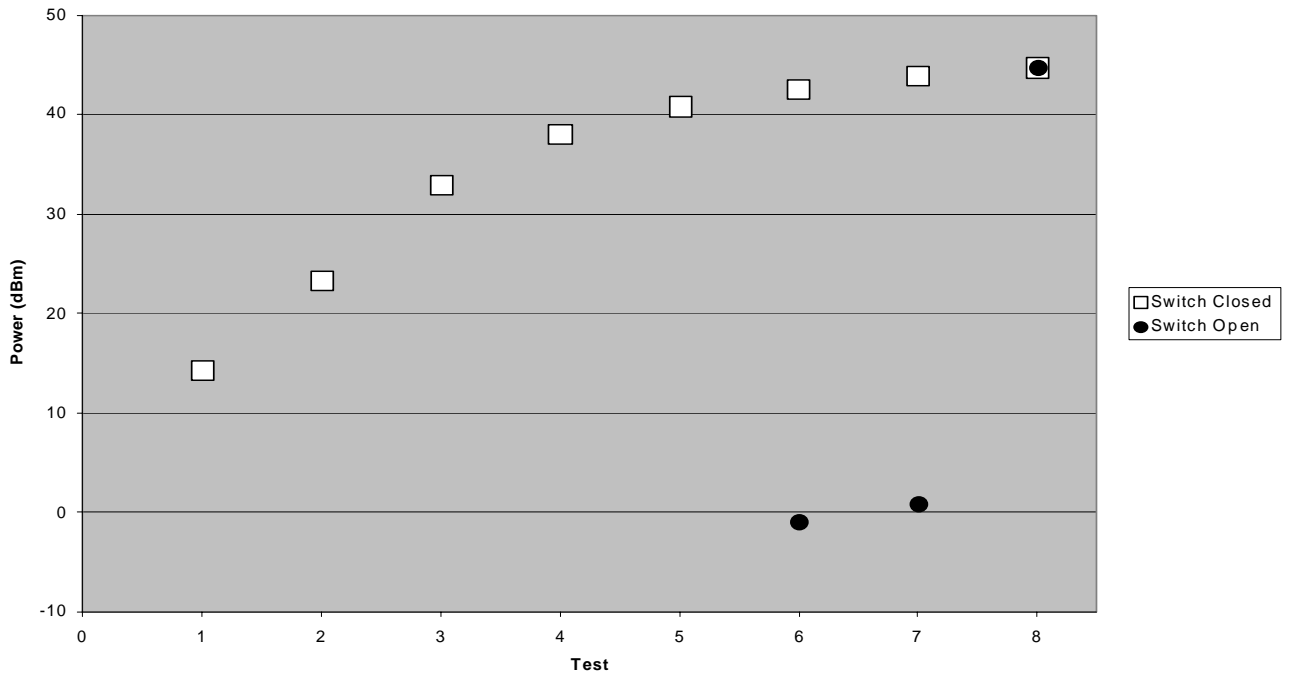


Figure A-3. Power Through HRL Device #4 (6AUG02)

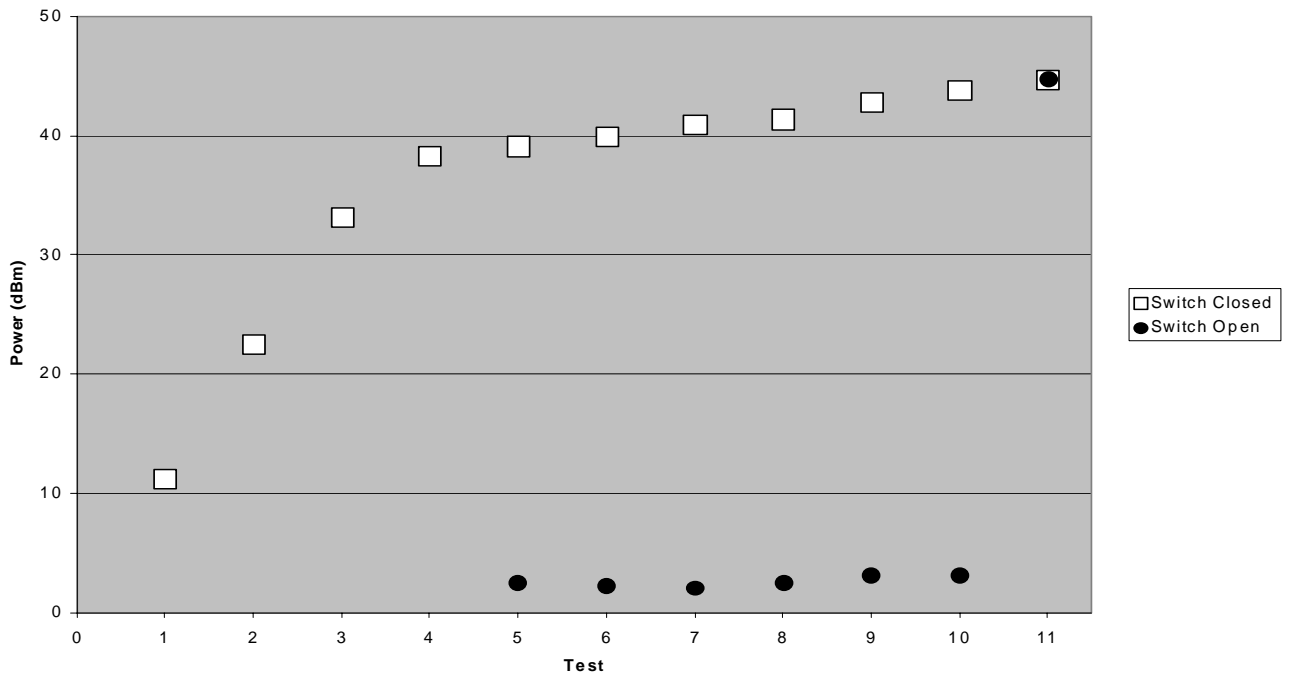


Figure A-4. Power Through HRL Device #5

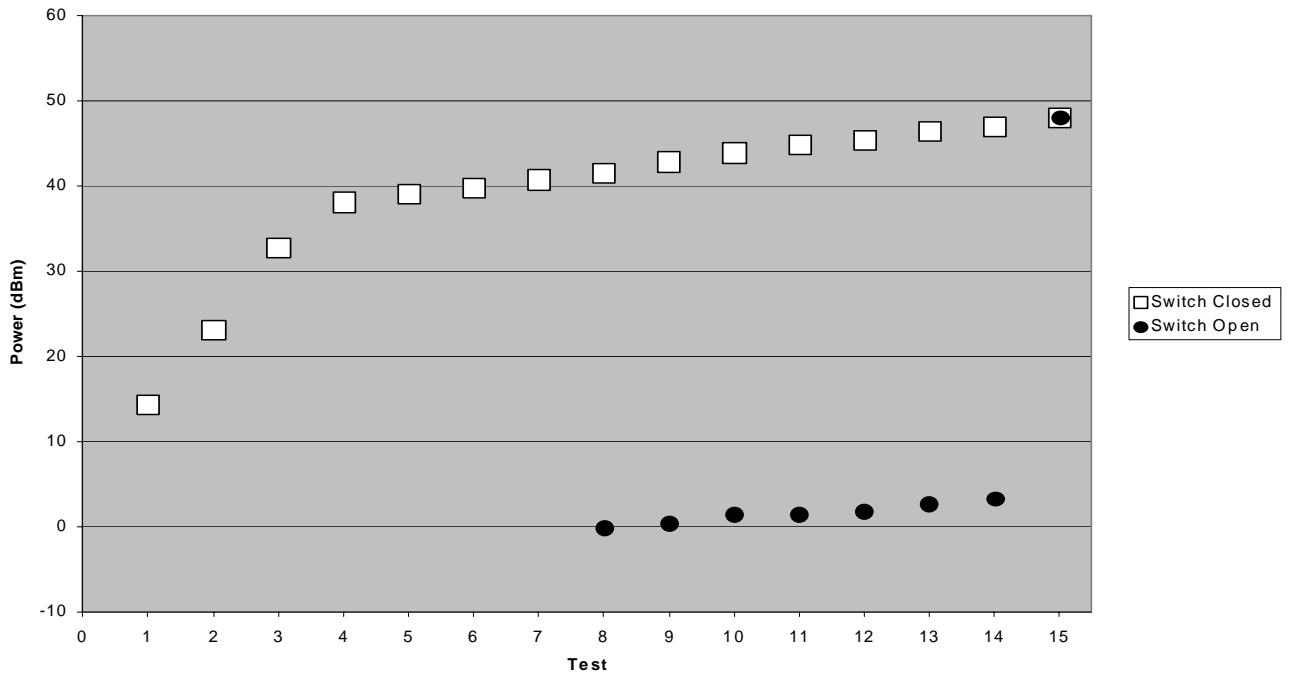


Figure A-5. Power Through HRL Device #6

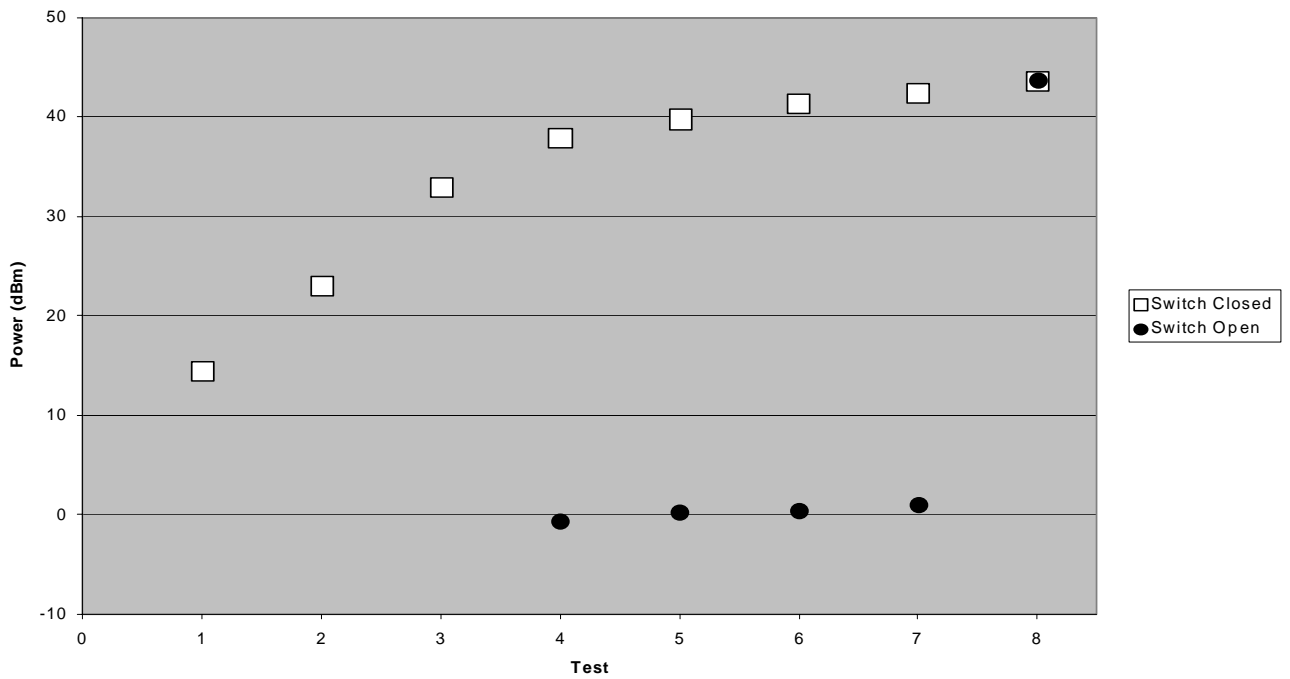


Figure A-6. Power Through HRL Device #7

# **APPENDIX B**

## **TeraVista RF MEMS Switches**

### **Isolation and Insertion Loss Data**

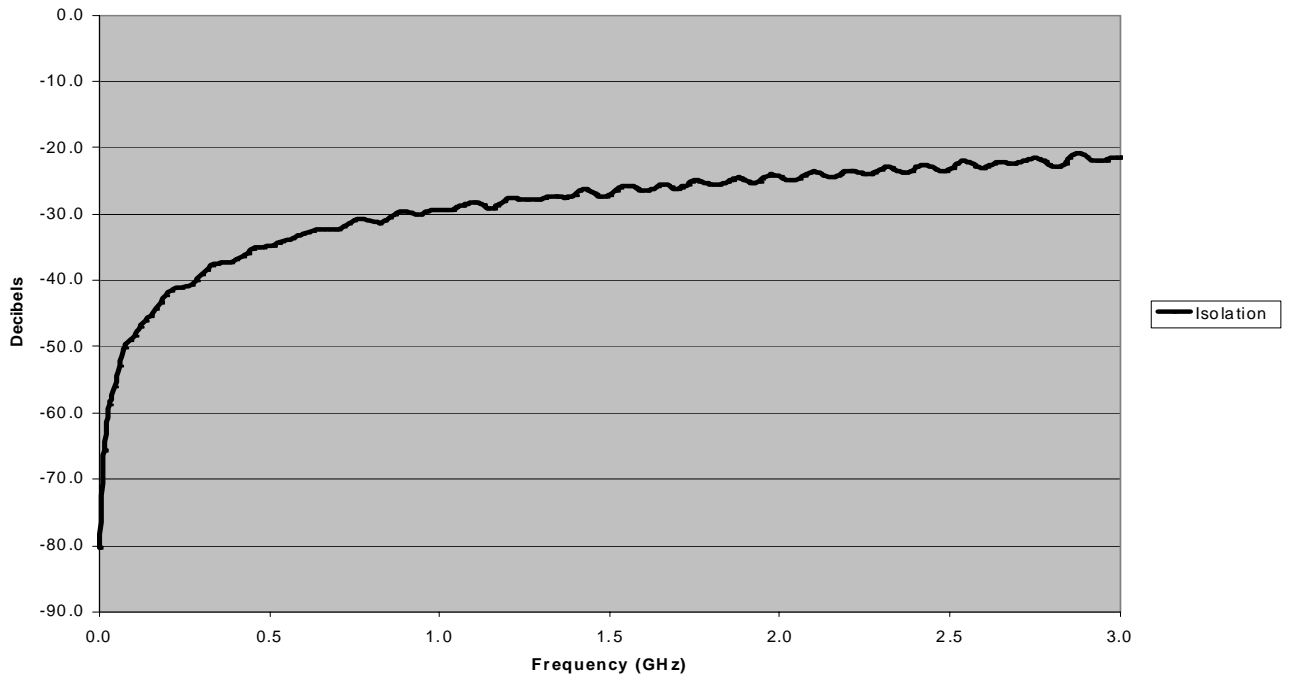


Figure B-1. TVM Device #2 RF1 isolation

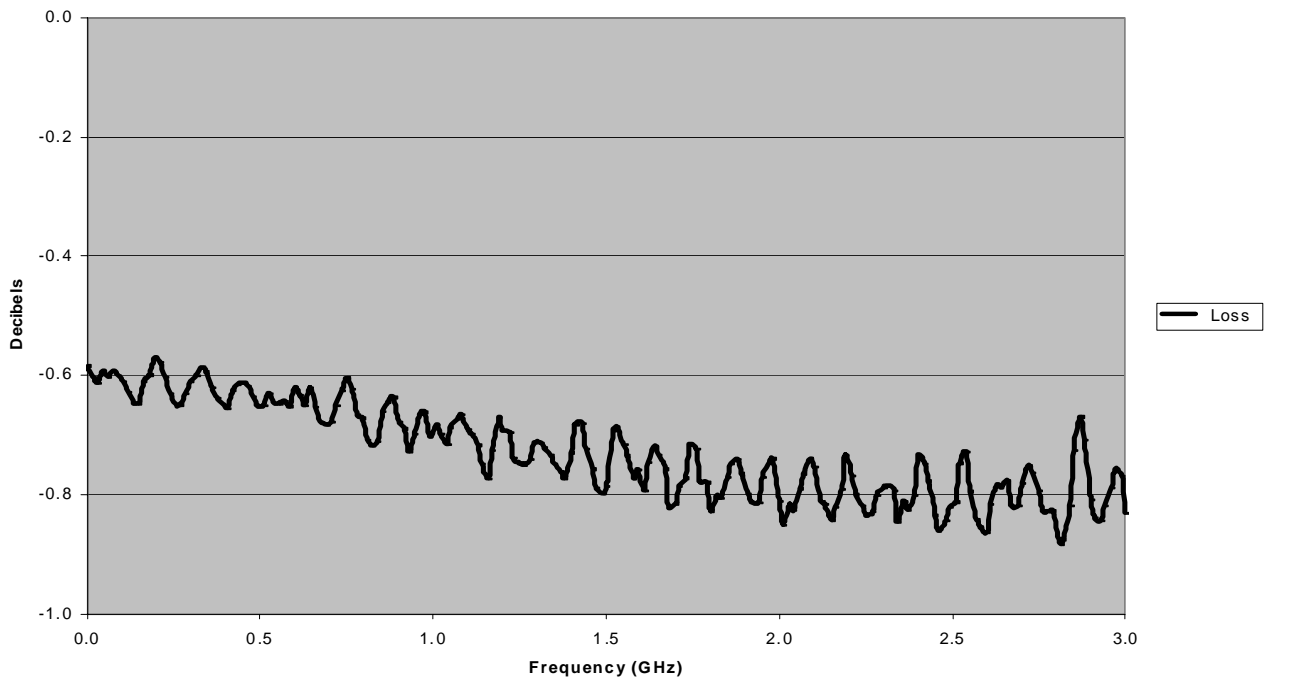


Figure B-2. TVM Device #2 RF1 insertion loss

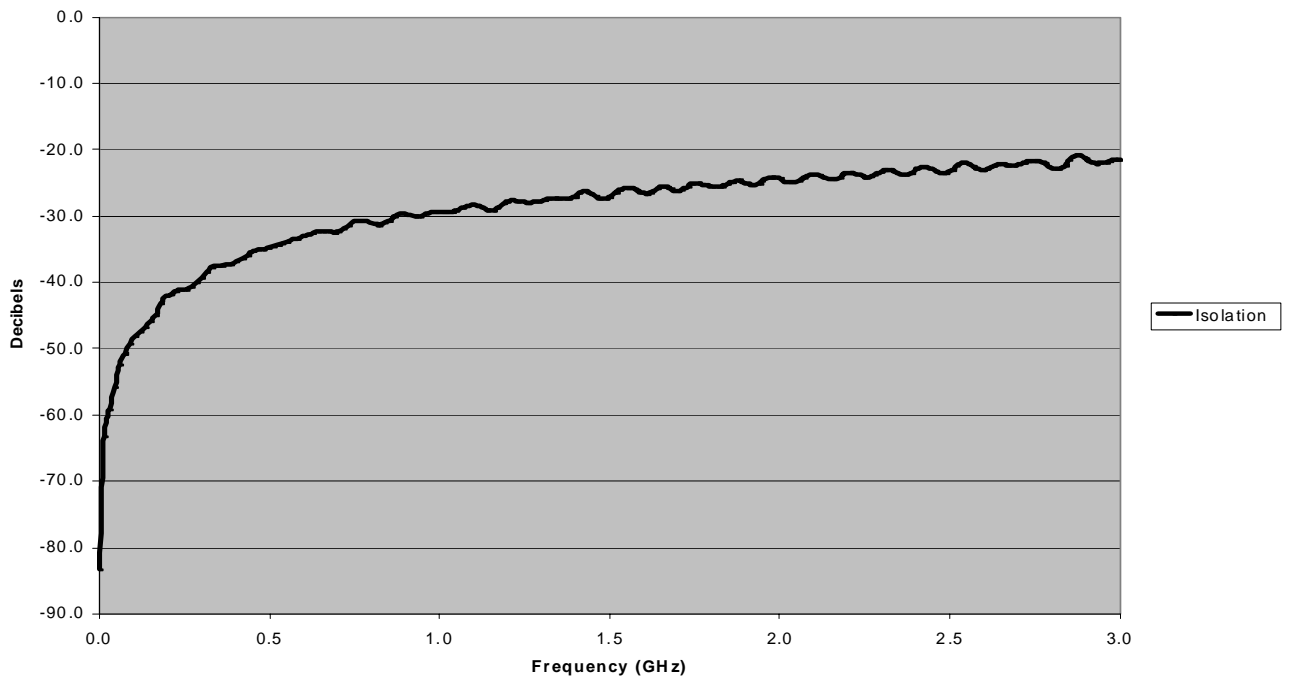


Figure B-3. TVM Device #2 RF2 isolation

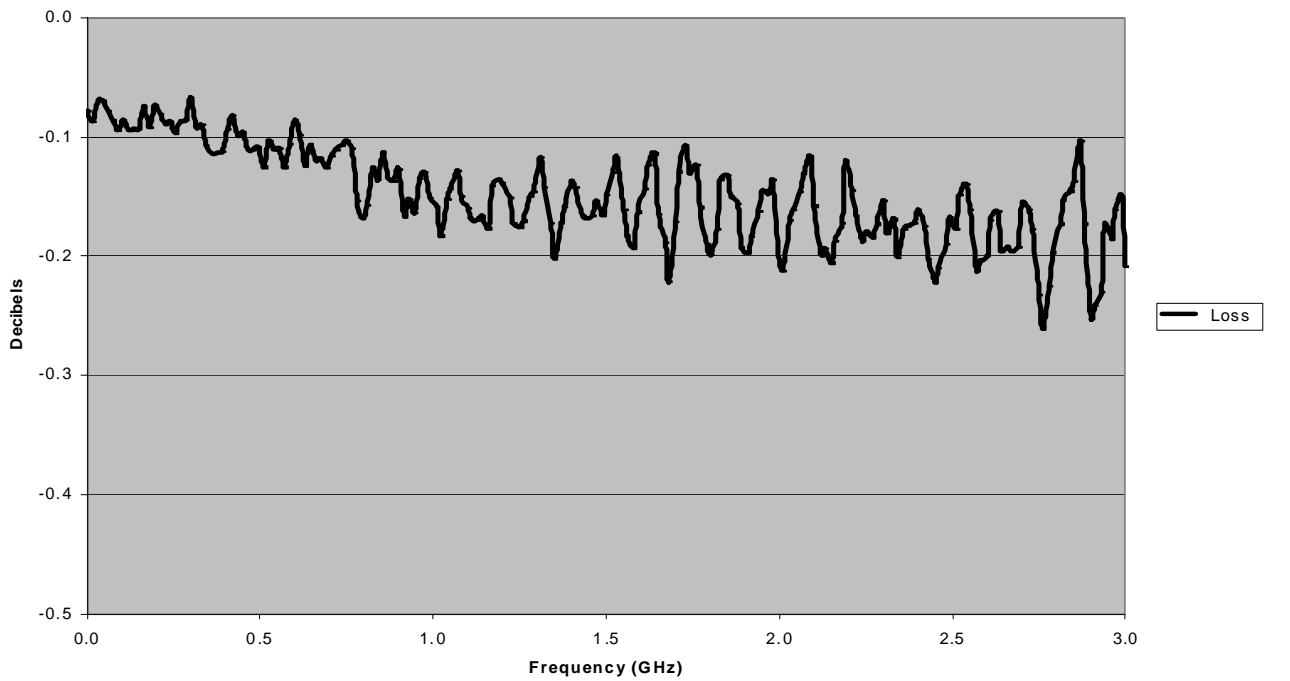


Figure B-4. TVM Device #2 RF2 insertion loss

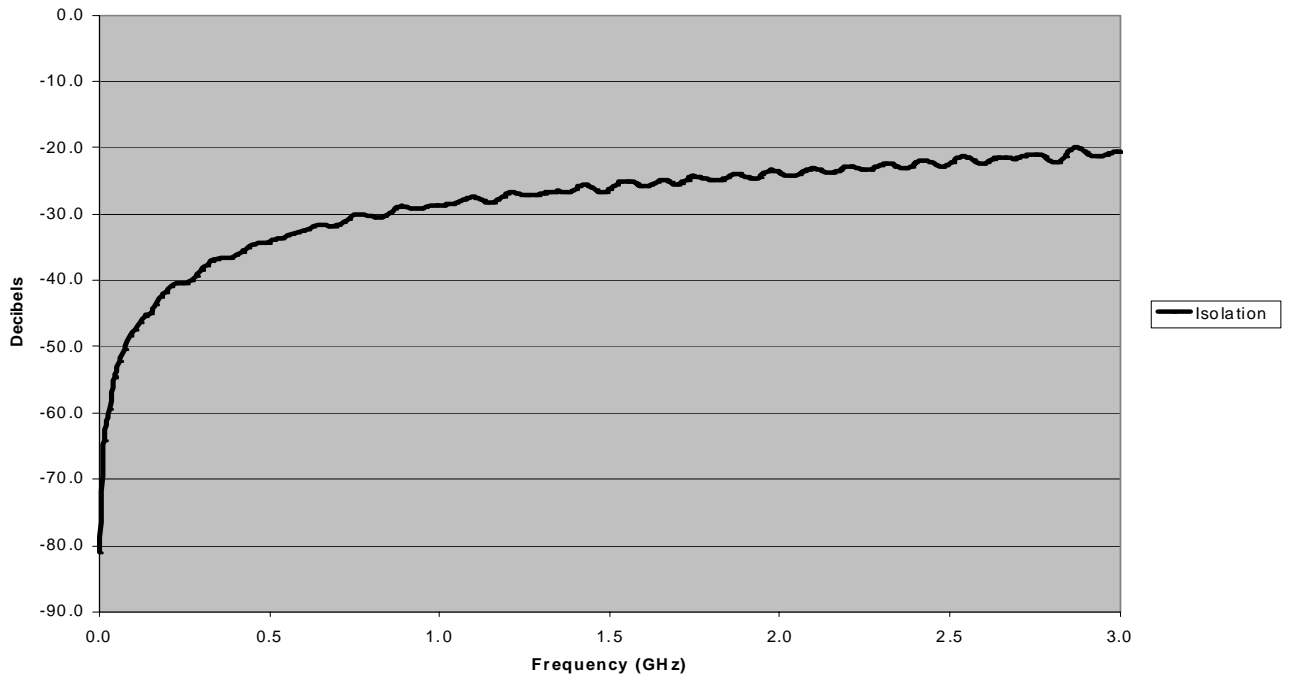


Figure B-5. TVM Device #4 RF1 isolation

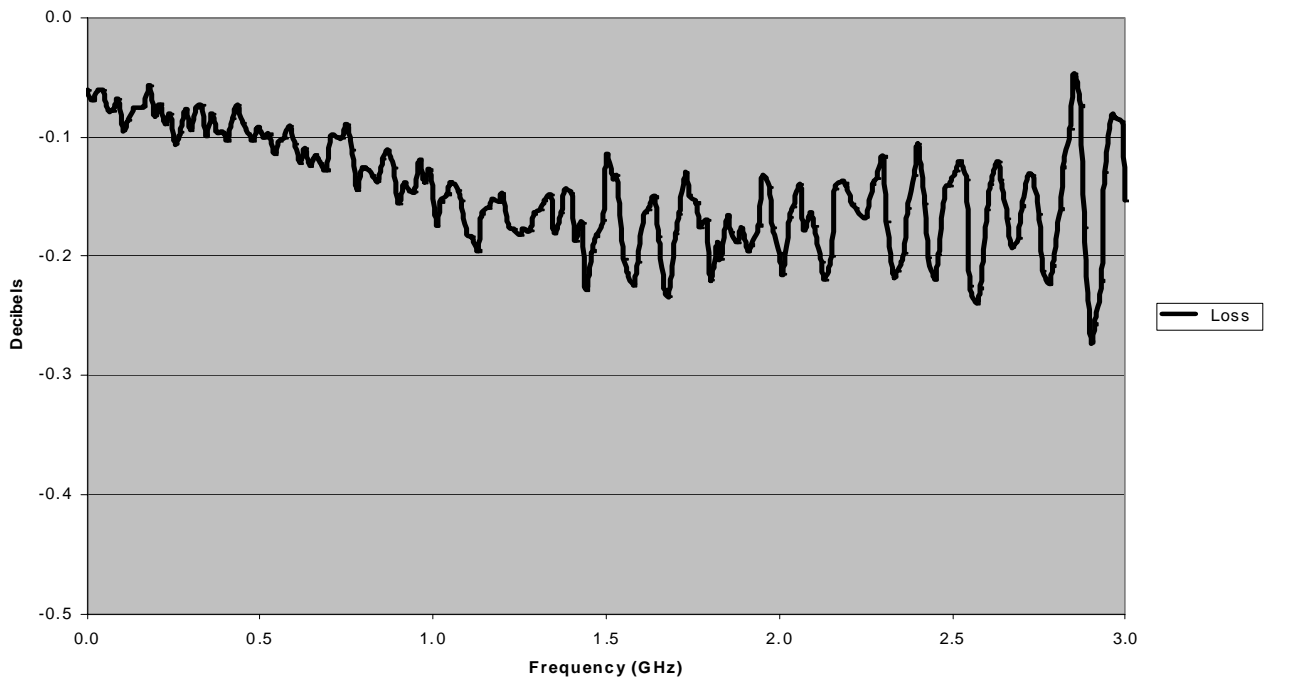


Figure B-6. TVM Device #4 RF1 insertion loss

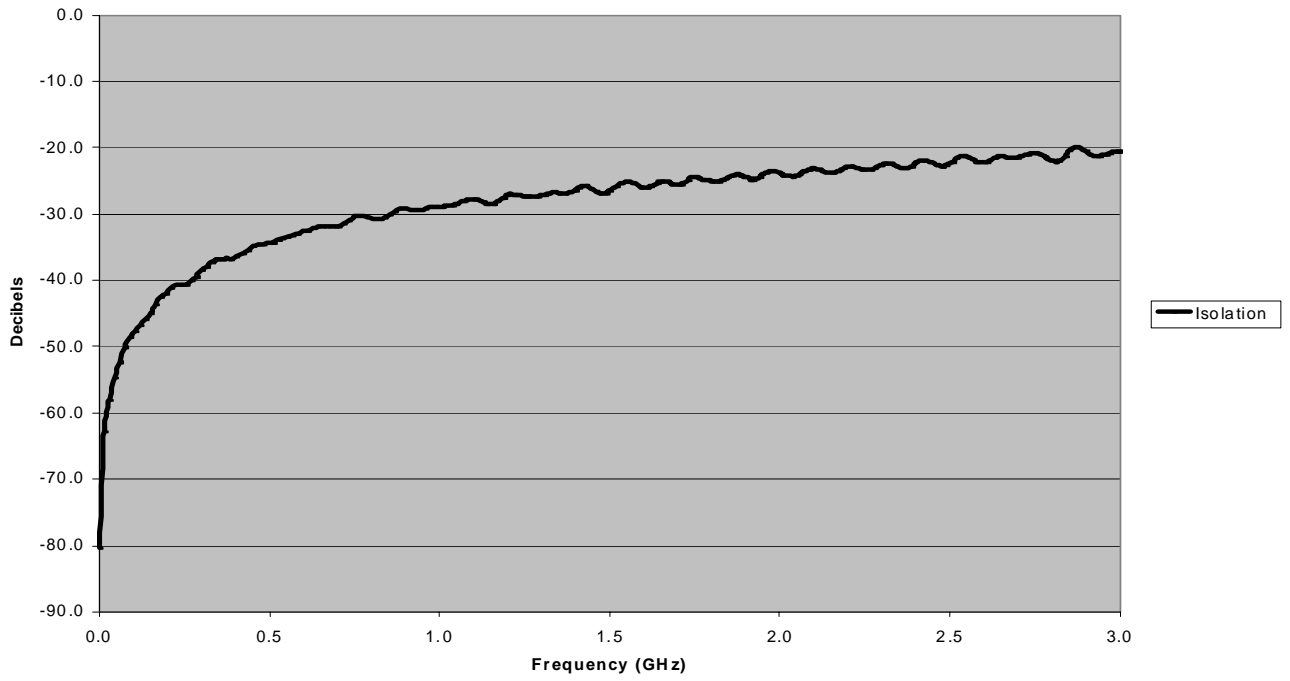


Figure B-7. TVM Device #4 RF2 isolation

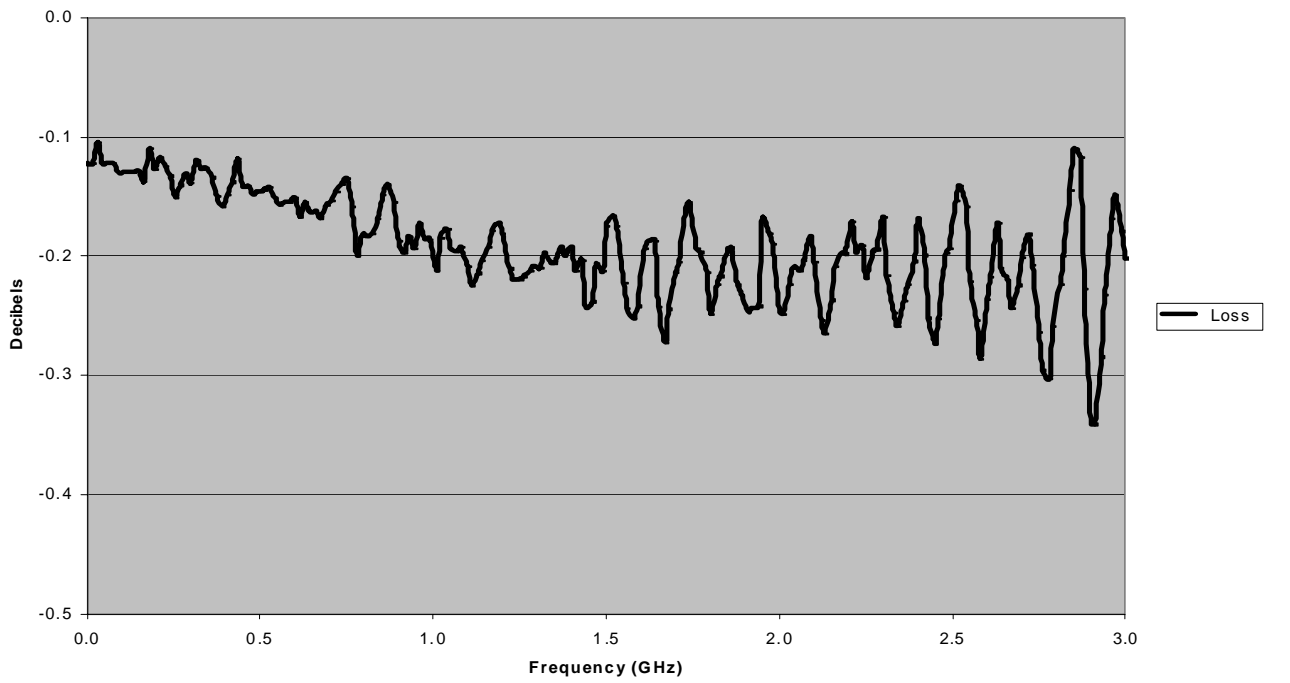


Figure B-8. TVM Device #4 RF2 insertion loss

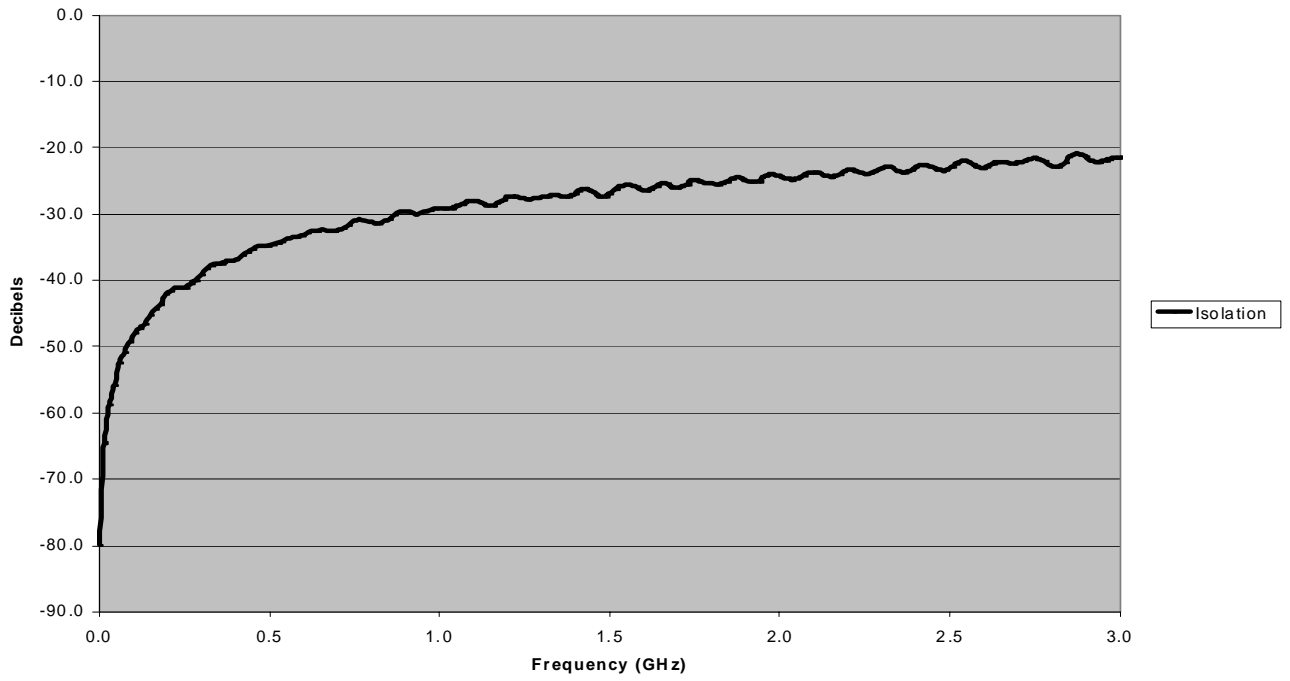


Figure B-9. TVM Device #5 RF1 isolation

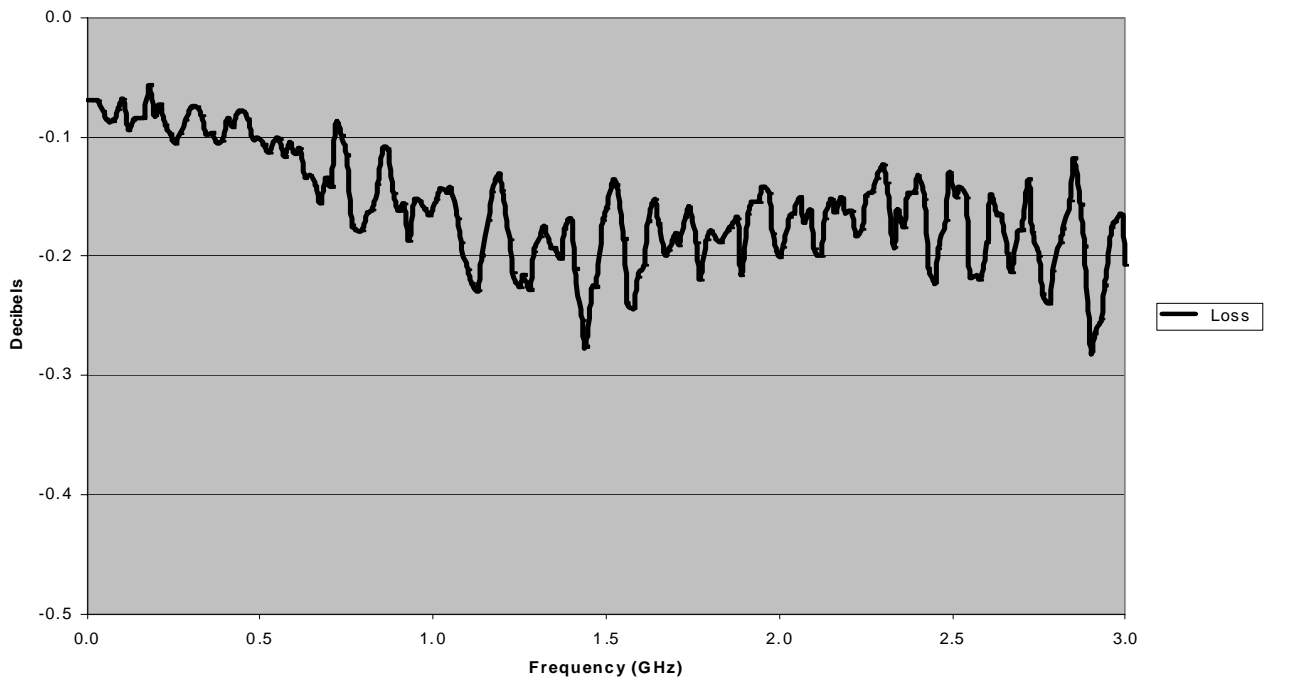


Figure B-10. TVM Device #5 RF1 insertion loss

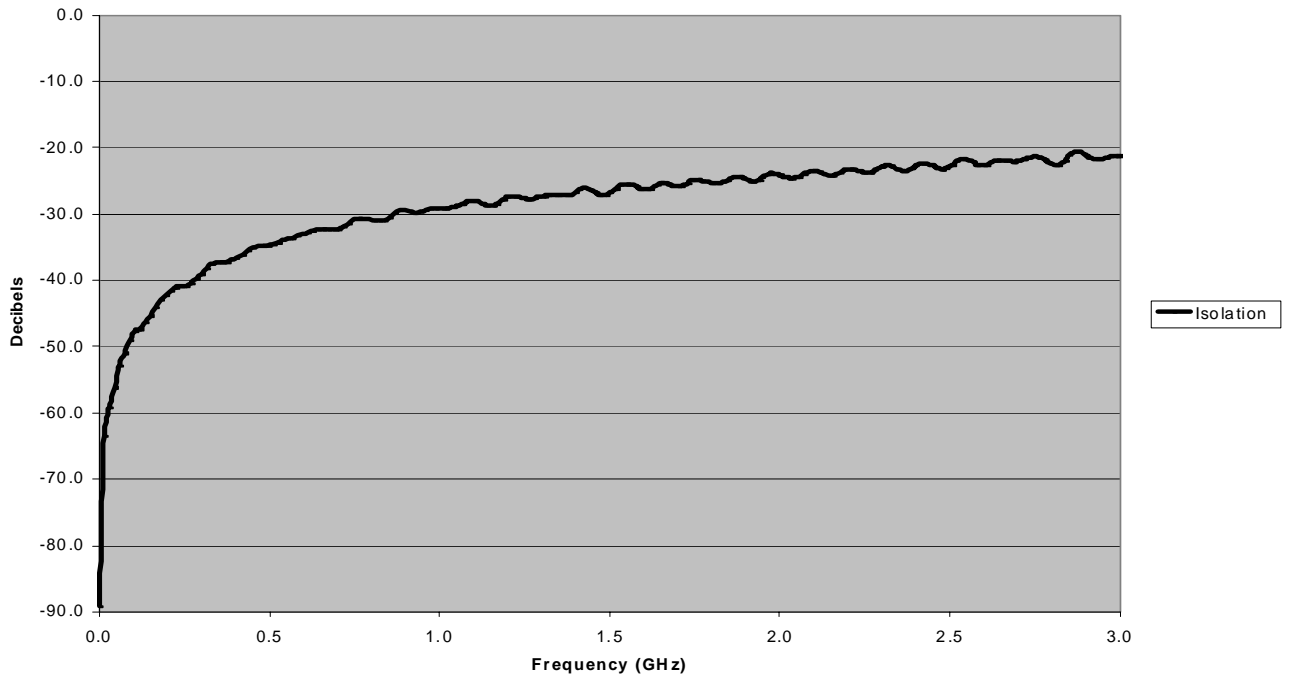


Figure B-11. TVM Device #5 RF2 isolation

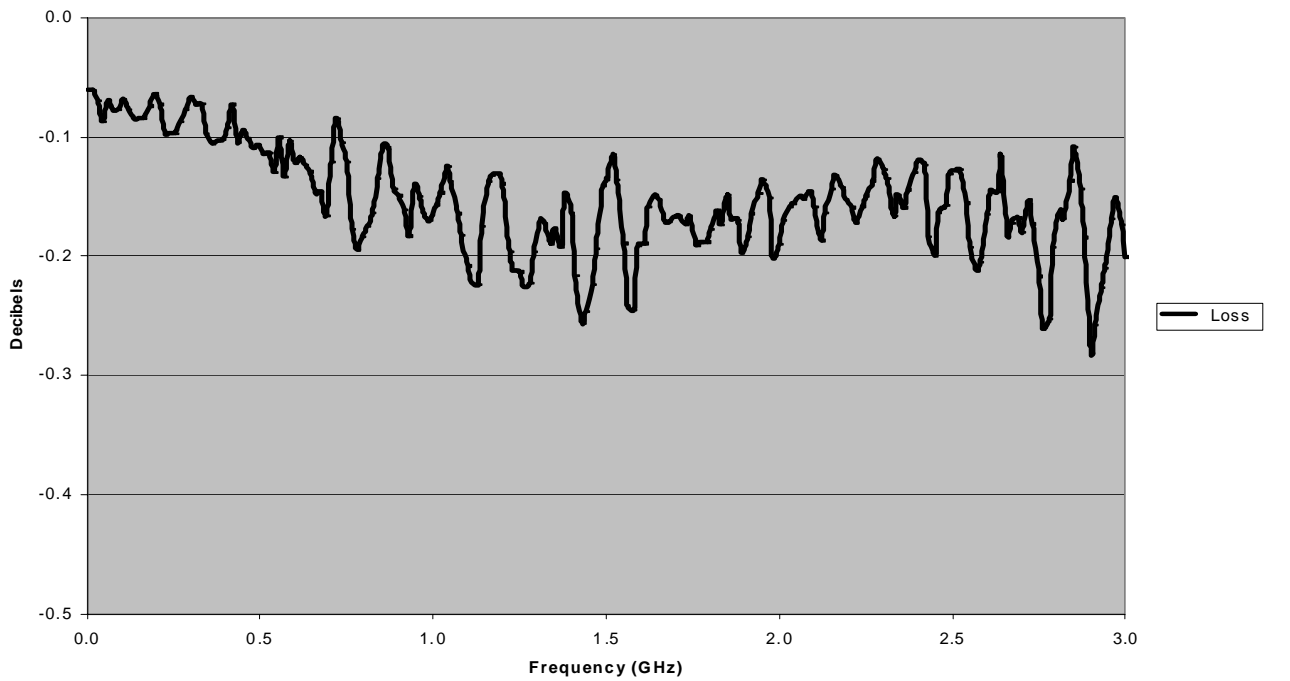


Figure B-12. TVM Device #5 RF2 insertion loss

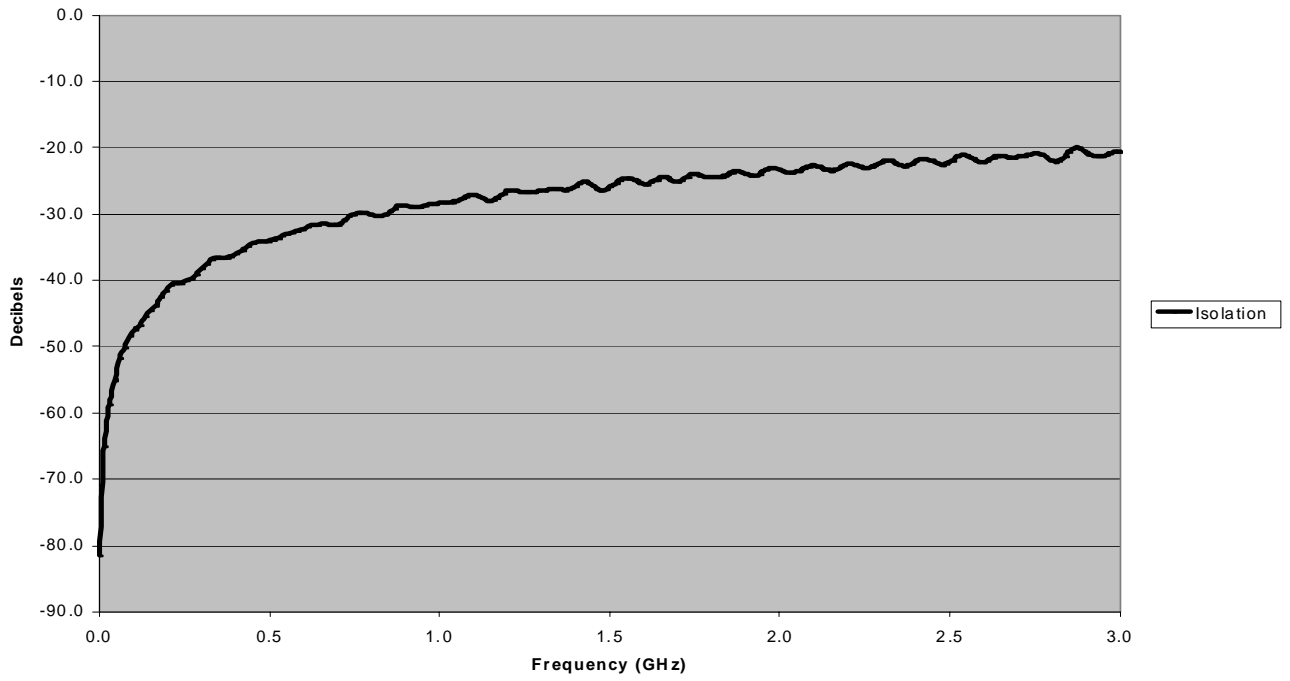


Figure B-13. TVM Device #6 RF2 isolation

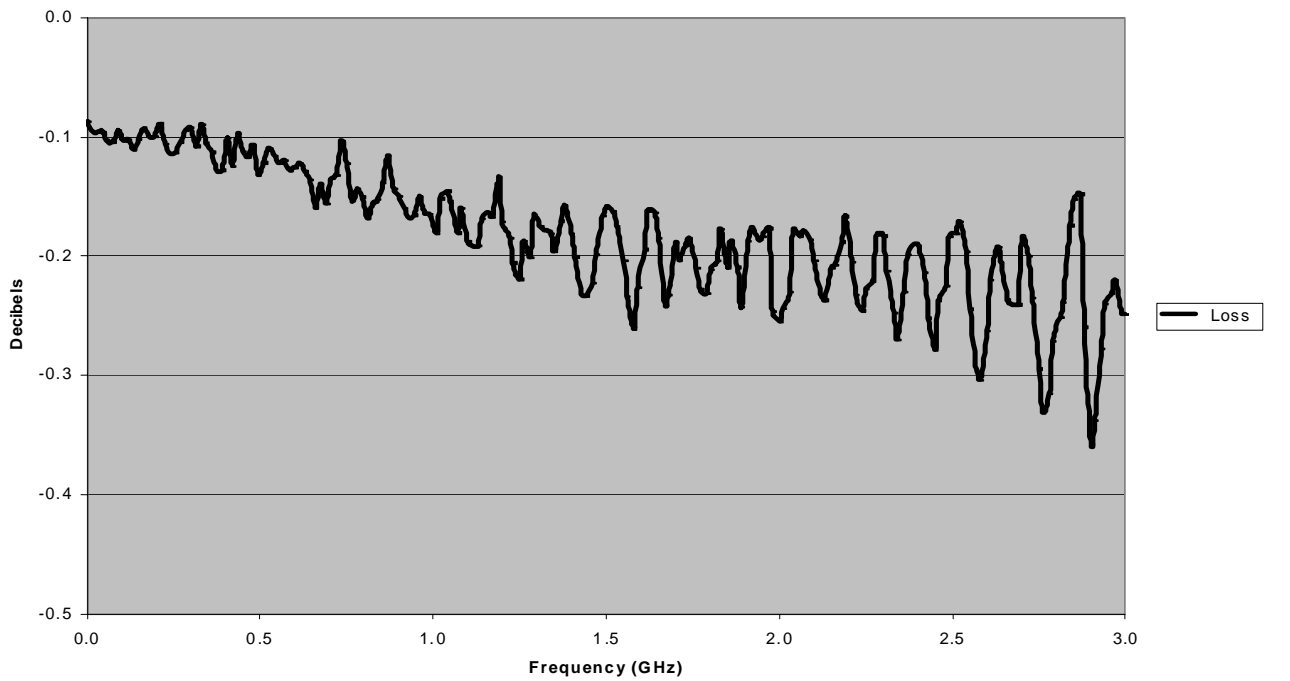


Figure B-14. TVM Device #6 RF2 insertion loss

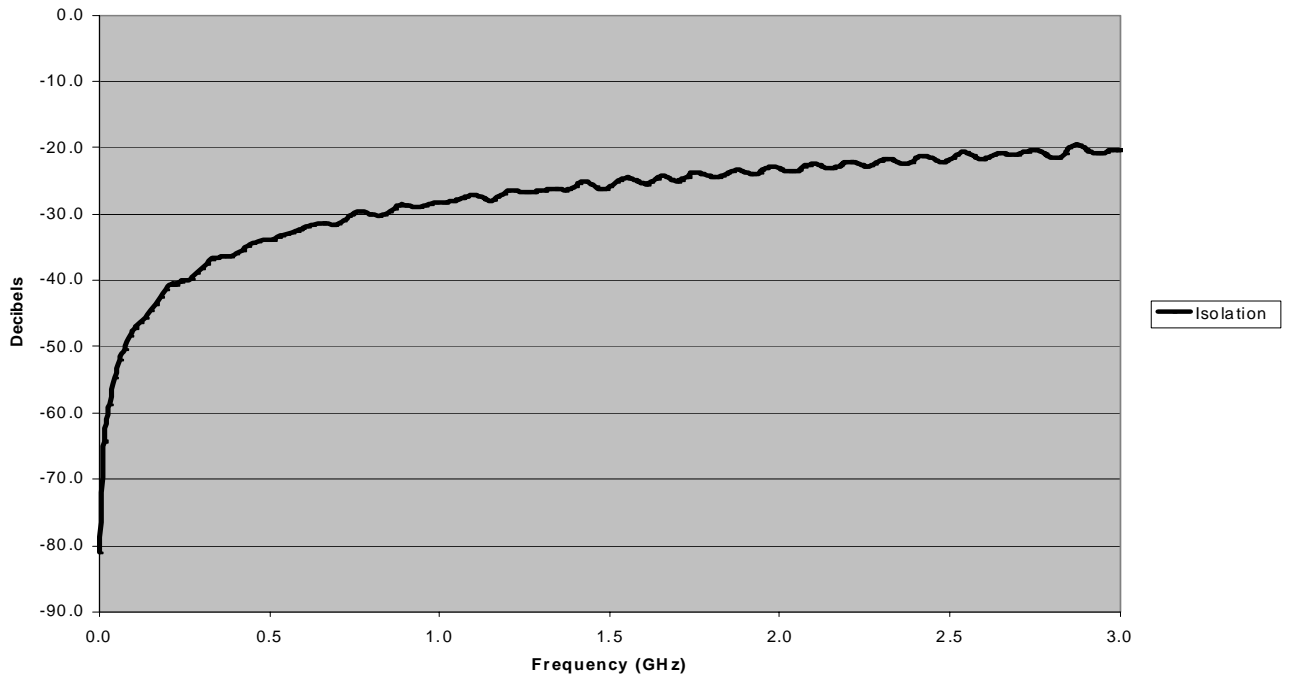


Figure B-15. TVM Device #7 RF1 isolation

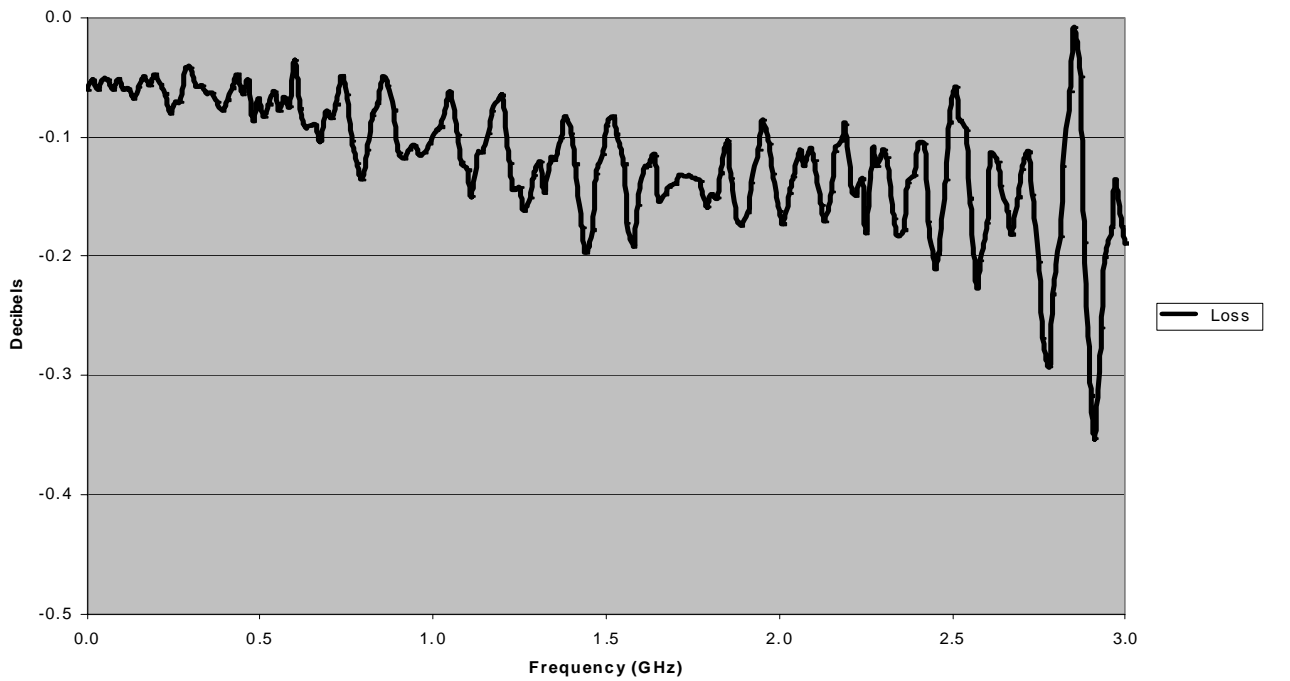


Figure B-16. TVM Device #7 RF1 insertion loss

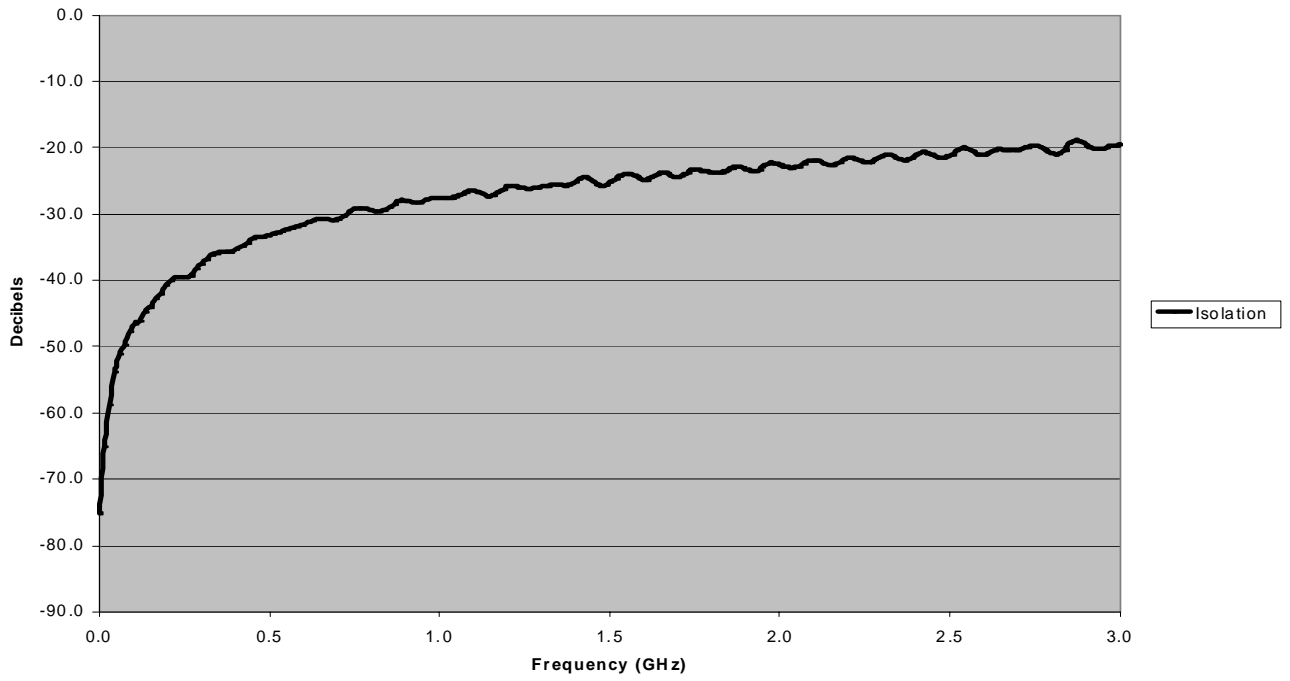


Figure B-17. TVM Device #7 RF2 isolation

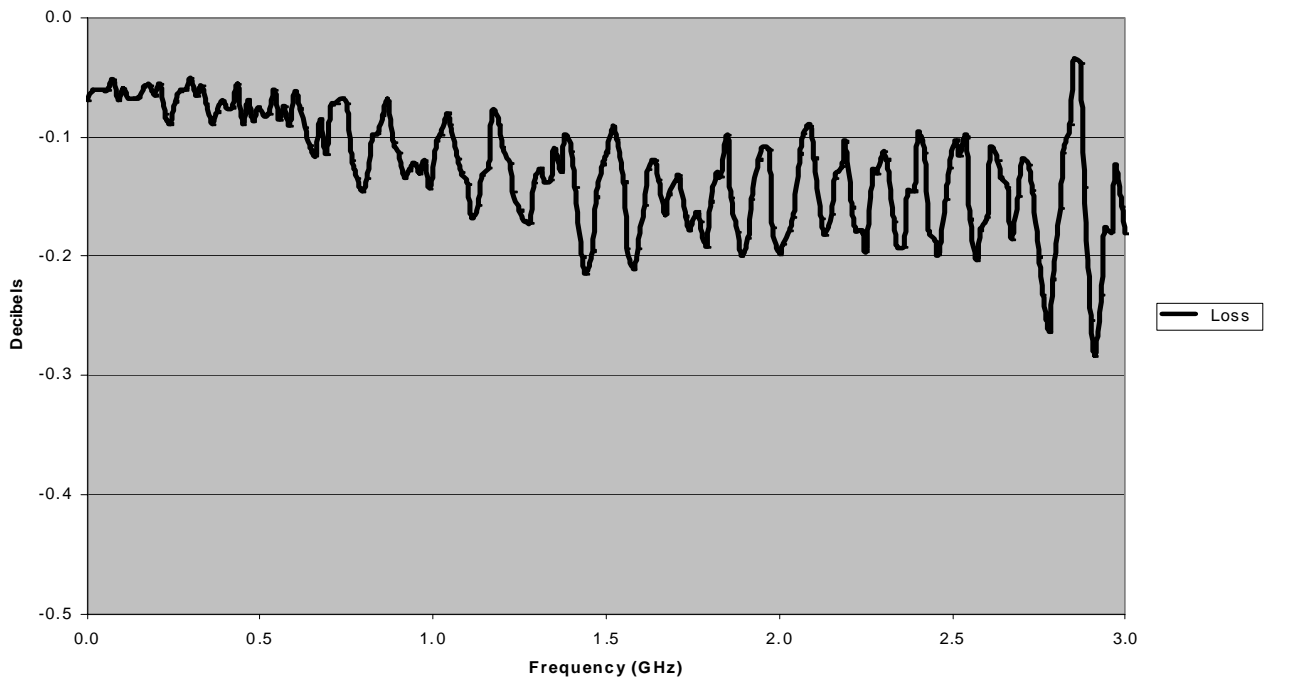


Figure B-18. TVM Device #7 RF2 insertion loss

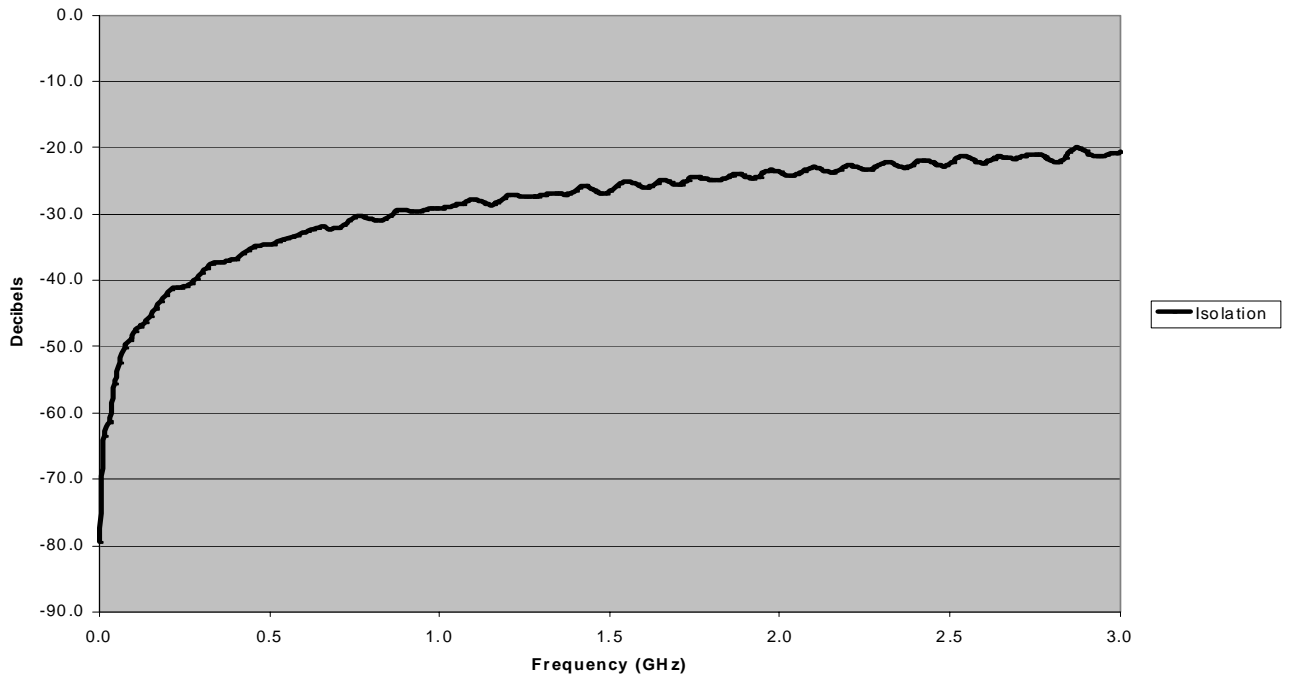


Figure B-19. TVM Device #8 RF2 isolation

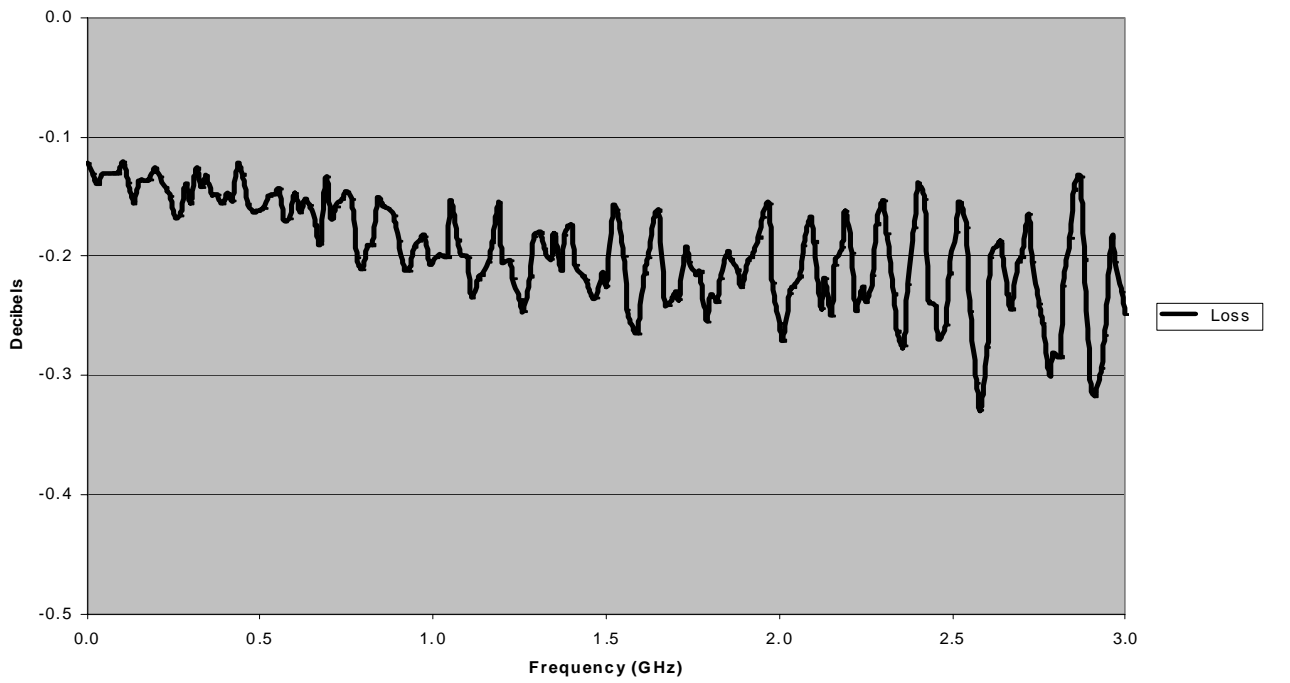


Figure B-20. TVM Device #8 RF2 insertion loss



# **APPENDIX C**

## **TeraVista RF MEMS Switches**

### **RF Pulse Power Test Data**

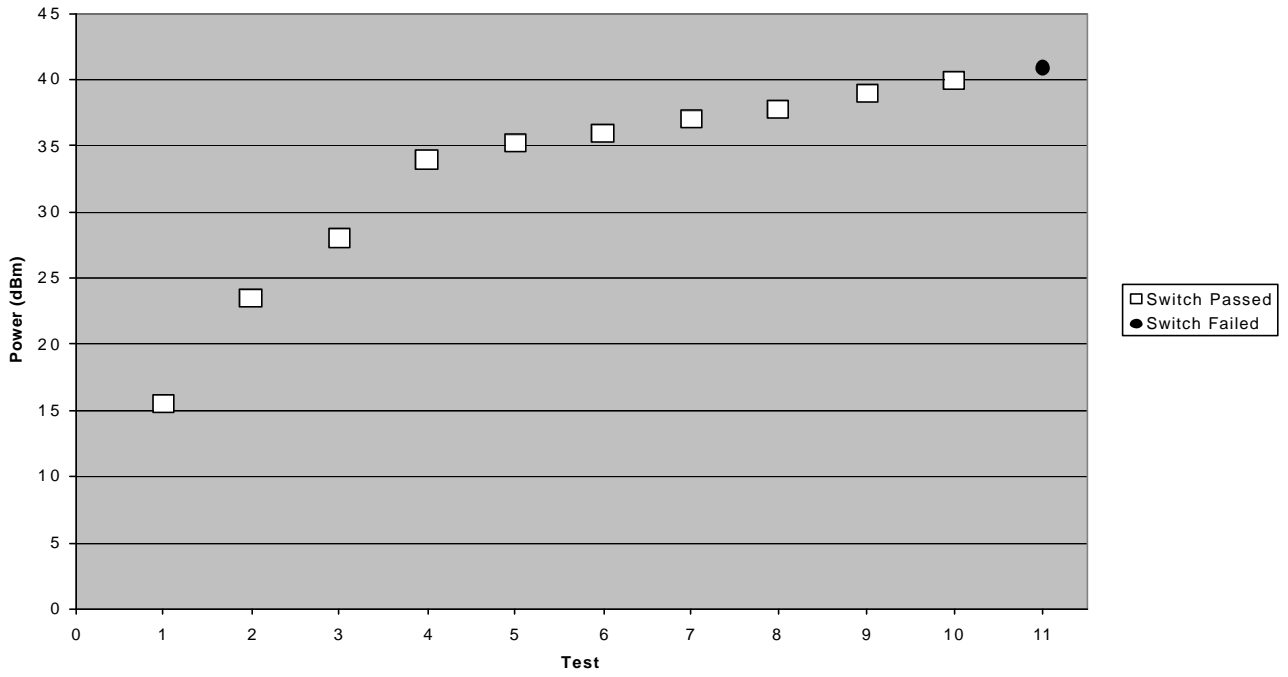


Figure C-1. Power Through TVM Device #1 RF2 Output

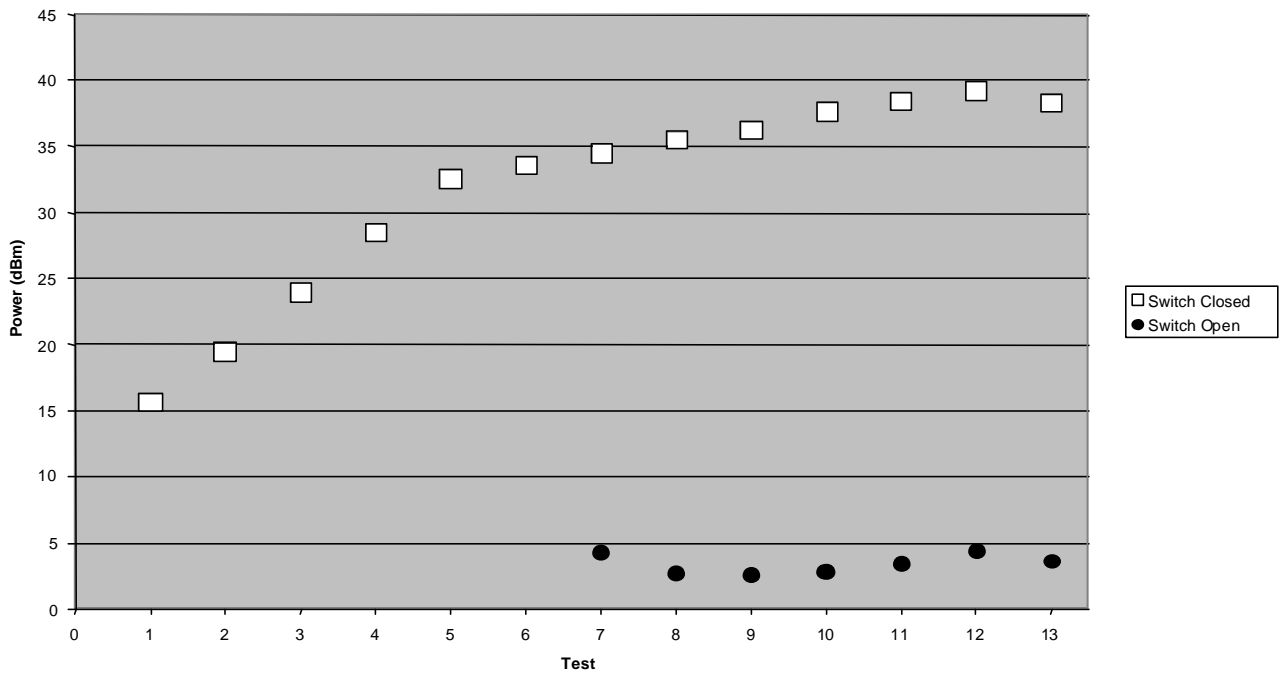


Figure C-2. Power Through TVM Device #2 RF1 Output

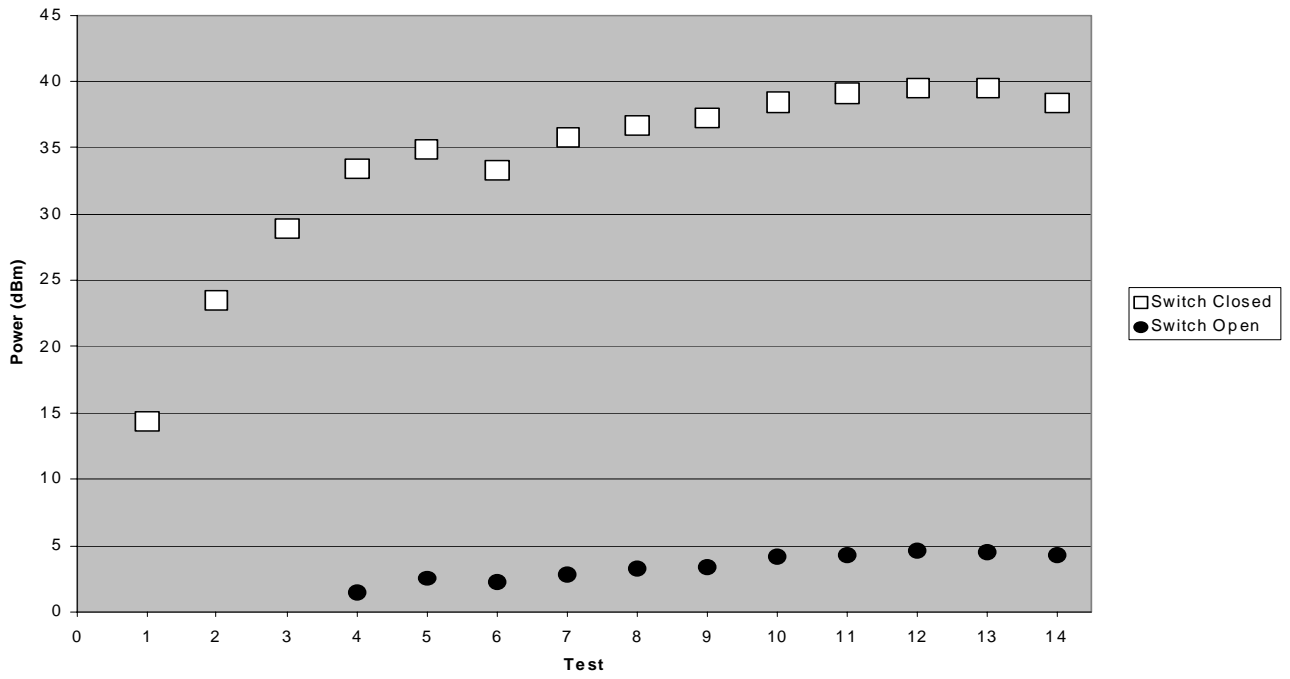


Figure C-3. Power Through TVM Device #4 RF1 Output

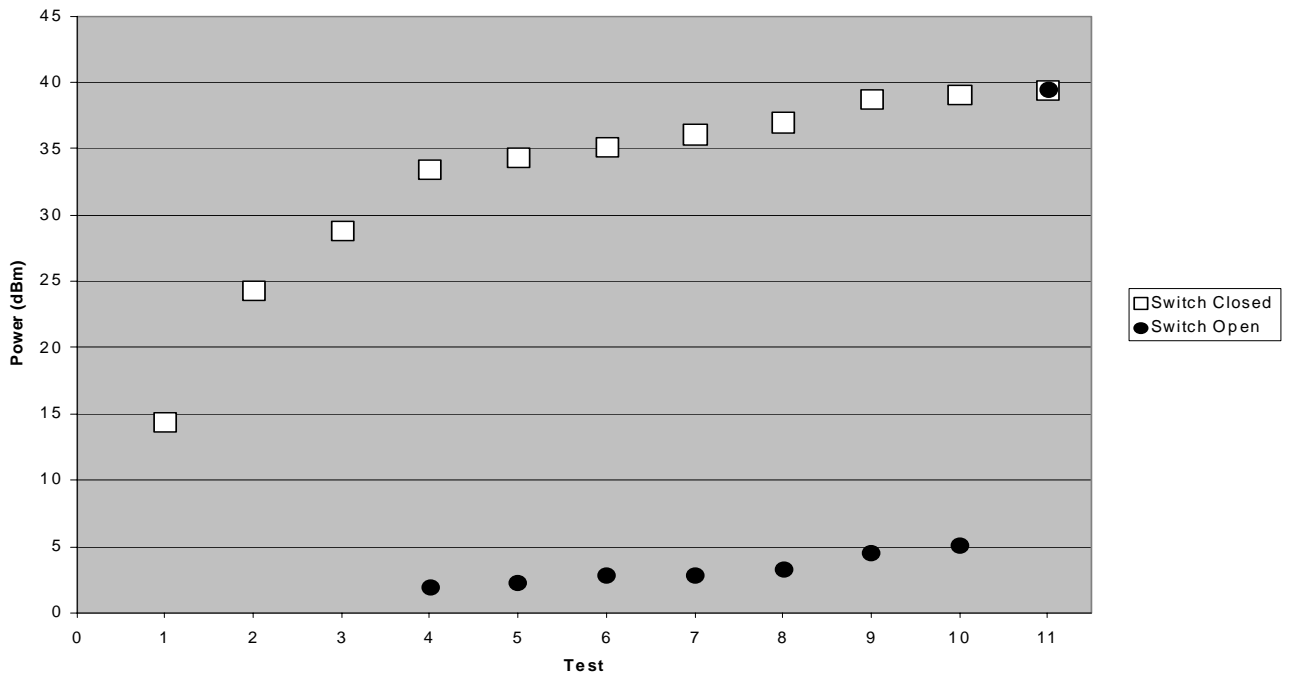


Figure C-4. Power Through TVM Device #4 RF2 Output

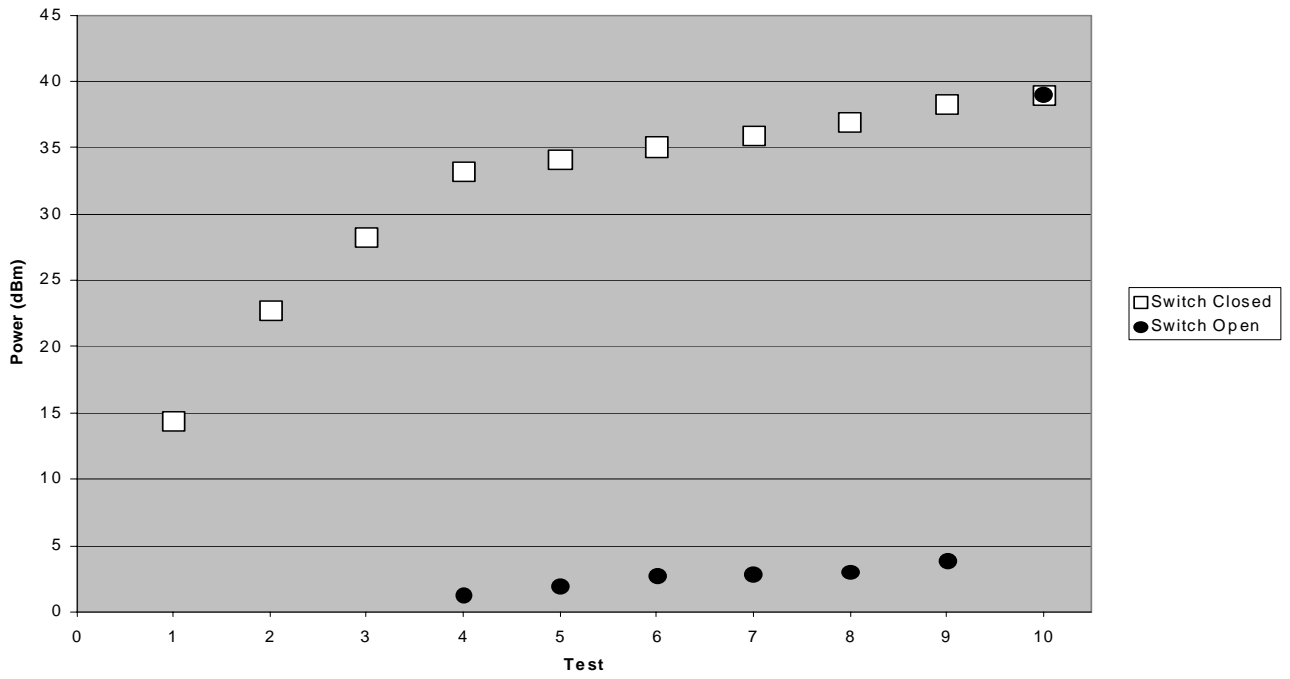


Figure C-5. Power Through TVM Device #5 RF1 Output

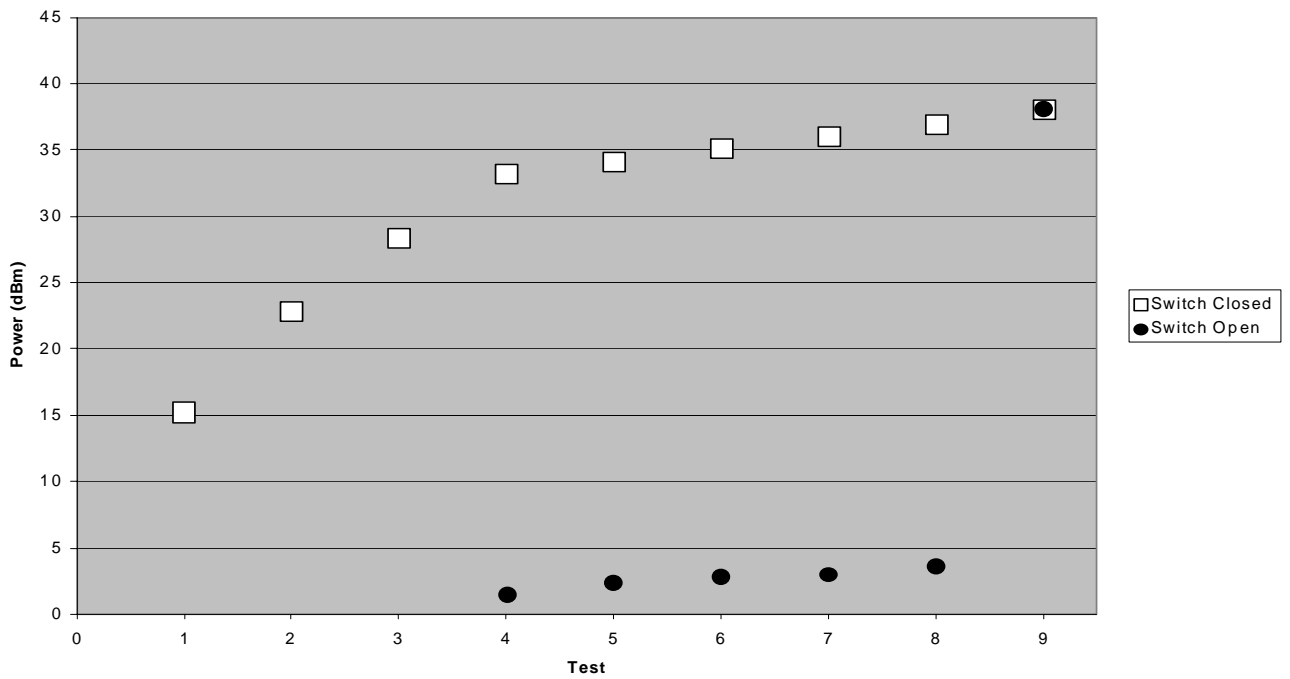


Figure C-6. Power Through TVM Device #6 RF1 Output

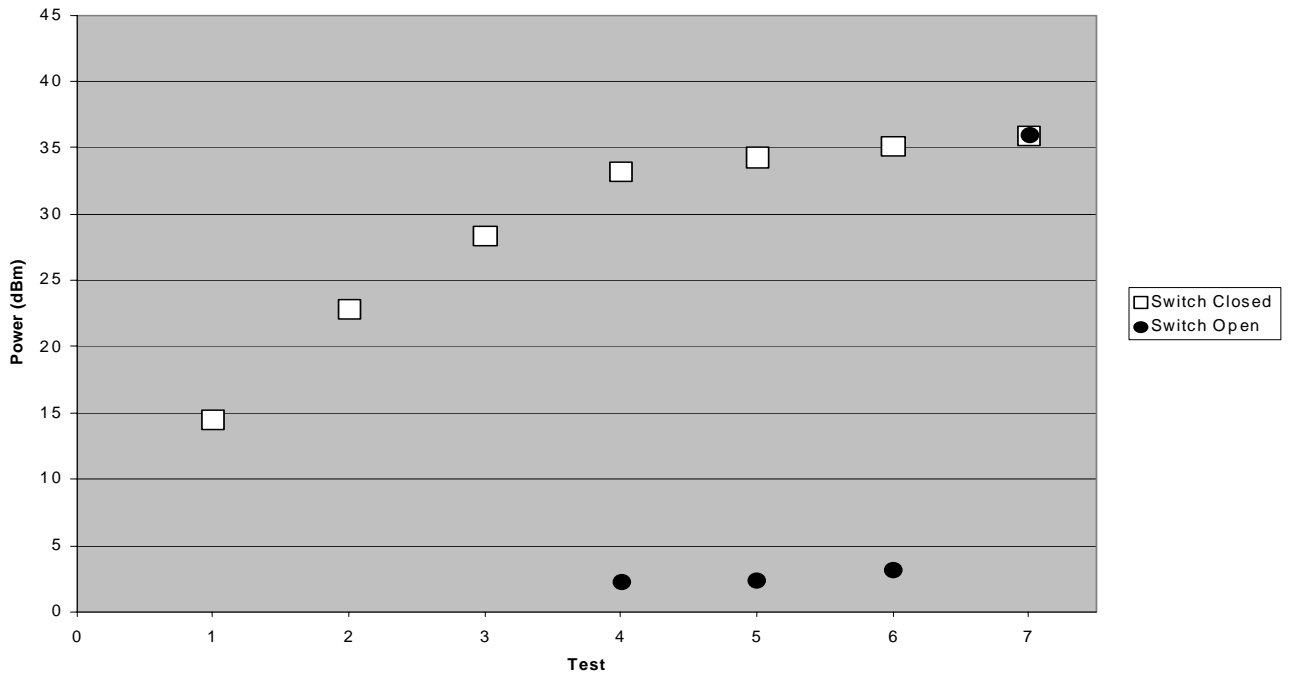


Figure C-7. Power Through TVM Device #7 RF1 Output

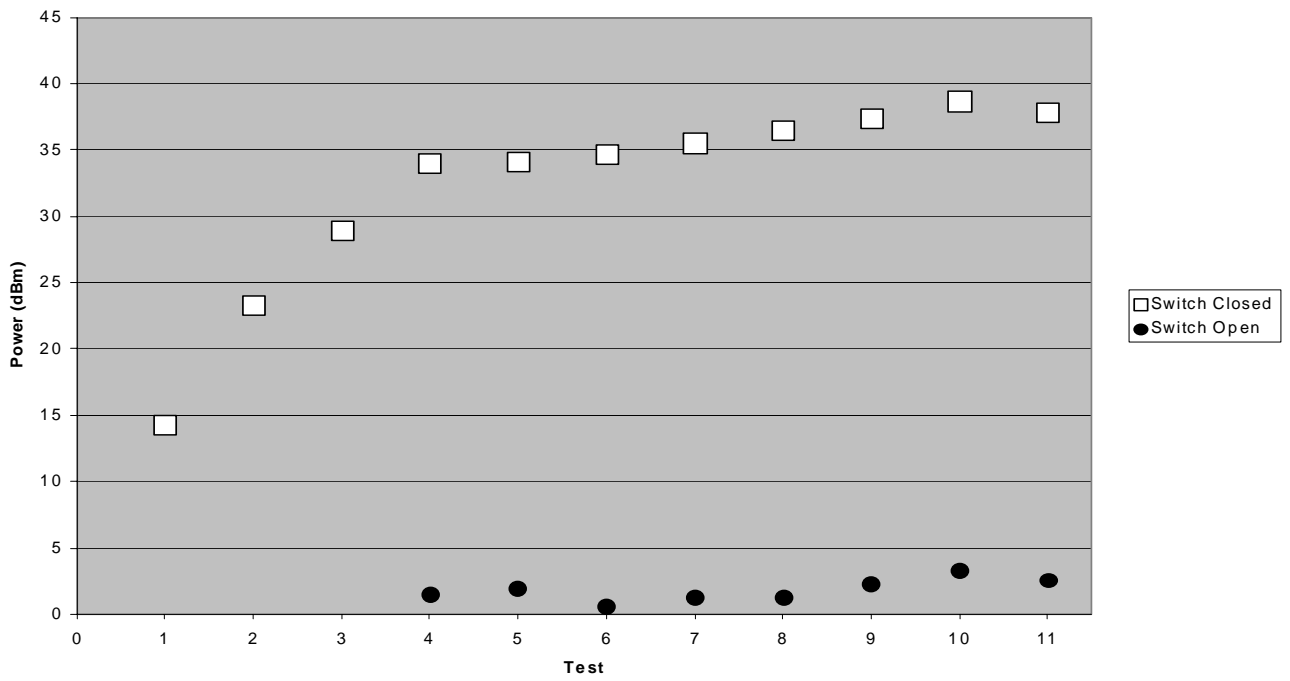


Figure C-8. Power Through TVM Device #8 RF1 Output (9JUL03)

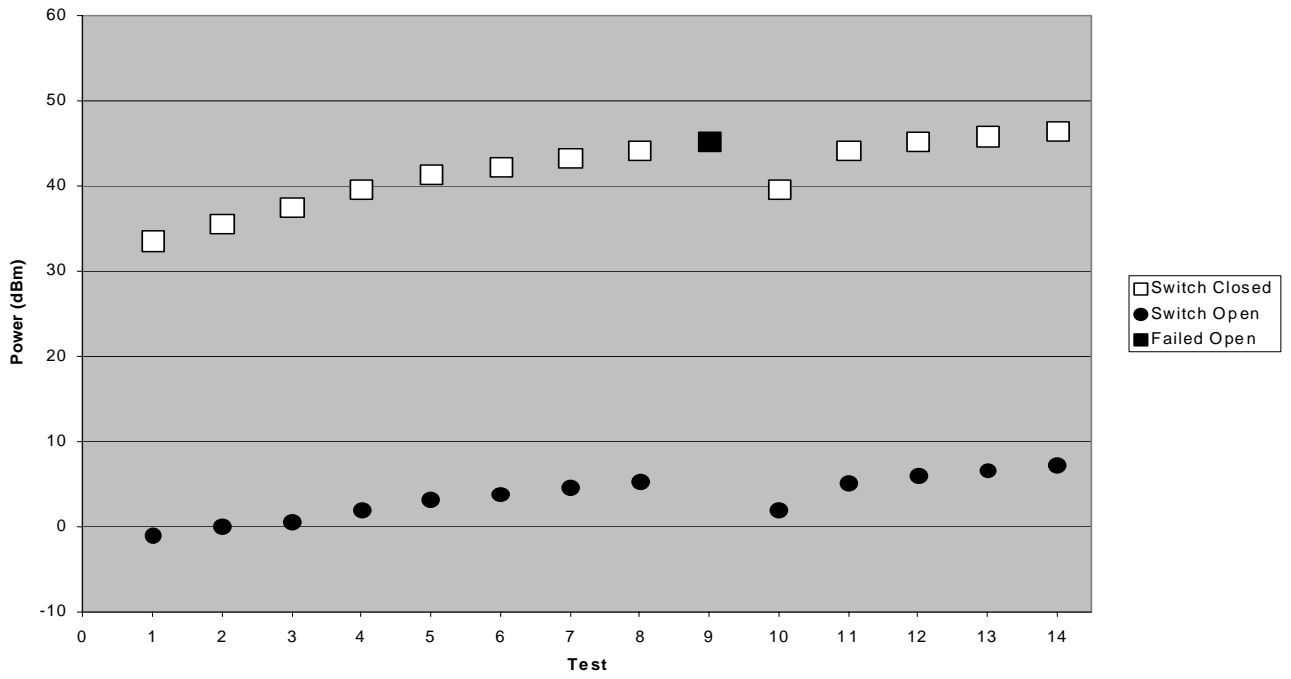


Figure C-9. Power Through TVM Device #11 RF2 Output (26AUG03)

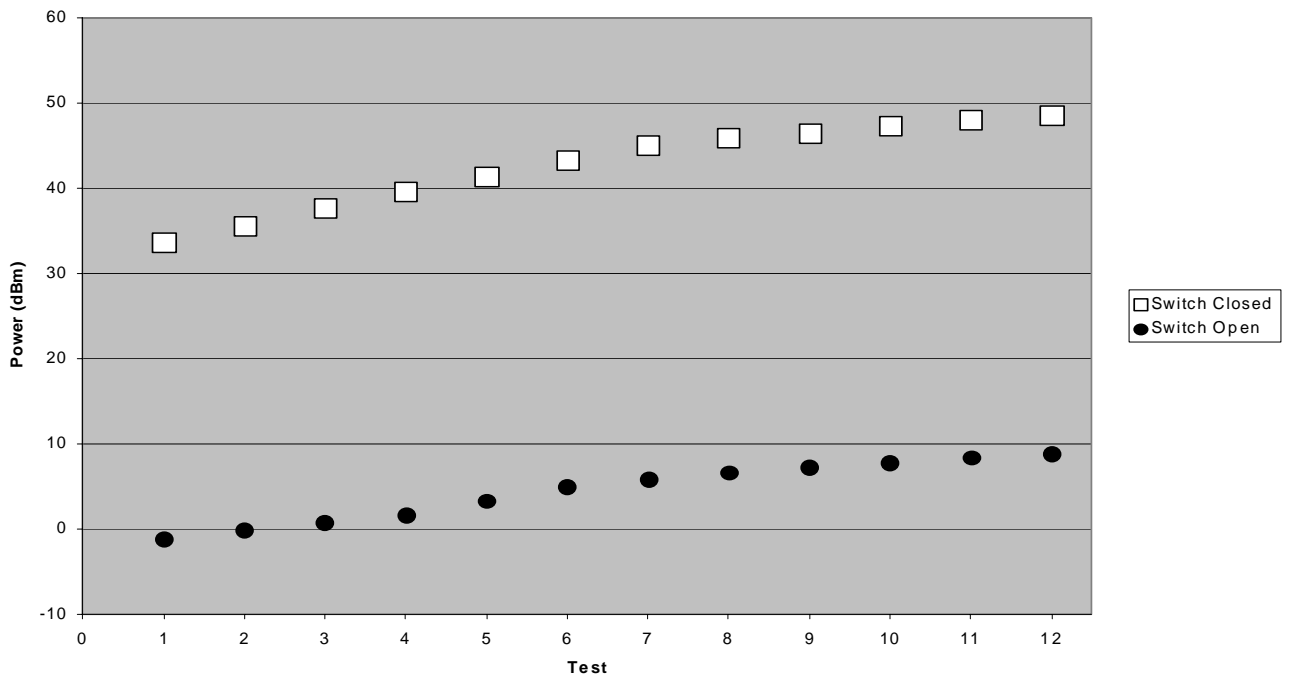


Figure C-10. Power Through TVM Device #11 RF2 Output (27AUG03)

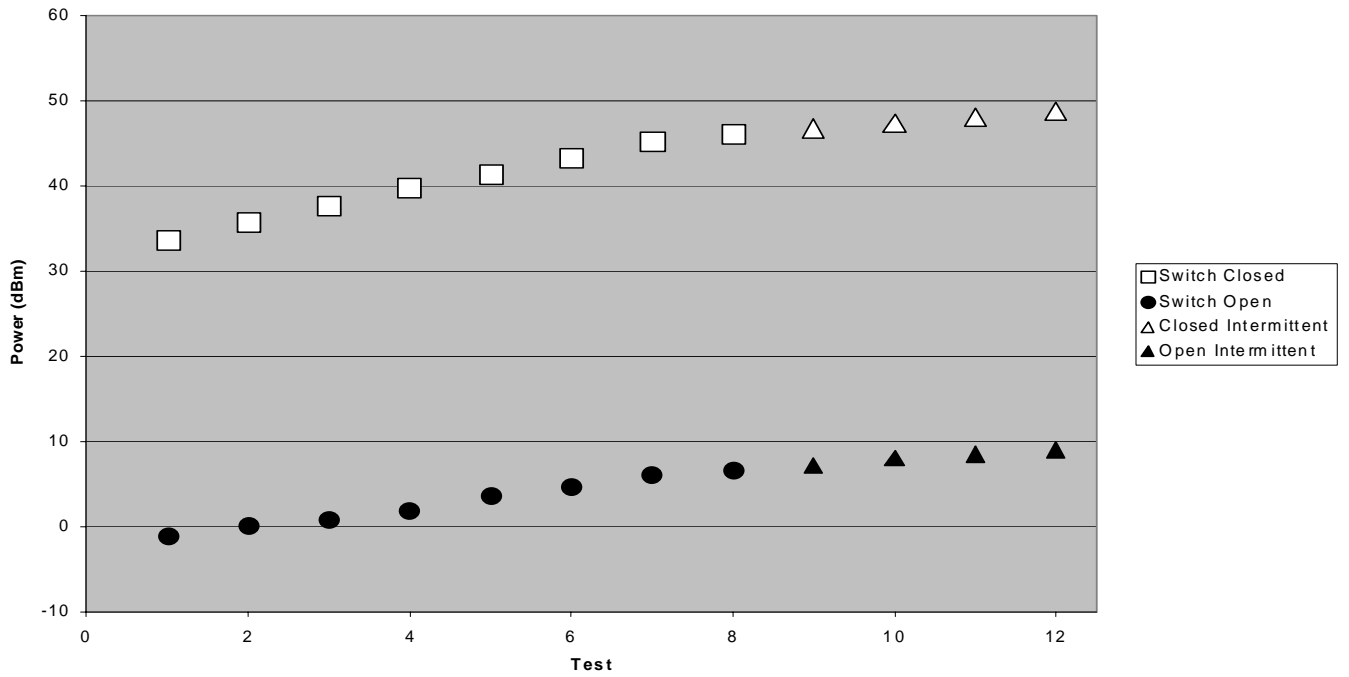


Figure C-11. Power Through TVM Device #8 RF1 Output (28AUG03)

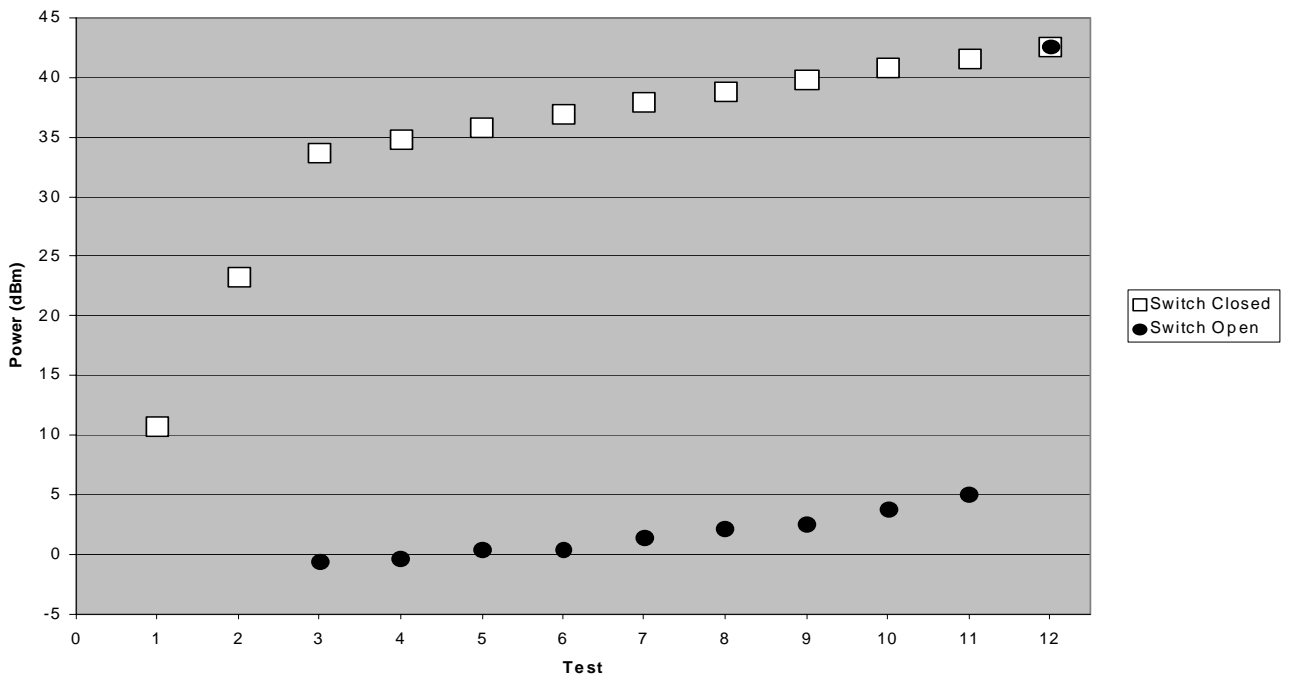


Figure C-12. Power Through TVM Device #11 RF2 Output (22SEP03)

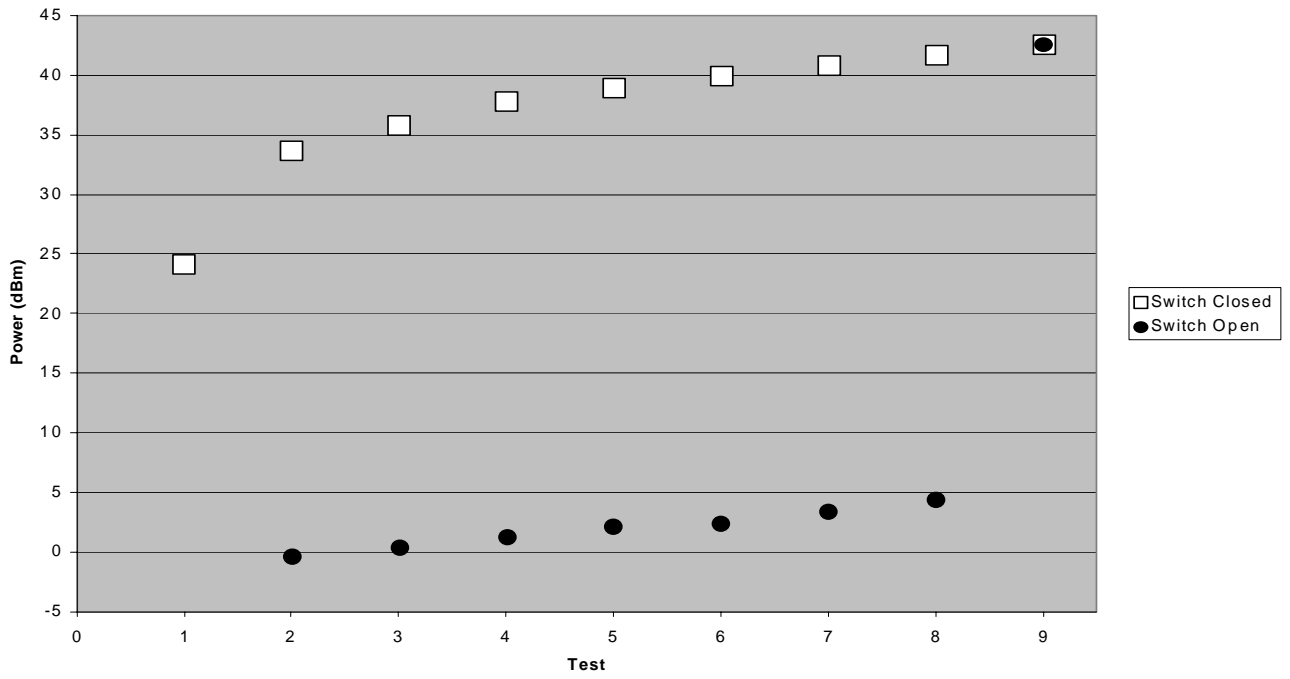


Figure C-13. Power Through TVM Device #8 RF1 Output (23SEP03)





Approved for public release; distribution is unlimited.